Macrophages in the pathophysiology of myxomatous mitral valve dystrophy

Dissertation

zur

Erlangung des Doktorgrades (Dr. rer. nat.)

der

Mathematisch-Naturwissenschaftlichen Fakultät

der

Rheinischen Friedrich-Wilhelms-Universität Bonn

vorgelegt von

Benjamin Le Vely

aus

Nantes, France

Bonn 2026

Angefertigt mit Genehmigung der Mathematisch-Naturwissenschaftlichen Fakultät

der Rheinischen Friedrich-Wilhelms-Universität Bonn

Gutachterin/Betreuerin: Prof. Dr. Elvira Mass

Gutachter: Prof. Dr. Falk Nimmerjahn

Tag der Promotion: 24. März 2026

Erscheinungsjahr: 2026

Summary

List of figures

List of abbreviations

BMP: Bone Morphogenetic Protein

CCR2: C-C motif chemokine Receptor 2

CD: Cluster of Differentiation

CRM: Cardiac Resident Macrophage

ECM: Extracellular Matrix

EMP: Erythro-Myeloid Progenitor

EMT: Endothelial to Mesenchymal Transition

FLNA: Filamin A

GAG: Glycosaminoglycan

HA: Hyaluronan/Hyaluronic acid

HAS: Hyaluronic Acid Synthase

HPS: Hematoxylin Phloxin Saffron

KI: Knock-In

KO: Knock-Out

MR: Mitral Regurgitation

MV: Mitral Valve

MVD: Mitral Valve Dystrophy

MVP: Mitral Valve Prolapse

NFATC: Nuclear Factor of Activated T Cell

PG: Proteoglycan

pMac: Precursor of Macrophage

SMAD: Small Mother Against Decapentaplegic

TGF-β: Transforming Growth Factor beta

TNF-α: Tumor Necrosis Factor alpha

VEC: Valvular Endothelial Cell

VEGF: Vascular Endothelial Growth Factor

VIC: Valvular Interstitial Cell

WT: Wild Type

I. Introduction

The human heart is a four-chamber muscle, which can be divided depending on the side they are located and which function they maintain. The right side of the heart is composed of the right atrium and right ventricle. Their function is to receive the blood from the veinous circulatory system and to pump it towards the pulmonary circulation for re-oxygenation. Therefore, the right heart is a low-pressure system. Conversely, the left heart is a high-pressure system. The left atrium receives oxygenated blood from the pulmonary vasculature, and the left ventricle pumps it toward the systemic circulation through the aorta to distribute oxygen to the organism (Figure 1).

To maintain a unidirectional blood flow, the heart is composed of four valves. Two are located between the ventricle and the vasculature and are classified as semi-lunar valves: the pulmonary valve, between the right ventricle and the pulmonary artery; and the aortic valve between the left ventricle and the aorta (Figure 1). They open during systole to allow blood ejection, and close during diastole to prevent backward blood flow towards the ventricle. The two other valves, classified as atrioventricular valves, are located between atria and ventricles. The tricuspid valve is located in the right heart, and the mitral valve between the left atrium and left ventricle (Figure 1).

Structural and/or functional defects of one or more valves have important impacts on the cardiac remodeling and function, and lead to heart failure and increased risk of cardiac death.[1–3] The manifestations of valvular heart diseases are stenosis, characterized by a reduction of the valve opening, and regurgitation, characterized by coaptation defects and backward blood leakage.

Throughout this thesis, the focus will be on the mitral valve (MV) and its most prevalent pathology, the myxomatous mitral valve dystrophy (MVD). MVD is the main etiology of mitral

valve prolapse (MVP). The consequence of MVP is the progressive development of mitral regurgitation (MR), increasing the incidence of heart failure, arrhythmia, endocarditis, and sudden cardiac death.[1,2,4,5] Even though this pathology has been described since the 1960s, no pharmacological treatment is available. Mitral valve surgery (repair or replacement) is the only therapeutic option for patients with severe MVD.[3] Thus, diagnosis as well as treatment of MVD represents a major challenge for healthcare system.

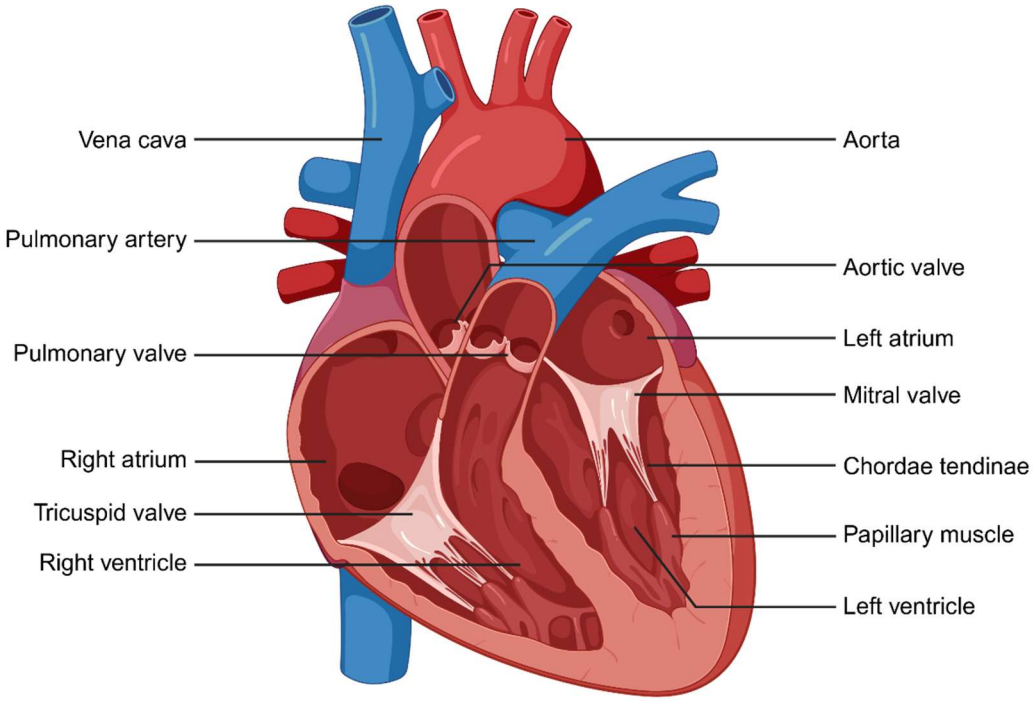

Figure 1. Human heart anatomy. Transversal section of the hear depicting the four chambers and valves. Created in BioRender.

1. Anatomy and physiology of the mitral valve

1.1 The mitral valve apparatus

The mitral valve apparatus is composed of the mitral valve, the papillary muscles, and the chordae tendineae (Figure 1 and Figure 2). The MV is the only bicuspid valve of the heart, and comprise the anterior and the posterior leaflets, each divided in 3 scallops (A1, A2 and A3 for the anterior leaflet, and P1, P2, and P3 for the posterior leaflet; Figure 2).[6] The leaflets are attached to the heart wall via the fibrous mitral annulus at the atrio-ventricular junction, and to the papillary muscles via the chordae tendineae.[7]

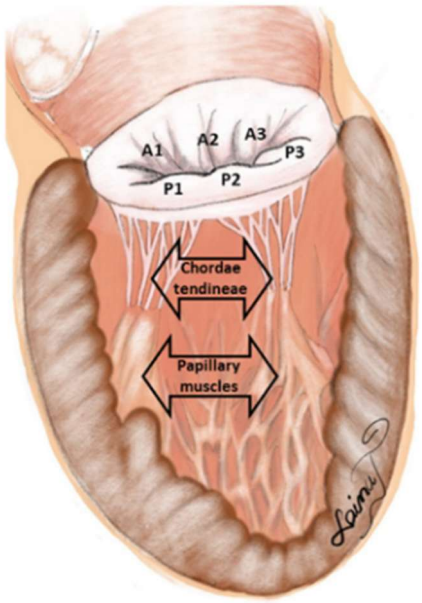

Figure 2. Mitral valve apparatus. Representation of the mitral valve apparatus showing the 3 scallops of the leaflets, the chordae tendineae and the papillary muscles. From Tumenas *et al.*[6]

The primary chordae attach the free edge of both leaflets, are rich in collagen and have low extensibility. The secondary chordae are attached to the leaflets central part, they are thicker and more extensible than primary chordae. The chordae allows the proper coaptation of both leaflets during systole and prevent MV leaflet prolapse.[8] The two papillary muscles are located at the anterolateral and posteromedial position of the left ventricle. During systole, the papillary muscles contract simultaneously with the left ventricle, and taut the chordae tendineae to prevent MV leaflet prolapse.[6,8]

1.2 Mitral valve function

The function of the mitral valve is to keep a unidirectional flow of blood between the left atrium and left ventricle. The coordinated opening and closing of the valve during the cardiac cycle is essential to the process.[8,9] During diastole, the mitral valve opens and the blood flows from the atrium towards the ventricle in two different phases: the passive filling of ventricle and the active filling caused by the contraction of the atrium. Then, during systole, as the ventricle starts contraction, the mitral valve closes and prevents the blood to flow backwards to the atrium. When closed, the aortomitral continuity also helps to guide the blood flow towards the aortic valve.

1.3 Mitral valve structure

The mitral valve leaflets are well-organized structures, the anterior leaflet is 18-24 mm long and 4-7 cm^2 in area, as opposed to 11-14 mm and 2-3 cm^2 for the posterior leaflet.[7] The structure of the MV is divided in three distinct layers: the atrialis, the spongiosa, and the fibrosa (Figure 3).[10–12] The atrialis, located on the atrial side of the leaflets, comprises a layer of elastic

fibers that allows the tissue to resist the laminar shear stress caused by the blood flow during the opening of the valve. The spongiosa is the thickest layer of the MV and is located in the middle part of the leaflet. It contains a high proportion of glycosaminoglycans and other extracellular matrix (ECM) components.[12] The purpose of this layer is to absorb the different mechanical forces the leaflets endure at each cardiac cycle, during opening and closing of the valve. Finally, the fibrosa is the layer at the ventricular interface, composed by a network of collagen fibers (Figure 3). The collagen fibers absorb the compression forces applied to the leaflet during the systole. The cellular composition of the MV leaflets relies on three cell types: valvular endothelial cells (VECs); valvular interstitial cells (VICs), and macrophages (Figure 3). Altogether with the extracellular matrix, those cell types contribute to maintain the valvular homeostasis.

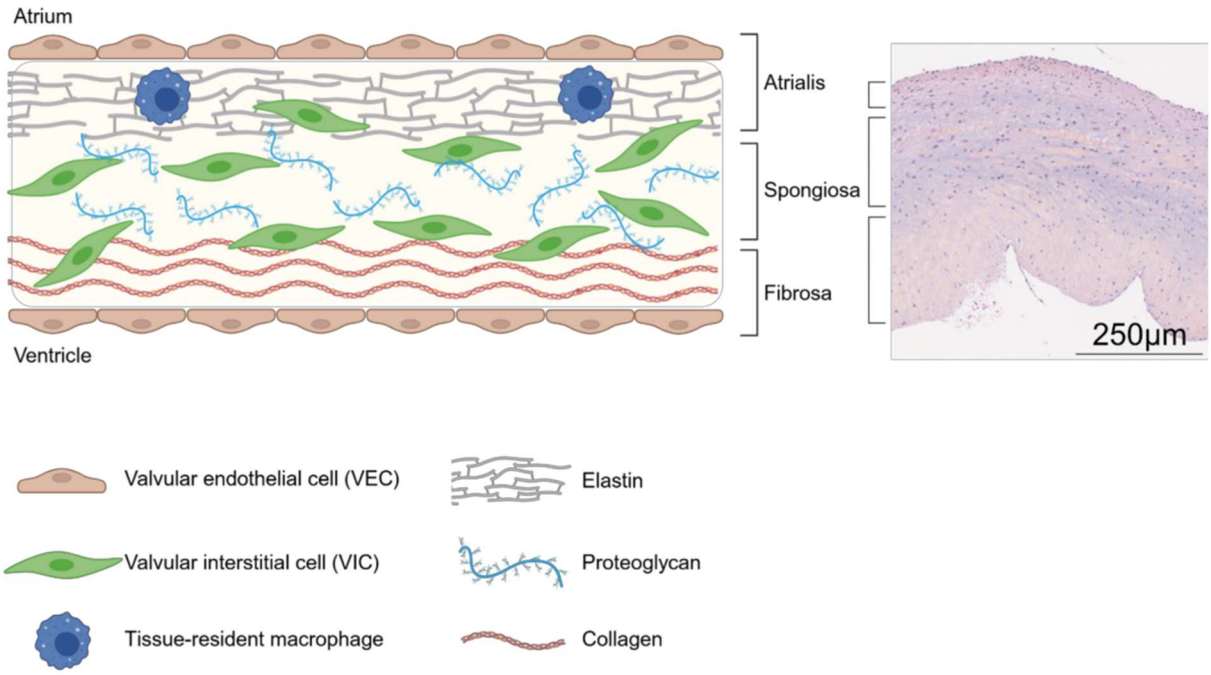

Figure 3. Healthy mitral valve leaflet structure. The three layers of the mitral valve are the atrialis, the spongiosa, and the fibrosa. The extracellular matrix comprises layers of elastin, proteoglycan, and collagen. Valvular endothelial cells, valvular interstitial cells and tissue-resident macrophages are the three main cell types populating the valve. Created in BioRender.

1.3.1 Extracellular matrix

The valvular extracellular matrix (ECM) is composed of elastin, collagen, and various glycosaminoglycans and proteoglycans (GAGs and PGs; Figure 3).[13] Three types of collagen are present in the MV-ECM: type I collagen, representing 74% of collagen in healthy valve, followed by type III collagen accounting for 24% of collagen content, and the 2% remaining are type V collagen, which is known to interact with type I to form heterotypic fibrils.[14,15] Collagen synthesis is at least partly regulated by VICs stiffness and valvular pressure.[16] Collagen fibers are found mostly in the fibrosa layer (ventricular side), they allow the tissue to cope with the compression forces during systole, and they also connect the leaflet to the chordae, which are also rich in collagen. Glycosaminoglycans are polysaccharide chains classified in five categories. Four of them are sulfated GAGs: chondroitin sulfate; dermatan sulfate; heparan sulfate; and keratin sulfate, and the last one is non-sulfated: hyaluronic acid (HA). Unlike other GAGs, HA doesn't require to be bound to a protein, and exist freely in the tissue.[13] Three different enzymes are known to synthetize HA: Hyaluronic Acid Synthase 1, 2 and 3 (Has1, Has2, Has3). HA is a highly hydrophilic GAGs that facilitates cellular proliferation and motility, and is important for proper heart development.[17,18] Proteoglycans consist of a core protein to which is bound covalently at least one GAG. In the MV leaflets, the major proteoglycans are versican, biglycan, and decorin. The distribution of proteoglycans is not uniform across MV leaflets and depends on the mechanical forces applied: biglycan and decorin are abundant in the center of the anterior leaflet (region of tensile forces), whereas versican is more abundant in the posterior leaflet and at the free edge of the anterior leaflet (region of compression forces).[13,19,20]

1.3.2 Valvular Endothelial Cells

Valvular endothelial cells, or VECs, are specialized cells derived from the endocardium during embryogenesis.[21,22] They form a monolayer surrounding the valve leaflets and are particularly important to maintain tissue homeostasis (Figure 3). As the first barrier of the MV leaflet, endothelial cells are submitted to a wide variety of mechanical constraints: opening and closing of the valve creates tension and strain, blood flow generates laminar and turbulent shear stresses as well as compression forces on the leaflets. To cope with those tremendous mechanical forces, VECs express a wide variety of receptors at their surface, such as integrins, mechanoreceptors, mechanosensitive ion channels, and adhesion molecules, that act as sensors of the microenvironment, and triggers signaling pathways to modulate endothelial cell -or other neighboring cell- properties in response to the microenvironment.[23–27] Endothelial cells also have immune functions, as the migration of monocytes to sites of inflammation depends on their interaction with endothelial cells. Particularly, through the release of chemoattractant and the modulation of adhesion molecules expression at their surface, endothelial cells finely regulates leukocyte trafficking and extravasation.[28,29] The regulation of endothelial immune functions is tightly linked to the level of activation of the endothelial cell, which is driven by different stimuli such as mechanical stress, and cytokines like Interferon γ (IFN-γ) or Tumor Necrosis Factor α (TNF-α).[23,30]

Different VECs subpopulation with specific functions and localization have been described in the literature.[31–33] Three mitral-VECs subtype were described by Hulin *et al*.[32] Typical VEC with high expression of endothelial markers (*Emcn*, *Edn1*, *Vwf*); Lymph-VEC characterized by *Prox1* expression and located on the fibrosa; and Coapt-VEC, located at the coaptation area of the leaflet and marked by *Hapln1* expression.[32] In a different study, Shu *et al*. identified via scRNAseq 5 distinct VECs states: Structural VECs, similar to the typical VECs described previously; Shear stress reactive VECs with high expression of endothelial-mesenchymal-

transition (EMT) signature; Protective VECs that express genes involved in repair processes; Metabolically active VECs; and inflammatory VECs.[31] Noteworthy, this study was performed on non-diseased human cardiac valve leaflets from aortic, pulmonary, tricuspid and mitral origins. The proportion of each VEC subtypes was variable depending on the type of valve, and MV had low proportion of shear stress-reactive VECs compared to the other valves.[31]

1.3.3 Valvular Interstitial Cells

Valvular Interstitial cells (VICs) are fibroblastic cells located in the inner layer of the valve leaflets, and are the most prevalent cell type in the mature valve, around 80% of cells (Figure 3).[32] They differ from typical fibroblast because of their unique origin. Indeed, VICs derive from endocardial cells that undergo EMT during development, and are then self-renewed in the fully developed heart.[32,34] These cells are in charge of the valves ECM homeostasis through secretion and degradation of the ECM components.[35] In order to understand valve physiology and pathophysiology, research studies have been conducted to decipher the cellular landscape of VICs and diverse classifications have been proposed.[31,32,36] Quiescent-VICs (qVICs) maintain the normal valve homeostasis in the adult valves .[36] They are also called fibrosa-VICs, or structural-VICs in some publications.[31,32] Activated-VICs (aVICs) are present in pathological valves and are cells involved in the ECM remodeling. As such, they have increased expression of genes involved in collagen organization, wound healing, and myofibroblast differentiation.[32,36] The aVICs have been compared to matrifibrocytes, a specific population of fibroblast observed in the infarcted myocardium. After infarction, cardiac fibroblasts are activated, highly proliferative, express α-smooth muscle actin (α-SMA) and secrete abundant ECM proteins to replace the necrotic core with scar tissue. It was shown that this population of fibroblasts persists within the scar and undergo a new phenotypic switch to express ECM and

tendon genes to support the mature scar.[37] Other types of VICs have been described but are restricted to a certain type of valves, like osteoblastic-VICs described in aortic valves, or a certain period like embryonic progenitors during development.[36] More recently, the studies of *Hulin et al.* and *Shu et al.* showed the presence of Antigen presenting-VICs and Complement response-VICs, and pro-inflammatory-VICs. Although different in terms of markers and function, those populations highlight the ability of VICs to have an immune phenotype.[31,32]

1.3.4 Macrophages

The presence of tissue-resident macrophages in the mitral valve is a relatively new concept that emerged with the identification of cells with hematopoietic origin in the mitral valve leaflets.[38,39] It was later shown an increase of hematopoietic $CD45^+$ cells in myxomatous valve disease from conditional endothelial Filamin-A knock-out mice model, highlighting for the first time the possible role of immune cells in MVD.[40] The immune cells infiltration was also confirmed in the model of Marfan syndrome related-MVD, and they further described those cells as predominantly macrophages ($CCR2^+$, $CD206^+$).[32,41]

A more detailed description of macrophages, their function, origin, and contribution to heart homeostasis and diseases will be developed in the section 4 of this manuscript.

1.4 Developmental origin of the mitral valve

The development of cardiac valves during embryogenesis is referred as valvulogenesis. It is an early process, starting at embryonic day E28 in human and E9 in mice.[26,42] After gastrulation, mesodermal mesenchymal cells give rise to the primary heart fields, which will first evolve in

the cardiac crescent and later the linear heart tube, composed of two cell layers: outer myocardial and inner endocardial cells. Those layers are separated by a hyaluronan and chondroitin sulfate-rich ECM called the cardiac jelly. Once formed, the linear heart tube initiates looping to form separate chambers. Concomitantly, swelling of the cardiac jelly leads to the formation of the endocardial cushions positioned at the atrioventricular junctions and at the outflow tract region for atrioventricular and semilunar valves respectively (Figure 4).[43] A subset of endocardial cells then loses their intercellular junctions and migrate into the cardiac jelly while transitioning from endothelial to mesenchymal phenotype (EMT), giving rise to the valvular interstitial cell population (Figure 4).[21,22,26,44,45] The finely regulated mechanisms behind this transition are not fully understood, but it is establish that it is locally triggered by various stimuli including shear stress, ECM composition, and Bone Morphogenetic Protein (BMP) signaling (Figure 5).[46–48]

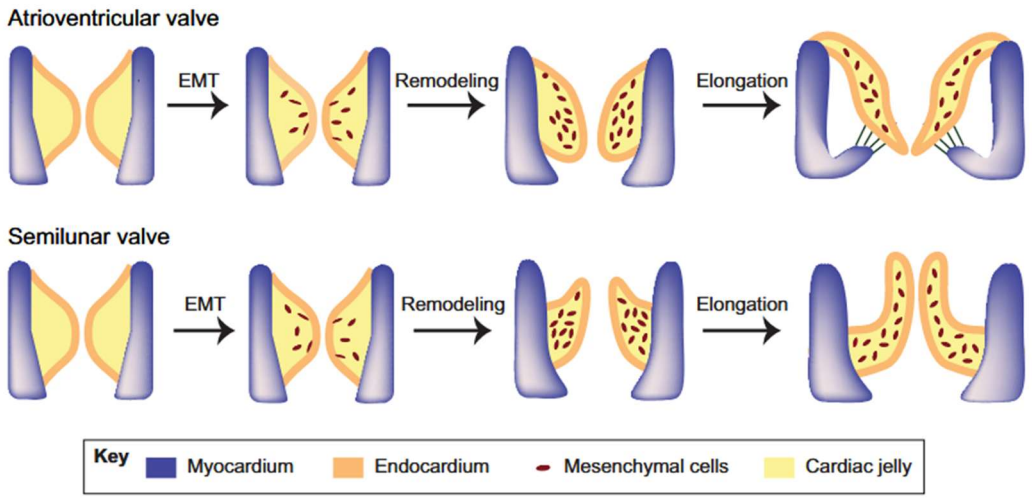

Figure 4. Valvulogenesis process. Endocardial cells undergo endothelial to mesenchymal transition (EMT) and invade the cardiac jelly. The newly formed VICs secrete extracellular matrix to remodel the endocardial cushion that undergo an elongation process until birth. From Lin et al.[45]

Several studies have investigated those mechanisms, and have revealed the importance of the Notch-WNT-BMP signaling axis.[46,49–51] Notably, Jagged1-mediated Notch1 activation in endocardial cells regulates WNT4 expression which in turn induce Bmp2 expression in the adjacent atrioventricular myocardium. Bmp2 then promote EMT of endocardial cells.[49] EMT is also under the control of Nuclear factor of activated T cells cytoplasmic 1 (NFATc1), an endocardial transcription factor which is highly expressed in endocardial cells.[52–54] It was shown that NFATc1 expression is restricted to endocardium at the endocardial cushion early in development, and that its expression is reduced upon EMT.[52] Precisely, Wu *et al.* demonstrated that a subset of endocardial cells downregulate NFATc1 before initiating EMT. The other NFATc1 endocardial cells remain in the endocardium as a proliferative population contributing to valve growth and elongation.[52] Moreover, endocardial deletion of NFATc1 results in failure of endocardial cushion to remodel and grow into mature valves.[52,53,55–58] The upstream regulator of NFATc1 in endocardial cells is not clearly identified, but the Vascular endothelial growth factor (VEGF) signaling pathway is thought to be involved. VEGF activates NFATc signaling in human endothelial cells postnatally, and there is a spatiotemporal overlap between NFATc1 and VEGF expression in the endocardial cushion (Figure 5).[54,59–61] In 2010, Stankunas *et al.* clarified the role of VEGF signaling in valvulogenesis. They showed that VEGF signaling is necessary for EMT at the outflow tract but not at the atrioventricular canal. This process involves VEGFR1, which is highly expressed in endocardial cells at early developmental stages but downregulated following EMT. On the other hand, VEGFR2 gets upregulated after EMT, and is involved in growth and elongation of the valve into mature leaflets.[60]

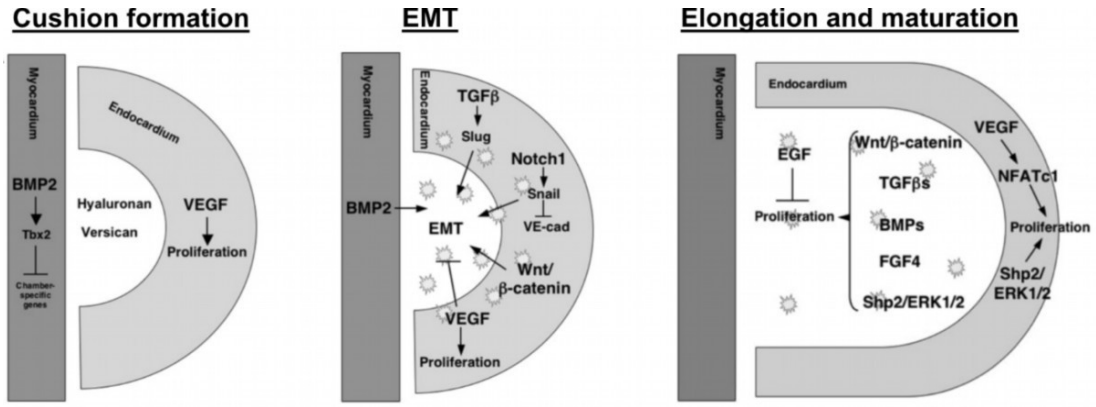

Figure 5. Valvulogenesis pathways. Representation and localization of the pathways involved in the formation of the endocardial cushion, the endothelial to mesenchymal transition and in the elongation and maturation phase of the valve during development. Modified from Combs and Yutzey.[62]

Other studies have focused on the role of mechanical forces in the event leading to valve development.[26,27,44,46,47] The mechanosensitive Transient Receptor Potential Vanilloid 4 (TRPV4) and Transient Receptor Potential Polycystin 2 (TRPP2), as well as the transcription factors Kruppel-like factor 2 (KLF2) and Early growth response 3 (EGR3) have been identified as key actors in the response to shear stress to modulate endocardial cell behavior, and thus regulate the cellular re-organization necessary for valve development.[27,46,63,64] Finally, it was also demonstrated that the composition of the ECM influence endocardial cell fate, as Hyaluronan Synthase 2 (*HAS2*) knockdown leads to embryonic lethality associated to abnormalities of the atrioventricular canal.[27,65]

The final maturation step of valve morphogenesis is not embryonic but occurs postnatally.[32,62,66,67] At birth the valve structure is still immature, and strong remodeling process takes place to reshape the valve ECM. Notably, increased collagen and elastin production after birth allows the proper delineation of the three layers visible in the adult valves.[32,62,67,68] The interstitial cells are in charge of the vast majority of the postnatal ECM remodeling. However, a few studies postulate that macrophages could participate to the process. At birth, macrophages

account for approximately 5% of aortic and mitral valve cells and seems to localize in areas with high mechanical stress: beneath the endothelium at the atrial side, and at the tip of the leaflet.[41] Macrophages of the post-natal valve leaflets are $CD206^+$ macrophages, denoting a pro-remodeling phenotype and MHC-II^+, denoting antigen-presentation phenotype. Over-time, new macrophages are recruited in the valve and the proportion of MHC-II^+ macrophages increase. Interestingly, both populations display different location with $CD206^+$ macrophages beneath the endothelium and MHC-II^+ macrophages at the free edge of the leaflet.[32,41] Despite those observation, the precise role of macrophages in the developing valve remains largely unknown.

1.5 Pathology of the mitral valve

Myxomatous mitral valve diseases are a major cause of cardiovascular morbidities and mortality worldwide. Mitral stenosis account for 12% of single valve diseases and is largely due to rheumatic heart disease and mostly prevalent in low-income countries. Prevalence of mitral stenosis in developed countries is between 0.02 – 0.2% according to the US population-based study, with good prognosis.[4,69] Mitral regurgitation (MR) is more frequent and its prevalence increase with age due to the predominance of degenerative form of MR. Accordingly, prevalence is 0.5% in patients aged 18-44 and increases to 9.3% in patients over 75-year-old.[4]

In 1980, Carpentier and colleagues established the first classification of mitral regurgitation (Figure 6).[70,71] The Carpentier classification, still used nowadays focuses on the function of the valve to classify the disease rather than lesions, that were previously used. In this functional

approach, the classification is based on the opening/closing function of the MV leaflets and three classes are described:

- Type I: normal leaflet motion, MR come from either annular dilatation or leaflet perforation
- Type II: excessive motion of the leaflet due to MV prolapse, chordae elongation or rupture, or papillary muscle rupture
- Type IIIa: restricted leaflet motion in systole and diastole, caused by rheumatic valve disease
- Type IIIb: restricted leaflet motion in systole only, caused by ventricular dilation and/or papillary muscle displacement.

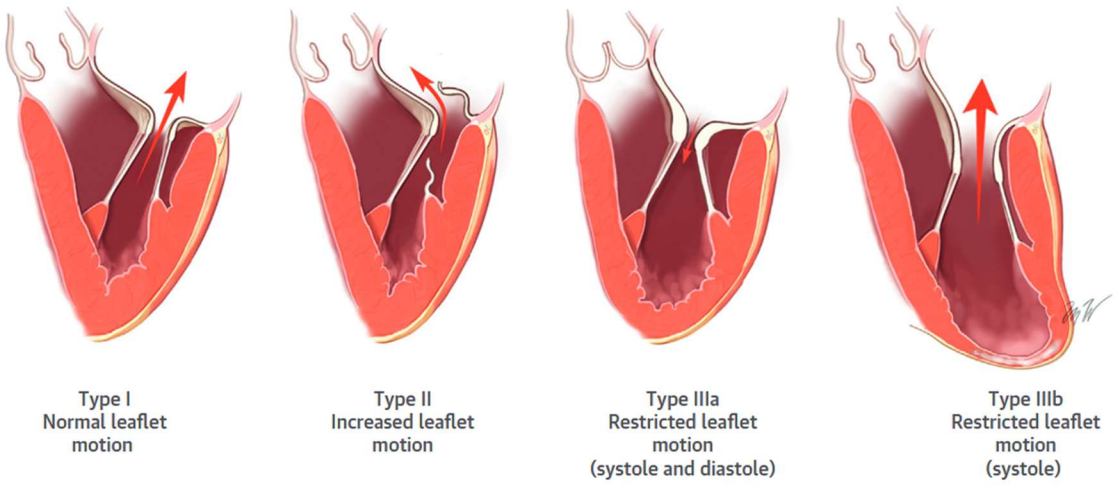

Figure 6. Carpentier classification of mitral regurgitation. Representation of the Carpentier classification of mitral regurgitation showing the different leaflet motions (red arrow). Modified from Stone et al.[72]

In line with the Carpentier classification, two forms of MR are distinguished. Primary MR results from a default in the MV apparatus, such as prolapsed leaflets, perforation or chordae rupture, whereas secondary MR is caused by left ventricle or atrium abnormalities.[2,7,72,73]

The main etiology of MR is the type II mitral valve prolapse (MVP), affecting 2 to 3% of the population.[4,74,75] To date, no pharmacological therapeutics are available to prevent or slow the disease progression. Thus, surgical valve repair or replacement represents the only option for patients with MVP-induced severe MR. Although most forms of MVP are sporadic, some syndromic forms exist, fueled by connective tissue disorders. Marfan syndrome is caused by a mutation in the gene encoding for Fibrillin-1 (*FBLN1*) with a prevalence of 1 in 5,000 individuals. More than 50% of patients with Marfan syndrome develop MVP.[76–79] Other connective tissue disorders, such as Loeys-Dietz or Ehler-Danlos syndrome, caused by mutations in TGF-β pathway genes, and collagens respectively, also induce MVP in a subset of patients (21% and 6% respectively).[80–82] Interestingly, although MVP is observed in every mutations associated to Leys-Dietz syndrome, Ehler-Danlos-associated MVP are related to mutations in the gene *COL1A2* only.

Non syndromic MVP are the most common forms and include Barlow's disease and fibroelastic deficiency.[83] Although pathophysiology is different for these two forms of MVP, both of them are classified as type II MR. Fibroelastic deficiency (FED) affects relatively old patients, over 60 years old. Patients are generally asymptomatic until chordal rupture, leading to prolapse and regurgitation. The prolapse is usually restricted to the middle scallop of the posterior leaflet (P2) at the chordae insertion where local thickening and proteoglycan accumulation is visible. It is probable that this local remodeling is responsible for chordal rupture. The rest of the leaflet is normal and thin. The mechanisms of FED are largely unknown but are most likely related to aging.[83,84] Conversely to FED, myxomatous mitral valve dystrophy (MVD), also known as Barlow's disease, affects younger patients and has a progressive development upon years.[85] It represents the first cause of MVP and is characterized by an accumulation of ECM that leads to thickening and lengthening of the entire MV leaflets, which impair the coaptation of the leaflets, resulting in mitral regurgitation.[84]

2. Myxomatous mitral valve dystrophy

2.1 Definition and etiology

The first description of what is now known as Barlow's disease is from 1887 by Cuffer and Barbillon[86], who described a syndrome of midsystolic click and systolic murmur. But it was only in 1963 that Barlow and colleagues were able to demonstrate the presence of mitral regurgitation in seven patients with midsystolic murmurs.[87] A few years later, Criley and colleagues described the mechanisms of regurgitation as an excessive leaflet motion towards the atrium in systole, and named this phenomenon mitral valve prolapse, which was soon recognized as degenerative rather than rheumatic etiology due to the myxomatous degeneration observed macroscopically on explanted valves (Figure 7).[88–90]

The clinical definition of MVP is the billowing of at least 2 mm of one or both leaflets above the mitral valve annular plane.[85,91] This definition is completed by the morphological changes of the tissue, with elongation and thickening of the MV leaflets. The three-layer organization of the leaflet is disrupted with fragmentation of elastin and collagen fibers in the atrialis and fibrosa. The spongiosa layer is largely expanded due to the accumulation of proteoglycan (Figure 7).[83]

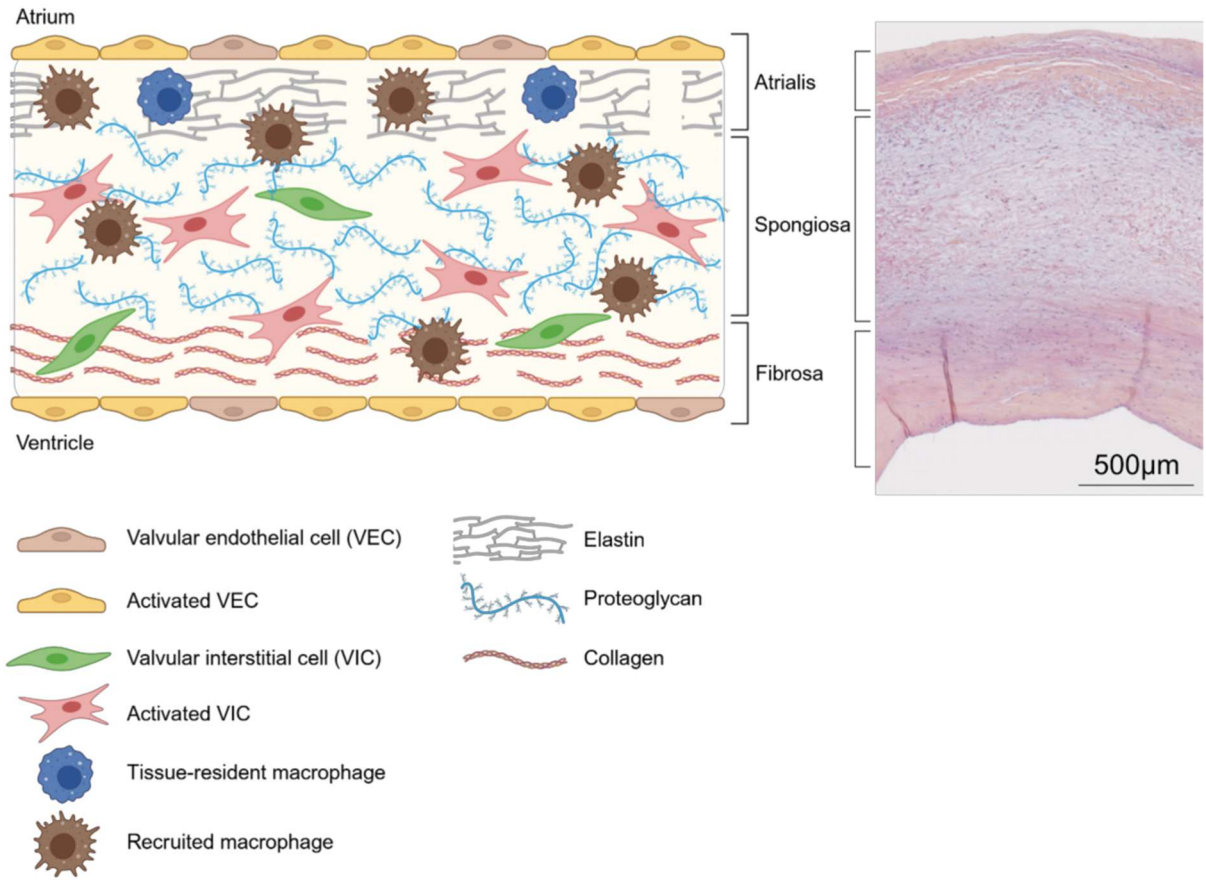

Figure 7. Myxomatous mitral valve leaflet structure. The spongiosa layer is enlarged due to proteoglycan accumulation. Elastin and collagen fibers are disrupted. VECs are activated, VICs differentiate in a myofibroblastic phenotype, and macrophages are recruited in the tissue. Created in Biorender.

2.2 Diagnostic and treatment

The development of MVD is slow and mostly asymptomatic in early phase, rendering its early detection rare. With progression to more advanced stages, symptoms such as dyspnea, dizziness, fatigue, chest pain, mid-systolic click at the apex during cardiac auscultation, and electrocardiographic abnormalities appears but are not specific to MVD. Such symptoms should guide towards further investigation to refine the diagnosis. Echocardiography is the first line imaging modality to confirm the diagnosis of MVD/MVP (Figure 8).[3,72]

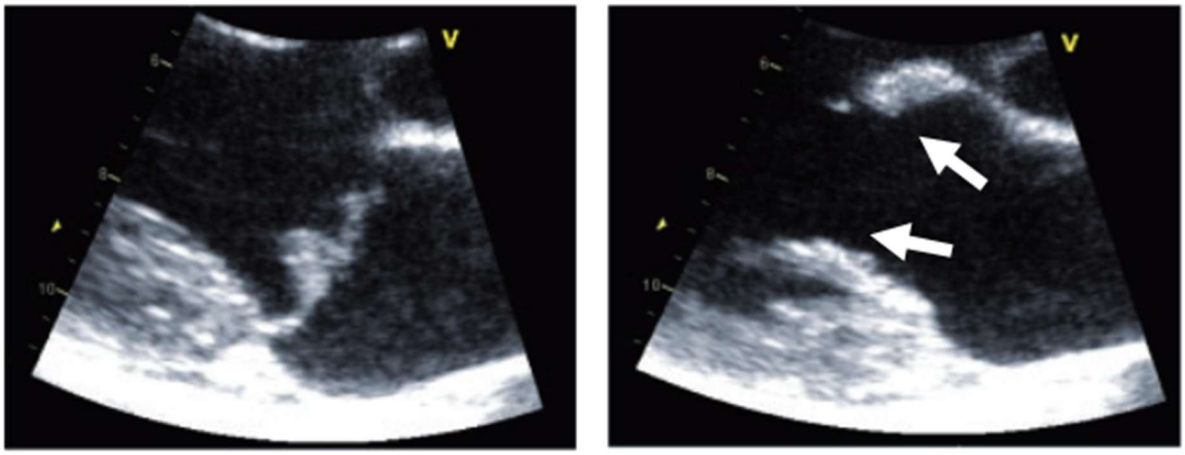

Figure 8. Echocardiography of MVD. Echocardiographic images of a MVD patient in systole (left panel) and diastole (right panel). Billowing of the leaflet is visible in systole and thickening of the leaflet is visible in diastole (white arrows). From Le tourneau *et al.*[92]

The evaluation of MVD should follow the guidelines for the management of valvular heart disease from the European Society of Cardiology and the European Association for Cardio-Thoracic Surgery (ESC/EACTS).[3] The evaluation of primary mitral regurgitation relies on 3 complementary methods:

- Trans-thoracic-echocardiography (TTE) is the gold standard method for the evaluation of valve morphology (presence of prolapse, length and thickness of the leaflets, annulus diameter; Figure 8), quantify ventricle and atrial dimensions and functions, as well as to assess the presence of regurgitation and grade its severity. Right heart catheterization can be important to verify pulmonary pressure and rule out any concomitant lung disease.

- Cardiac biomarkers, although non-specific, can be good indicators of disease severity. Notably, NT-proBNP level is related to the New-York Heart Association (NYHA) functional class of primary MR.[93]

- Cardiac magnetic resonance is an alternative to echocardiography to determine cardiac dimensions and volumes as well as regurgitation. Magnetic resonance imaging can also detect myocardial fibrosis, which has been associated with ventricular arrythmia and sudden cardiac death.[94]

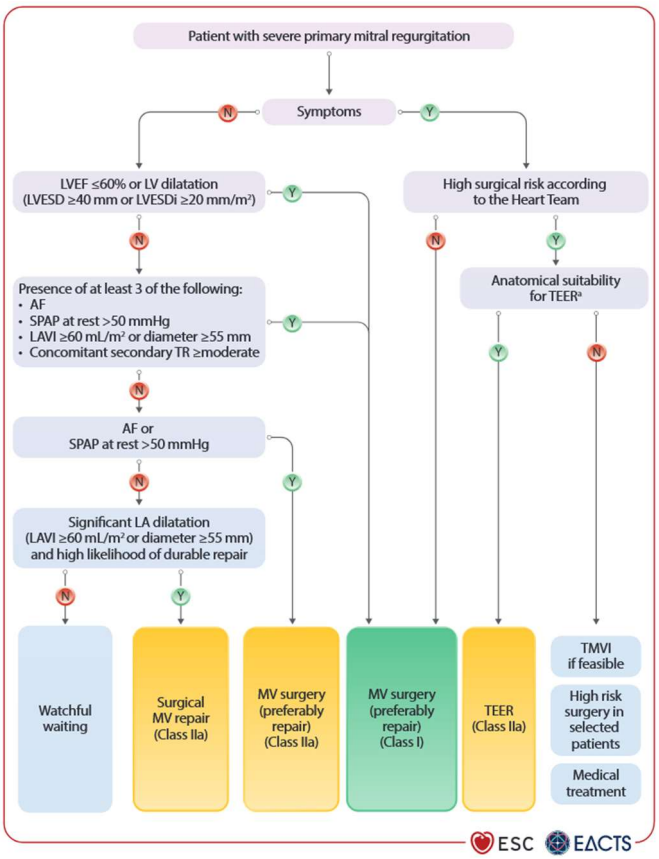

Figure 9. Decisional tree of primary mitral regurgitation management. AF: atrial fibrillation; LA: left atrial; LAVI: left atrial volume index; LV: left ventricle; LVEF: left ventricular ejection fraction; LVESD: left ventricular end-systolic diameter; LVESDi: left ventricular end-systolic diameter indexed to BSA; MV: mitral valve; SPAP: systolic pulmonary artery pressure; TEER: transcatheter edge-to-edge repair; TMVI: transcatheter mitral valve implantation; TR: tricuspid regurgitation. From Praz F *et al.*[3]

Due to rather low effect and poor long-term outcome, medical therapy is only recommended for patients at prohibitive surgical risk. For other patients with severe MR, the type of recommended surgery recommended is based on the functionality of the leaflet and the severity of MR as detailed in Figure 9.[3,7] The goal of MV repair surgery is to correct the coaptation default to reduce the severity of MR. Depending on the anatomy of the valve, it can be whether

by reducing the annulus diameter, reducing the chordae length, or reducing the opening orifice. Recently, new techniques have emerged bypassing the need of open-heart surgery like the transcatheter edge-to-edge repair (TEER) using the MitraClip (Abbott Laboratories) or PASCAL (Edwards) technology that allows the reduction of MR by placing a clip between the free edge of both leaflets, thereby reducing the orifice during systole and limiting the extent of regurgitation.[95–97] When repair is not possible, the last option is the replacement of the valve. It can be done surgically or by TMVR (Transcatheter Mitral Valve Replacement).[98]

2.3 Genetics of MVD

Myxomatous mitral valve dystrophy was long thought to be a degenerative disease due to aging.[84] However, the observation of familial forms of MVD, lead the researchers to explore genetic inheritance of MVD.[99,100] Thus, in 1998, *Kyndt et al.* successfully linked MVD to chromosome Xq28 in a large French family of MVD.[101] Later in 2007, the same authors refined their analysis and identified a P637Q mutation in the gene encoding the actin-binding protein Filamin A (*FLNA*), making it the first causal gene associated to MVD.[102] The mutation is located in the fourth repeat consensus sequence, close to the actin binding domain. Four other mutations were later found in non-related families: G288R, V711D, H743P and a 182 amino acid deletion, all of which are located within the same N-terminal region of the *FLNA* gene.[102–104] A genotype-phenotype and outcome study was conducted by *Le Tourneau et al.* in 2017 and described classical MVD phenotype with prolapse, elongation and thickening of the leaflets. It also revealed specific features, including restricted leaflet motion in diastole. Of note, the mutated patients present abnormalities as early as childhood, suggesting developmental disease and evolution of the MV remodeling from prodromal form to MVD with functional impact.[92] Clinical identification of familial forms and genetic screening later lead to the identification of

mutations in other genes.[105,106] *Durst et al*. described mutations in Dachsous 1 (*DCHS1*) gene coding for a cadherin superfamily member, and confirmed the role of *DCHS1* mutation in MVD using animal and cellular models.[105,107] Another pedigree lead to the identification of a missense mutation in the primary cilia gene *DZIP1*, and a mouse model validated the pathogenicity of the variant.[106]

Genetic screening of familial forms of MVD allowed for the detection of rare variants with a strong effect on the development of the disease, but were restricted to the limited number of familial cases. Genome Wide Association Study, or GWAS, are genetic studies based on very large cohort of patients and controls, to identify common variants in the population that are more prominent in the diseased group. The first MVP-GWAS was performed by *Dina et al*. in 2015, and included 1412 cases and 2439 controls.[108] Six loci (*TNS1*, *LMCD1*, *SIPA1L1*, *SMG6*, *SETD4*, *PITPNB*) were associated to MVP and replicated in a follow-up cohort of 1422 cases and 6779 controls. Downstream analysis used knockdown of target genes ortholog in Zebrafish, and showed atrioventricular valve regurgitation for *LMCD1* and *TNS1*.[108]

A meta-analysis of six GWAS studies including 4884 cases and 434649 controls was conducted in 2022 by Roselli *et al.* (Figure 10). This meta-analysis increased the number of loci associated with MVP up to 16 including previously described *LMCD1 TNS1*, and *SMG6*.[109] Integration with epigenetics, transcriptional and proteomic data identified candidate genes at these loci, including *LMCD1*, *SPTBN1*, *LTBP2*, *TGFB2*, *NMB* and *ALPK3* (Figure 10). This study strongly supports the hypothesis of TGF-β contribution to MVP as two candidate genes belong to the TGFβ superfamily. *TGFB2* encoding for the TGF-β2 protein, and Latent TGF-β Binding Protein 2 (*LTBP2*), encoding for an extracellular matrix protein that regulates TGFβ signaling. Interestingly, a recent publication from 2025 identified a *LTBP2* mutation in a large family with MVP, and confirmed the causality of the mutation in a mice model carrying the mutation.[111]

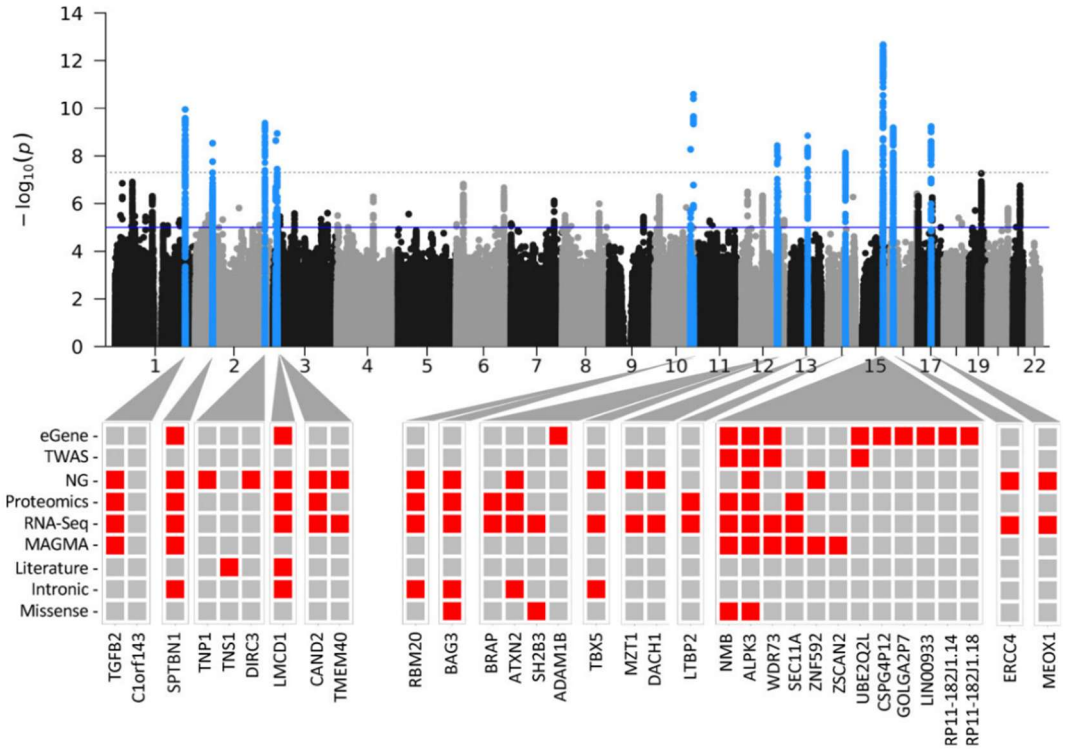

Figure 10. Manhattan plot of the GWAS meta-analysis. The 14 loci with a genome-wide significance are in blue. The significance threshold is represented by the grey dotted line. Below are the candidate genes for each locus and the different lines of evidence for the candidate gene. Red square indicate that the evidence is present. TWAS: transcriptome-wide association study, NG: nearest gene, MAGMA: multi-marker analysis of genomic annotation. From Roselli et al.[109]

2.4 Pathophysiological mechanisms

Over the last decades, several pathophysiological mechanisms have been studied and proposed as a cause of myxomatous degeneration. It appears that the development of MVD is a complex and multifactorial process, with interconnected pathways.[112,113]

Those mechanisms have been described in 2024 in a short review in the French journal *Archive des maladies du Coeur et des vaisseaux Pratique.*[112]

2.4.1 Transforming Growth Factor β pathway

The TGF-β superfamily is a highly conserved group of proteins known to regulate a wide range of cellular processes, including cell differentiation, proliferation, migration, survival and apoptosis, in a variety of cell types. The TGF-β superfamily comprises 37 ligands and 12 different receptors (Figure 11).[114] Within the canonical pathway, two branches are described depending on the signaling effectors. The TGF-β-Activin-Nodal branch signal through the phosphorylation of Small Mother Against Decapentaplegic 2/3 (Smad2/3), and the BMP-GDF branch signal through the phosphorylation of Smad1/5/8. Two types of receptors co-exist: type I and type II receptors. The ligand fixation occurs on a homodimer of type II receptors, and induce the recruitment of a type I receptors homodimer. Once the heterotetramer is formed, autophosphorylation of different residues of the receptors occurs and leads to the phosphorylation, of Smad2/3 or Smad1/5/8. Smad4 is then recruited as a co-Smad, and the Smad complex is translocated to the nucleus to regulate gene expression (Figure 11).[114]

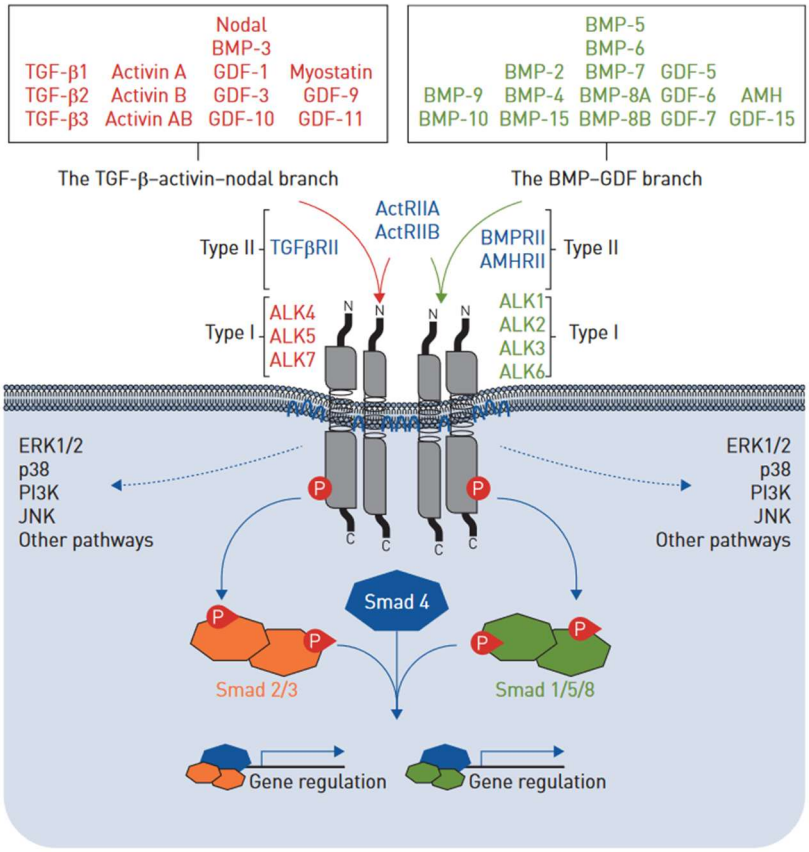

Figure 11. Signaling pathway of the TGF-β superfamily. The TGF-β superfamily is divided in two branches: TGF-β/Activin/nodal on the left and in red, and BMP/GDF on the right and in green. The ligands are in the square box on top. Binding to type I and type II receptors triggers either Smad2/3 or Smad1/5/8 phosphorylation. The co-Smad Smad4 is recruited for the translocation to the nucleus where the complex will regulate gene expression. Modified from Guignabert and Humbert.[114]

In Marfan syndrome, in which 50% of patients develop MVD, the fibrillin-1 deficiency causes an upregulation of TGF-β activity, and the inhibition of the pathway in murine models of Marfan syndrome prevent the development of MVD.[115] Moreover, in 2005, Loeys and colleagues reported families carrying mutations in the genes coding for TGF-β receptors *TGFBR1* and *TGFBR2*. The phenotype of these patient is close to Marfan syndrome, and some display mitral valve prolapse.[77,80] More recently, in 2025, Shpitzen *et al*. described a mutation in the Latent TGF-β Binding Protein 2 (*LTBP2*) gene in a family with MVP.[111] Interestingly, both *TGFBR2* and *LTBP2* loci have been identified as candidate genes associated to MVP in the latest GWAS for MVP by Roselli *et al*.[109]

In vitro experiments have further shown that primary culture of VICs from MVD patients have increased expression of TGF-β1 associated with increased level of phosphorylated-Smad2/3. Oxidative stress in the MVD micro-environment could, at least in part, explain this increased TGF-β signaling.[116] Another study by Blomme *et al.* showed that a cyclic stretch imposed to human VICs induced an early and transient over-expression of TGF-β2.[25]

2.4.2 Serotonin

Serotonin, also known as 5-Hydroxytryptamine (5-HT), is a neurotransmitter derived from tryptophane under the action of tryptophane hydroxylase 1 (TPH1), and synthetized primarily by the enterochromaffin cells of the intestinal mucosa (95% of total 5-HT), and in less part in the raphe nuclei of the brain (5% of total 5-HT).[117,118] Serotonin plays multiple physiological roles in brain functions such as behavior, mood, or memory, but also in gastrointestinal function, such as food intake or intestinal motility.[119] After liberation in the bloodstream, circulating serotonin is rapidly internalized and stored in dense granules of blood platelets through the serotonin transporter SERT. Upon platelets activation, serotonin is released through degranulation and can act locally. Serotonin signaling is mediated by a variety of 5-HT receptors. Seven families of receptors are described (5-HT_1R to 5-HT_7R), and several subtypes can be distinguished inside families. In total, 20 subtypes of receptors have been identified, all of them are G protein coupled receptors (GPCR) with the exception of the 5-HT_3R which is a ion-gated channel.[120]

The first evidence suggesting a role for 5-HT in the development of MVD comes from the observation in the 1980s that patients with a carcinoid tumor, a type of tumor affecting the enterochromaffin cells of the gut and releasing high levels of serotonin in the circulation, often presented cardiac symptoms.[121] Those symptoms were referred as carcinoid heart disease, and

includes valves thickening.[122,123] The second evidence came in the 1990's, when the role of the anorexigen treatments fenfluramine, dexfenfluramine and benfluorex, were recognized as causative of pulmonary hypertension and valvulopathy because of their action on the serotoninergic system, leading to their suspension.[124–126] Several studies were then conducted to understand how serotonin participates to the development of valve diseases. It was shown that the effect of serotonergic treatment on valve dystrophy were mediated by the 5-HT_{2B} receptor in VIC, that triggers the MAP kinase pathway via Erk1/2 activation.[127–130] Other more recent studies point out the fact that an increase in serotonin or a decrease of SERT activity lead to a myxomatous degeneration of the mitral valve (Figure 12).[126,131–133]

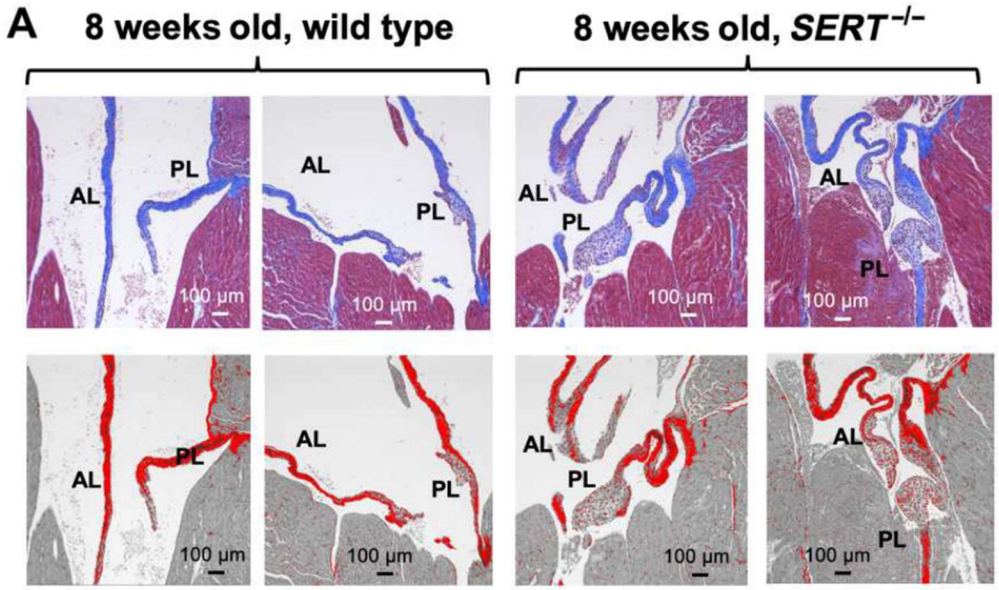

Figure 12. Serotonin transporter deficiency induce myxomatous mitral valve. Histology of SERT knock-out mice showing myxomatous remodeling of the mitral valve leaflet at 8 weeks. AL: anterior leaflet, PL: posterior leaflet. From Castillero *et al.*[133]

2.4.3 Primary cilia

Primary cilia are extrusion of the plasma membrane present in most mammalian cell types, composed of an axoneme of nine microtubules doublets that extend from an intracellular basal body (Figure 13). Primary cilia differ from motile cilia by the lack of two dynein-associated microtubules that confers the ciliary motility.[134] Along the axoneme is the intraflagellar transport system (IFT) that allows the anterograde transport of proteins towards the tip or anterograde transport to the basal body of the cilia. Thus, primary cilia serve as hub for a wide variety of receptors, making the primary cilia a mechanosensor and chemosensor of the cellular microenvironment (Figure 13).[135] The first descriptions of primary cilia are from the 1960's, and they were named in 1968 by Sorokin.[136] Since then, many diseases related to cilia gene mutations have been identified, and are now referred as ciliopathies.[106,137–140] Indeed in a 2023 review, Morleo *et al.* performed an Online Mendelian Inheritance in Man (OMIM) database search using the term 'ciliopathies', and identified 147 transcripts, of which 127 were associated to a specific clinical phenotype.[138] During embryonic development, primary cilia are only sparsely present at the surface of endocardial cells, but present on the majority of interstitial cells. Interestingly, cilia expression correlated with the nature of the ECM, with most of the cells expressing cilia in a proteoglycan-rich matrix at early developmental stage, to only few ciliated cells in postnatal collagen-enriched matrix.[106]

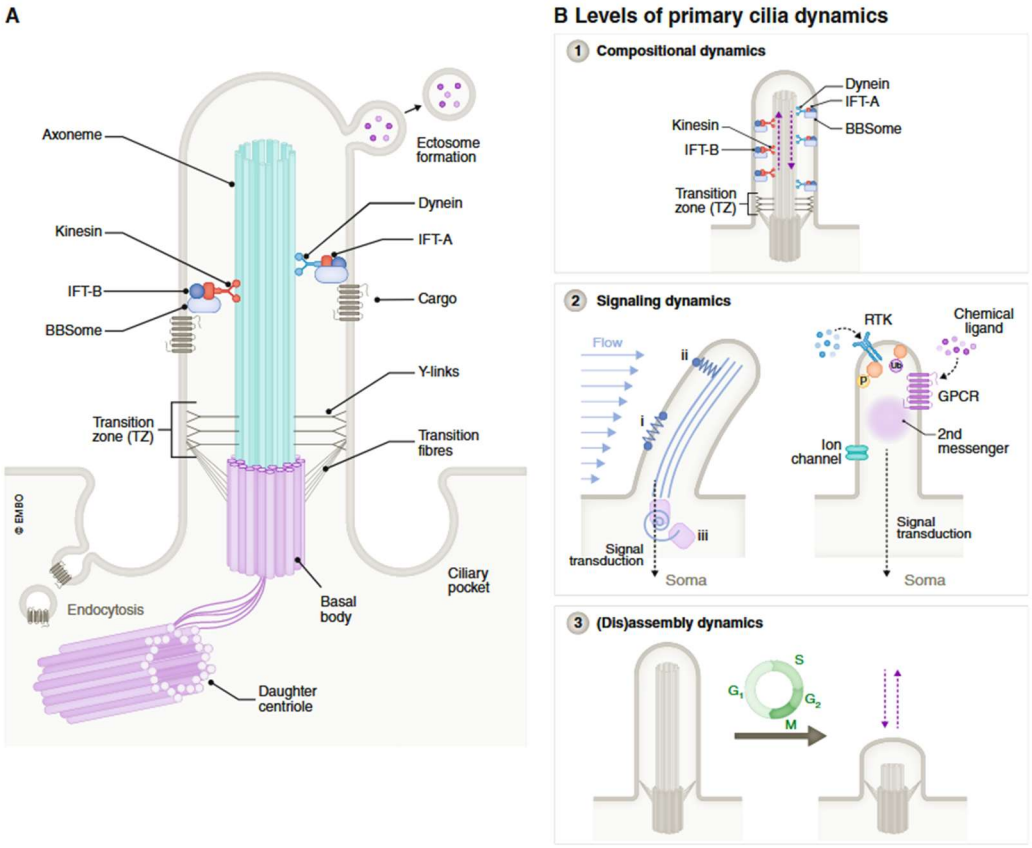

Figure 13. Primary cilia structure. A: Structure of the primary cilia showing the basal body and the axoneme along which the intraflagellar transport (IFT) machinery transport proteins anterogradely in a kinesin-dependent manner, and retrogradely in a dynein-dependent manner. B: Dynamics of primary cilia is regulated at three levels: the composition of the cilia (1), the signaling dynamics refers to the molecular adaptation to the signals perceived by the cilia (2), and the assembly/disassembly of the cilia which is coupled to the cell cycle. From Gopalakrishnan et al.[135]

In 2005, Nesta *et al*. published the discovery of a new locus on chromosome 13 associated with MVP.[141] It is only in 2019 that this locus was linked to DAZ Interacting Zinc Finger Protein 1 (*DZIP1*), a gene known to regulate ciliogenesis and cilia signaling.[106,142] In their study, the authors show that the introduction of the mutation in a mice model result in myxomatous mitral valve dystrophy. They further demonstrate that cilia dysfunction is causal, as deletion of the ITF88 gene, a specific cilia gene, also leads to myxomatous mitral valve disease.[106]

2.4.4 Endothelial to mesenchymal transition

Endothelial to mesenchymal transition is a developmental process during which endothelial cells (ECs) undergo a phenotypic switch towards mesenchymal type.[143–145] Importantly, in the cardiac valves, EMT is the process that gives rise to the valvular interstitial cell population as described in 1.4. It has been hypothesized that under pathological conditions, EMT could be reactivated in adult mitral valve endothelial cells.[146] The mechanisms behind EMT are not completely understood but it is known that it can be triggered by mechanical forces, as well as several signaling pathways and growth factors such as TGF-β, WNT, NOTCH, Yes-associated protein 1 (YAP1), IL1-β, or Fibroblast growth factor 2 (FGF2) as represented in Figure 14.[143,145,147–149] Those various signaling pathways activate a small set of transcription factors (TFs) that regulates EMT, and that include: Snail1, Snail2, Zinc finger E-box binding homeobox 1 (Zeb1), Zeb2, Twist1 and Twist2.[149] Those TFs collectively repress expression of endothelial genes, while activating mesenchymal gene expression (Figure 14).[149]

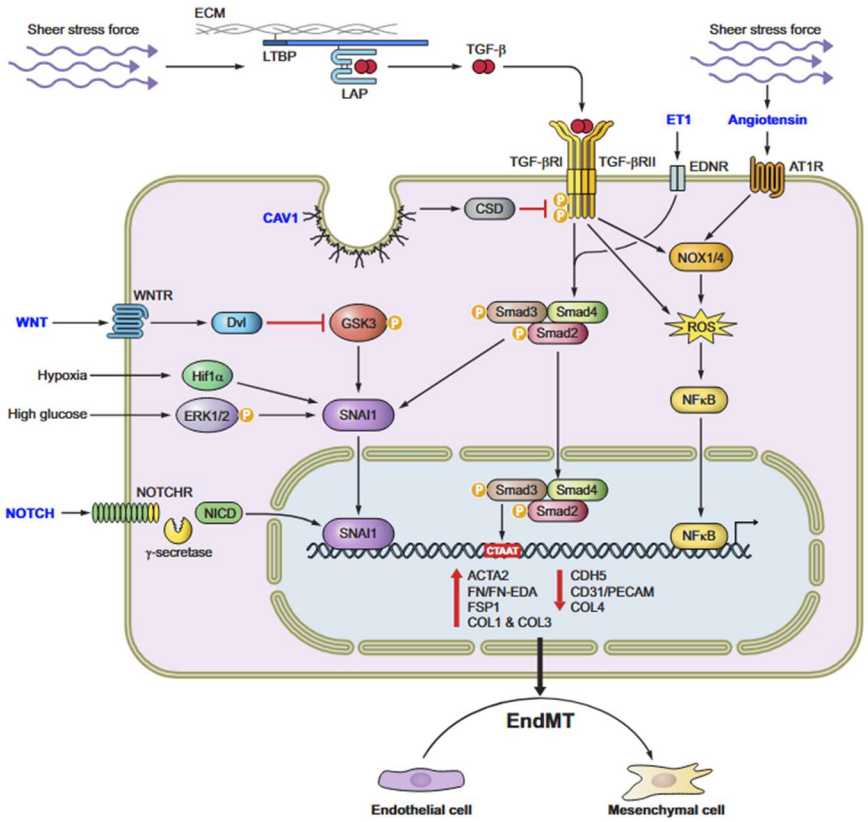

Figure 14. EMT signaling pathway. Schematic representation of the pathways involved in EMT. From Piera-Velazquez *et al.*[145]

The ability of VECs to undergo EMT has been previously described in aortic and pulmonary valves both *in vitro* and *in vivo*.[150,151] In 2009, Dal-Bianco *et al*. performed papillary muscle shortening surgery in adult sheep to mimic tethering of the mitral valve and induce secondary MR.[146] They showed that after 60 days, stretched MV were 2.8 times thicker, mostly due to spongiosa thickening. They also described that stretched MV had significantly increased proportion of $CD31^+$ endothelial cells positive for α-smooth-muscle-actin (α-SMA), a mesenchymal marker that could suggest EMT. Finally, they showed that TGF-β could induce α-SMA expression *in vitro* in primary culture of MV-ECs.[146] The ability of mitral valvular ECs to undergo EMT *in vitro* has later been confirmed in other studies.[152–155] However, these studies relied on α-SMA expression, which could be triggered by myofibroblastic differentiation rather than actual endothelial-mesenchymal transition. Moreover, *in vivo* re-activation of EMT in adult mitral valve has never been reported. A study in the context of Marfan-related MVD used endothelial lineage tracing (Tie2-Cre and Cdh5-$CreER^{T2}$ mice model), and demonstrated the absence of endothelial-derived mesenchymal cells in both healthy and pathological valves.[156]

2.4.5 Mechanotransduction

The MV opens and closes approximately 3 billion times in a lifetime, while facing high mechanical forces.[26,85] On the atrial side, the blood flow during ventricular filling in diastole generates shear stress and tension. During systole, the closure of the leaflets coupled to the contraction of the ventricle generates compression forces and turbulent flows against the ventricular face of the leaflets.[157] Therefore, a dysregulation of the mechanotransduction pathways is thought to be involved in the pathophysiology of MVD.

During valvulogenesis mechanical forces participate to shape the MV structure.[26,27,47] The unique hemodynamic of the developing heart starts with the first contraction at E8.5 in mice

and 22 days in Humans. All along heart development, the hemodynamic environment is spatially and temporally modified, inducing distinct transcriptional program that contributes to valvulogenesis.[26,46,47,63] Particularly, the mechanosensitive transcription factor Kruppel-like factor 2 (KLF2) has been shown to be important during valvulogenesis as it regulates WNT-9a expression in endocardial cells, and fibronectin deposition in the atrioventricular cushion.[46,63,158–160] In a recent study from 2022, *Pham et al.* looked into the elongation phase of semilunar valves, and found that endocardial cells respond differently depending on their location due to the different mechanical stress imposed.[47] As such, endocardial cells from the vascular side endure oscillatory shear stress that induces canonical WNT/β-catenin signaling which activate BMP signaling pathway with increased SMAD1/5 phosphorylation, leading to endocardial proliferation. Conversely, endocardial cells of the ventricular side of the leaflet endure laminar shear stress that induce NOTCH signaling which inhibits WNT pathway, thereby limiting proliferation of endocardial cells.[47]

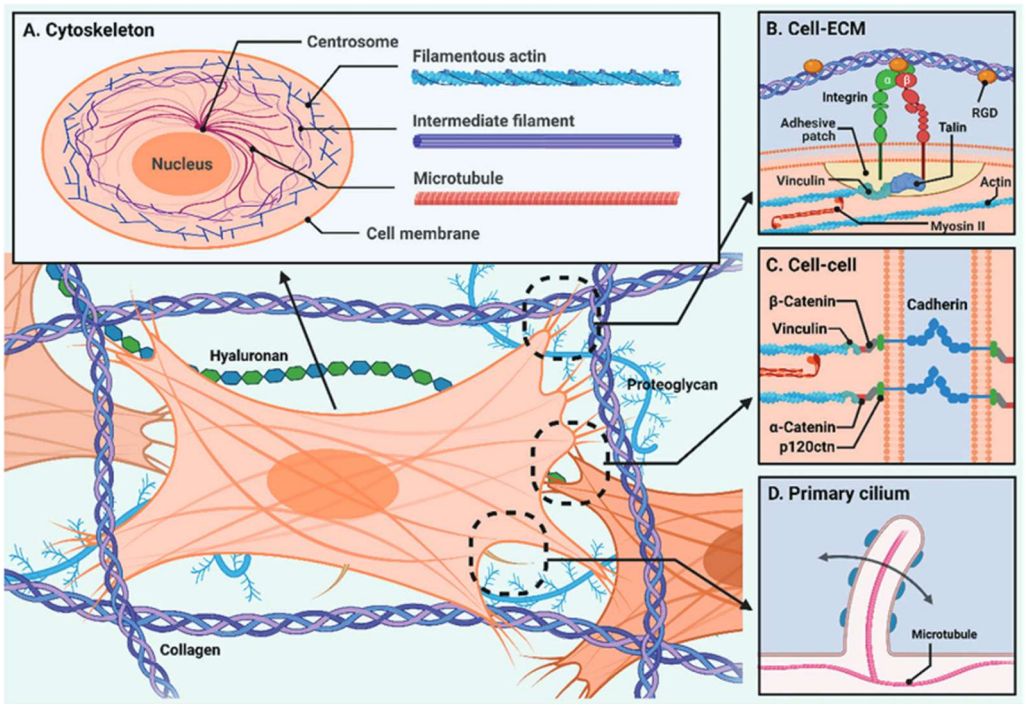

Figure 15. Cellular mechanosensing. A. The cell cytoskeleton plays a key role in the mechanosensory machinery. B. Transmembrane proteins like integrins transduce external stimuli to the actin cytoskeleton via adaptor proteins. C. Intercellular adhesion can also transmit mechanical stimuli to the cytoskeleton. D. Primary cilia are mechanosensitive element via their unique structure, and via the numerous receptors expressed at their surface. From Shou *et al.*[161]

The sensing of mechanical forces is permitted by a range of specialized mechanosensitive receptors expressed at the surface of the cell, such as G protein-coupled receptors (GPCR), ions channels and integrins (Figure 15). Integrins are known to be involved in many cellular functions like adhesion, migration, angiogenesis, permeability, signaling transduction, cytoskeletal organization, and are thus crucial to maintain tissue homeostasis.[161,162] They are transmembrane adhesion proteins that connect the ECM to the actin cytoskeleton by specific actin-binding proteins (Talin, Filamin, α-Actinin, Vinculin), making integrins the primary sensor and transducer of external mechanical stimuli to the cell (Figure 15). In addition, integrins can also react to the intrinsic properties of the ECM, like its composition, rigidity or elasticity.[163,164] Integrins are heterodimers of 18 α and 8 β subunits that can assemble into 24 subtypes.[165,166] Each subunits has a specificity for a ligand, and the signaling pathway induced by the binding differ depending on the subunits engaged and the ECM ligand.[164–168] The mechanisms by which integrins bidirectionally sense the mechanical stimuli are well described. The inside-out signaling is induce by traction forces of the cell cytoskeleton that induces binding of intracellular actin-binding proteins to the cytoplasmic tail of the integrin triggering interaction with the extracellular ligand. On the other hand, the outside-in signaling occurs when an external force is applied to the ECM leading to activation of the integrin and binding of the ECM ligand which leads to intracellular signaling.[166,169]

2.4.6 Crosstalk between pathways

It is important to mention that all the previous pathways described are not independent of each other, and that a dysregulation of one of them can affect the others through the many crosstalk between these pathways (Figure 16). For example, it was shown that the activation of the serotonin receptor 5-HT_{2A}R causes an increase of TGF-β1, and that both serotonin and TGF-

β1 induced collagen and proteoglycan synthesis *in vitro* with sheep VICs.[170] Another study identified that antagonism of the 5-HT_{2B}R could prevent the non-canonical TGF-β1 signaling through P38-MAPK in porcine VICs, preventing their differentiation *in vitro*.[171] The mechanical stress, which can be sensed via primary cilia or integrins, was shown to induce differentiation of VICs through activation of TGF-β pathway in the model of leaflet tethering in sheep.[146]

Additionally, the familial and population-based studies identified associated genes that are all related in some ways to the response to mechanical stress. Among them, *TNS1* codes for the protein Tensin-1, localized at focal adhesion and linking the actin cytoskeleton to integrins cytoplasmic tails. *DZIP1* mutation induce a shortening of primary cilia that could impair their mechano-sensory functions. *LMCD1* is a regulator of GATA6, a key transcription factor in cardiac development, and LMCD1 is thought to be involved in the cardiac remodeling caused by hypertensive stress.[172] Finally, *FLNA* is an actin-binding protein involved in the transduction of external stimuli to the actin cytoskeleton.

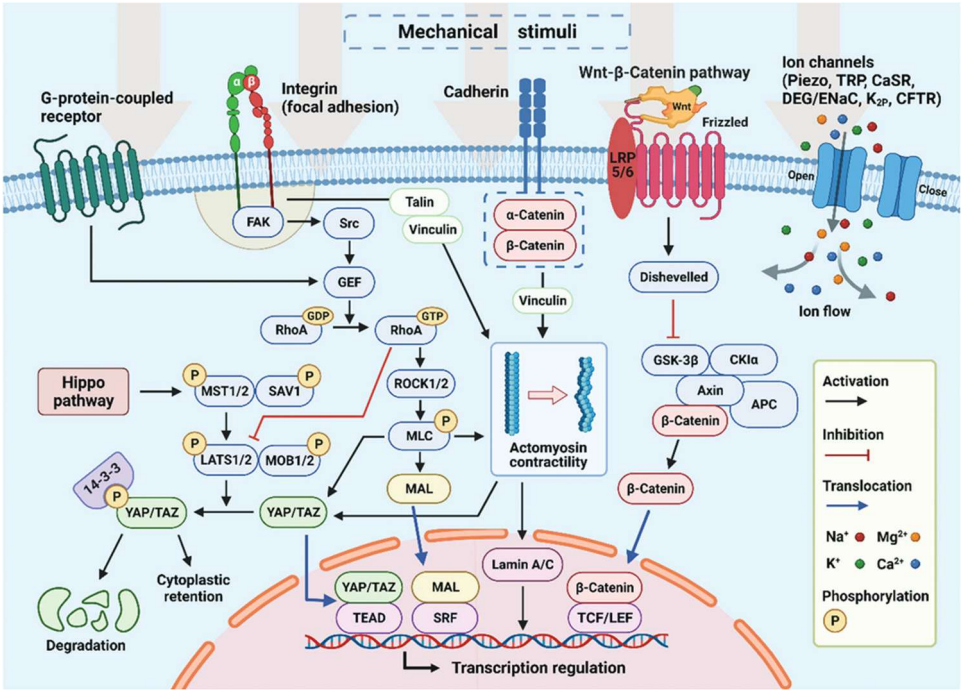

Figure 16. Mechanotransduction pathways. Mechanical stimuli are sensed by various transmembrane receptors. Those receptors can transduce the signal via several pathways like WNT/β-catenin, or RhoA-Rho kinase. From Shou *et al.*[161]

2.5 Filamin A

Filamin proteins were discovered and described for the first time in 1975 in chicken gizzard.[173] At the same time, a similar protein was described in rabbit alveolar macrophages.[174,175] It was later identified that among the three filamin isoforms (Filamin A, B and C), filamin A is the most abundant in adult and coded by the *FLNA* gene located on the X chromosome.[176–178] Filamin A is a ubiquitously expressed actin-binding protein that promotes actin filament reticulation and connect the actin cytoskeleton to the cell membrane by binding to transmembrane receptors or ion channels.[178–182] The structure of Filamin A consist of a N-terminal actin binding domain followed by 24 immunoglobulin-like repeated domains, the 24th domain being involved in the dimerization of Filamin A (Figure 17).[183] As an actin-binding protein, Filamin A serve as a scaffold for many other proteins, including membrane receptors, integrins, ion channels, enzymes, GTPase, or transcription factors, and can modulate the activity of these partners. This place Filamin A as a central actor of many cellular functions such as cellular migration, proliferation, adhesion, filopodia formation, cell spreading, cell-ECM crosstalk, and mechanosensing.[177,178,184–190] Notably, it has been well described that the Rho-GTPase activating protein FilGAP can bind Filamin A specifically to site of membrane protrusion to antagonize Rac activity and regulate cell spreading via a RhoA-dependent mechanism.[190,191] Moreover, FilGAP binding to Filamin A was demonstrated to be mechanosensitive in a *in vitro* network of actin. Deformation of the actin network increased β-integrin binding to Filamin A and induced dissociation of FilGAP from Filamin A.[192]

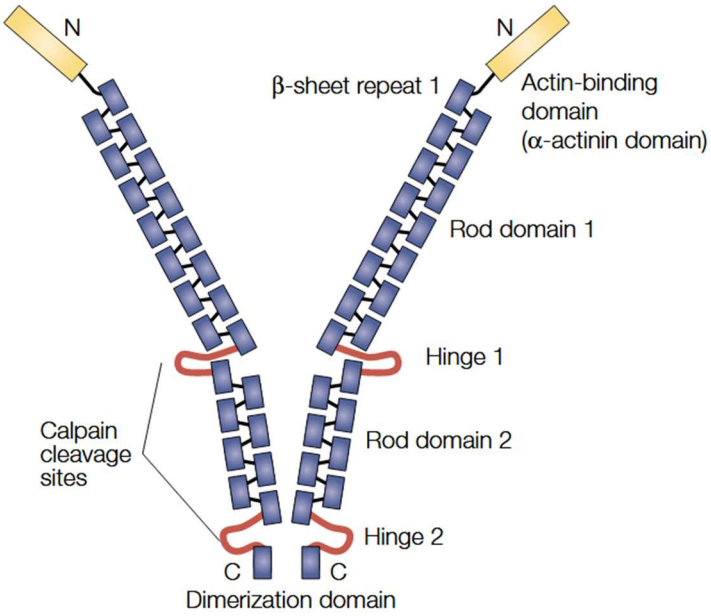

Figure 17. Filamin A structure. The actin-binding domain is located at the N-terminal region (yellow box) and is followed by 24 repeats of immunoglobulin-like domain with 2 calpain cleavage sites. The dimerization domain is at the C-terminal region. Modified from Stossel et al.[178]

Mutations in the Filamin A genes has been associated to several pathologic phenotype that include mainly periventricular nodular heterotopia, but also skeletal alterations, otopalatodigital syndrome, Melnick-Needles syndrome, congenital heart disease, pulmonary hypertension, interstitial lung disease, gastrointestinal disorders, dilation of the thoracic aorta, thrombocytopenia, and, as developed in the section 2.3 'Genetics of MVD', valvular dystrophy with the identification of the first MVD causal mutation.[102,193–197]

Four mutations have been associated with to induce MVD: P637Q, G288R, V711D and H743P. They are all located in the N-term region of the protein, but little is known on how these mutations affects Filamin A function or its partners. Our group previously demonstrated that the mutations P637Q, G288R and H743P destroyed the folding of the 5th domain, affected the ability to transmit cellular forces, and abolished the interaction between Filamin A and protein tyrosine phosphatase non-receptor type 12 (PTPN12), a regulator of the response to mechanical stress and cytoskeleton dynamic.[188,198,199] Specifically, mutations in Filamin A impaired the

activation status of the focal adhesion kinase Src and the RhoA specific activating protein p190RhoGAP, two PTPN12 substrates.[188] This could partly explain why the *FLNA*-mutated cells have a failed response to mechanical stress, leading to their activation and the acquisition of a myofibroblastic phenotype.[188]

3. Models of MVD

Over the years, several models of myxomatous remodeling of the MV have been developed to study the involved signaling pathways, relying on three different species: dog, rodent, and zebrafish (Figure 18).[113] Each of these models presents advantages and limits.

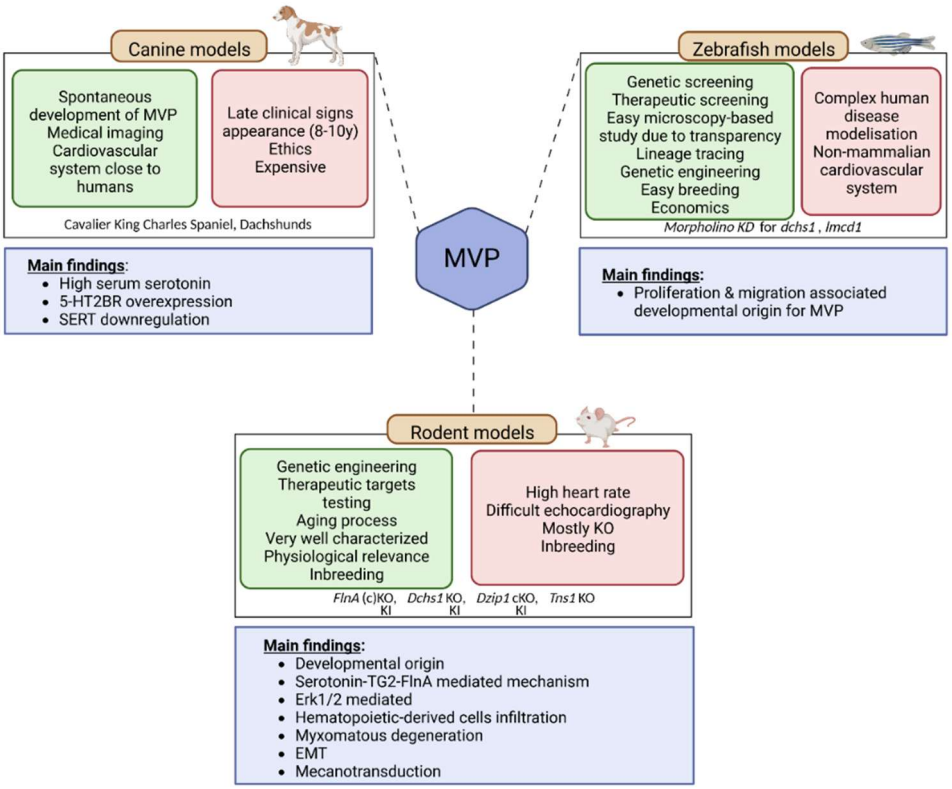

Figure 18. Animal models of MVP. 3 categories of animals are available for modeling MVP: canine, zebrafish and rodent. Advantages and limits are presented in the green and red squares respectively. From Delwarde *et al.*[113]

3.1 Canine spontaneous MVD

Myxomatous mitral degeneration is spontaneous in some small-breed dogs like Cavalier King Charles Spaniel and Dachshunds. The clinical evaluation of such dogs show that the pathology recapitulates the MVD phenotype observed in Human Barlow disease with proteoglycan accumulation and disruption of the layered architecture of the leaflets.[200] It was

shown that dogs with spontaneous MVD has elevated plasmatic serotonin level, reduced serotonin clearance, and that this was associated with TGF-β mediated activation of VICs.[201] The spontaneity of the disease in dogs has the advantage of better representing the human pathology. This model is suitable for pre-clinical studies or to identify biomarkers.[130,201–203] However, there are some limits regarding the access of samples that can be collected (late appearance of MVD, mostly limited to veterinary research center), as well as regarding ethical considerations and costs.

3.2 Zebrafish

If dog is the largest model for MVD, on the other hand, zebrafish is the smallest. Nonetheless, zebrafish are "easy-to-use" models for translational or fundamental researchers. Moreover, zebrafish can be genetically manipulated to study the role of specific genes in various processes. Notably, zebrafish have been extensively used to study valve developmental processes, and the impact of mechanical forces. It was shown in Zebrafish, that blood flow activates the Klf2-Wnt signaling pathway which participate to the regulation of heart development.[26,27,46,63,158,160] Zebrafish was also the model of choice to validate candidate loci identified in genetic studies, and zebrafish confirmed the causal role of *TNS1*, *LMCD1*, and *DCHS1* to MVD.[105,108]

3.3 Rodent models

Rodents are the most used animal to model cardiovascular diseases, including MVD.

3.3.1 Syndromic models

Notably, a mice model of Marfan syndrome has been generated by introducing the Fibrillin-1 ($Fbn1^{C1041G/+}$) mutation discovered in Marfan patients. Though only half of Marfan patients develop MVD, all homozygous $Fbn1^{C1041G/+}$ mice present myxomatous degeneration of the MV by the age of 2 month.[115] This model has been used to characterize the cellular population of the mitral valve during development and disease, but also to demonstrate macrophage recruitment during myxomatous remodeling.[32,41,204] Moreover, Xu and Yutzey established that therapeutic blockade of C-C motif chemokine receptor 2 (CCR2) was sufficient to prevent macrophage recruitment and development of myxomatous mitral valve disease.[205]

3.3.2 Non-syndromic model

Following the discovery of mutations associated to MVD, new mice models have emerged. Notably, the Tensin-1 knock-out mice (*Tns1*-KO) has been developed to validate the association of the candidate gene identified by GWAS, and deletion of Tensin-1 effectively induced a myxomatous phenotype of the MV.[108] Among the other mutations involved in MVD, *Dchs1* and *Dzip1* were both studied through knock-out and/or knock-in studies. *Dchs1*-KO mice exhibit prolapse and thickening of the MV leaflets.[105] As for *Dzip1*, both the full knock-out and the mutated form induce myxomatous degeneration of the MV associated to increased prolapse. The authors also showed that *Dzip1* mutation induced a shortening of primary cilia length in the MV.[106]

Following the identification of the first causal mutation in *FLNA* gene, genetic engineered rodent models were studied. The *Flna*-null mice is embryonically lethal at day E14.5 with vascular defect and hemorrhage, abnormal septation of the outflow tract, defective vascular

endothelial cells junctions, and mitral valve dysplasia.[187,193] These observation demonstrated a central role of Filamin-A in developmental process, not only restricted to valvulogenesis. To better understand the role of Filamin-A in mitral valve, an original approach was developed by *Sauls et al.* in 2012.[206] Their strategy was to breed Filamin-A floxed mice with Tie2-Cre mice to generate conditional endothelial knockout of Filamin-A (*Flna*-cKO). By doing so, they take advantage of the fact that VICs derive from endothelial cells through EMT during embryogenesis. This results in valvular knockout of Filamin-A, viable in mice in contrast to the full knockout.[206] The cKO mice exhibit a significant MV leaflet thickening with increased collagen and hyaluronan deposition at the age of 2 month. Surprisingly, the analysis of embryonic stage revealed that valvular enlargement was detectable at E17.5 but was not yet associated to increased ECM deposition, suggesting that matrix production didn't contribute to the embryonic phenotype. The authors examined the interaction of filamin A with serotonin and demonstrate that during embryonic development only, the interaction of filamin A with serotonin and transglutaminase 2 (TG2) was important for the formation of stress fibers. Thus, the knock-out of filamin A disrupted this interaction and VICs lost their capacity of matrix compaction *in vitro*.[206]

To overcome the limitations of knocking-out a protein involved in several processes, our group generated in 2017 a new model by introducing the *FLNA*-P637Q mutation in a rat using CRISPR-Cas9 technique.[207] The newly developed *FLNA*-P637Q Knock-In rat model was then phenotyped by Delwarde *et al.*[208] The *FLNA*-KI rat was analyzed at the age of three weeks, and the observed phenotype was similar to those of MVD patients (Figure 19). Specifically, FLNA-KI rats had elongated leaflets and enlarged annulus, as assessed by echocardiography, increased MV volume quantified by micro-computed tomography, as well as leaflet thickening and proteoglycan accumulation as determined by histological analysis (Figure 19). This phenotype was the confirmed over a 6-months follow-up. Finally, at the transcriptomic level, a gene-

ontology terms (GO-terms) analysis of the differentially expressed genes revealed five metaclusters: chemotaxis and immune cell migration; extracellular matrix; epithelial cell migration; endothelial to mesenchymal transition; and molecular stress pathways. Unexpectedly, 30% of all GO-terms were classified under the metaclusters chemotaxis and immune cell migration (Figure 19).

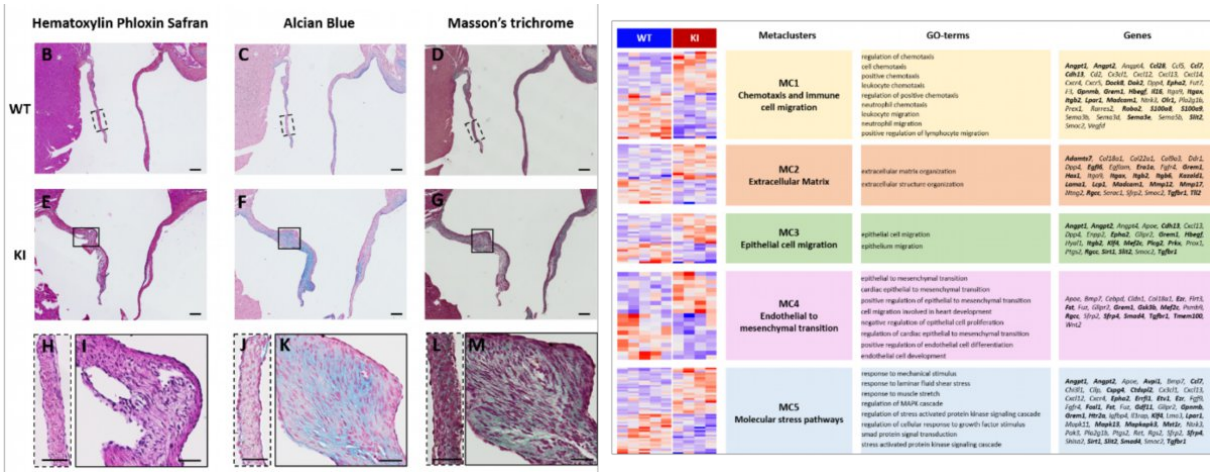

Figure 19. Morphological and molecular phenotyping of the *FLNA*-KI rat model. The top panel show the histological analysis of WT and *FLNA*-KI rats MV by hematoxylin phloxin saffron, Alcian blue and Masson's trichrome staining. Bottom panel is the enrichment analysis of the transcriptomic data from 3 weeks WT and KI rats MV. Modified from Delwarde *et al.*[208]

Overall, the different animal models used for the study of MVD allowed the identification of several key pathways involved in the development of the pathology. Recently, the identification of macrophages involvement in the development of Marfan syndrome-related MVD using the Fbn1$^{C1041G/+}$ mice, and the transcriptomic signature of chemotaxis in FlnA-related MVD paved the way to study macrophages as a new pathophysiological pathway of particular interest. Indeed, MVD was considered as a non-inflammatory disease, and the role of immune cells was left aside, but the comprehension of the immune mechanisms at play during the development and the maintenance of MVD could potentially offer new therapeutic targets.

4. Innate immune system and macrophages

4.1 Innate immune system

The innate immune system is one of two defense system of the organism, and is conserved across all multicellular organisms. It consists of all the immune defense mechanisms that lack immunologic memory and provide an immediate but non-specific response, in opposition to the adaptive immune system. Innate immunity has developed earlier on the history of evolution, but it remains the first defense mechanism of host organisms to a variety of infections, pathogens, or toxins.[209–211] The very first lines of defense of innate immunity system are the skin and mucosa that form a natural barrier which prevents most pathogens from entering the host organism. The second line of defense is cellular, and comprise granulocytes, natural killer (NK) cells, dendritic cells, monocytes and macrophages. To support their role, those cells have a wide range of effector molecules, from cellular receptors for recognition, to secreted soluble mediators that allow immune cell communication (i.e. cytokines and chemokines), opsonization (i.e. complement factors) or antigen presentation (i.e. major histocompatibility complex).[209,211,212]

To ensure their function of defense, innate immune cells harbor different mechanisms. For the clearance of abnormal cells, NK cells are capable of "killing" via a cytolytic process involving perforin and granzyme. Specifically, NK cells express a series of specific activator and inhibitory receptors, and the balance between activator or inhibitory signals govern the activity of the NK cells. [211,213] The Complement system is another mechanism of innate immunity. It comprises over 50 plasmatic or surface proteins that can be activated in three ways: the classical pathway, the lectin pathway or the alternative pathway.[214,215] Each pathways initiate a signaling

cascade with different actors that all ends up by the activation of C3 and C5 convertases. This will lead to either opsonization of the pathogen for recognition by immune cells, or lysis of abnormal cells through the formation of the membrane attack complex (MAC).[214]

Finally, the last mechanism of innate immunity is phagocytosis, a complex process by which a phagocytic cell engulfs a particle into a vesicle called phagosome to degrade it intracellularly via the formation of a phagolysosomes (Figure 20).[216–218] The professional phagocytes are neutrophils, eosinophils, dendritic cells, osteoclasts, monocytes and macrophages.[219] Phagocytes must recognize a large variety of particles larger than 0.5µm, ranging from microbial pathogens, to apoptotic cells.[216] Thus, phagocytosis is utterly important for immunity against external pathogens, but also for tissue homeostasis.

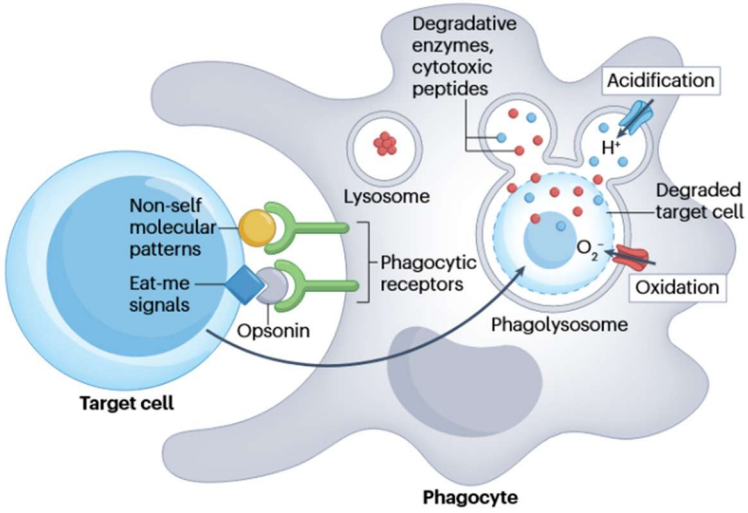

Figure 20. Phagocytosis. Schematic representation of the phagocytic process. A target cell is recognized through surface signals by a phagocyte. It is then internalized into a phagolysosome for degradation. From Brown et al.[218]

In order to recognize their target, professional phagocytes are equipped with a large panel of recognition receptors (Figure 20 and Figure 21).[217,220] Those receptors are designed to recognize four types of signal from the target cells: find-me signal, a chemotactic factor to attract the phagocyte; eat-me signal, a surface ligand from the target cell to initiate phagocytosis; don't-

eat-me signal, a surface ligand preventing phagocytosis; and opsonin, a soluble molecule bound to the target cell surface to stimulate phagocytosis (Figure 21).[217] It is important to note that the clearance of apoptotic cells by phagocytes is a specific phagocytic process called efferocytosis.[220,221] Thus, efferocytosis plays a major role in the maintenance of tissue homeostasis, and in tissue repair.[220]

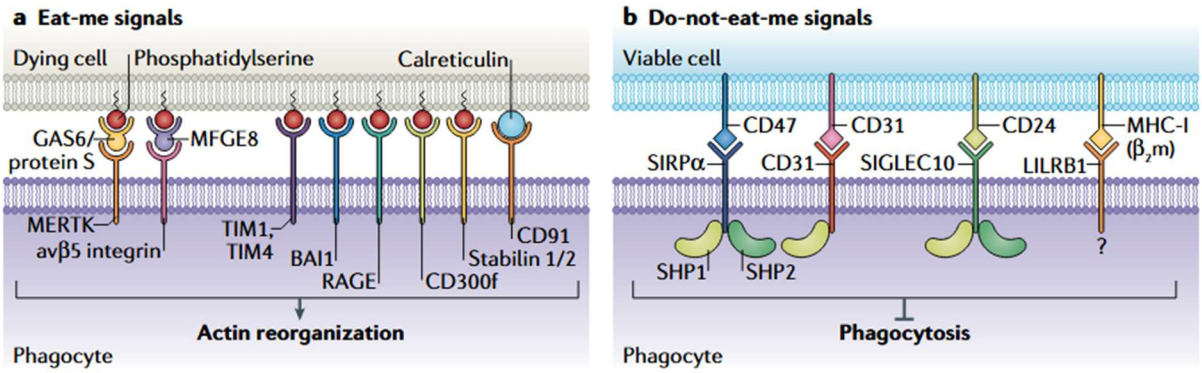

Figure 21. Efferocytosis cell surface signals. Eat-me and Do-not-eat-me signals are expressed at the surface of dying and viable cells respectively. Eat-me signals are recognized by phagocytic receptors either directly or through adaptor proteins like GAS6. From Boada-Romero *et al.*[220]

Once the target cell is bound to the phagocytes, the latter will rapidly rearrange its actin cytoskeleton to form filopodia that will engulf the target cell (or particle) in a vesicle called phagosome (Figure 22).[220,222–224] The actin remodeling occurs via Low density lipoprotein related protein 1 (LRP1)- or DOCK180-dependant activation of RAC1.[220,225] Intracellularly, the phagosome will undergo a multistep maturation process and merge with a lysosomal vesicle into a phagolysosome which will enzymatically and chemically degrade the target (Figure 22).

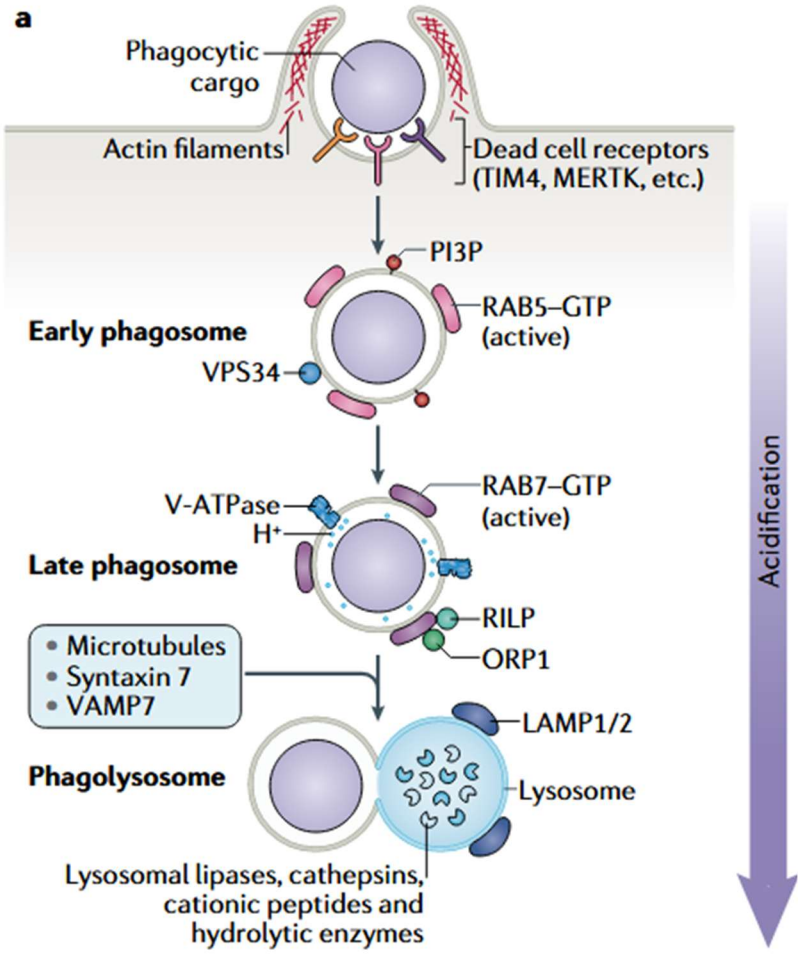

Figure 22. Efferocytosis internalization process. The dying cell, or phagocytic cargo is engulfed by actin cytoskeleton remodeling in an early phagosome. After maturation steps the phagosome merge with a lysosome vesicle to form a phagolysosome. From Boada-Romero et al.[220]

Among the professional phagocytes, macrophages are the most prevalent. They are present in all tissue at steady state to maintain tissue homeostasis, and they can be locally recruited to sites of inflammation via differentiation of circulating monocytes.

4.2 Macrophages

Described for the first time in the late 19th century by Ilya Metchnikov, co-laureate of the physiology Nobel prize in 1908, macrophages are mononuclear phagocytes of the innate immune system.[226] Macrophages plays a critical role in the clearance of pathogens, cellular debris, or apoptotic corpses, and in the maintenance of tissue homeostasis. They are also crucial for immune function as they regulate local inflammation and immune response to pathogen. Macrophages are ubiquitously distributed in the body, and meet different tissue-specific functions. The tissue specificity of macrophages is guided by the surrounding cells and microenvironment, known as the macrophage 'niche'.[227–230] The vast diversity of macrophages raised questions about their origin and the developmental programing that shapes their function depending on their localization.[230]

4.3 Ontogeny of macrophages

In adult, hematopoiesis relies on hematopoietic stem cells (HSCs), a pluripotent and self-renewed cell population located in the bone marrow that give rise to all circulating cell types, from erythrocytes to innate and adaptive immune cells. Over the years, several evidences were provided leading to the conclusion that some populations of tissue-resident macrophages were not HSC-derived, but rather originates from a developmental hematopoiesis.[229–238]

Developmental hematopoiesis refers to the spatiotemporal processes that lead to the generation of several hematopoietic progenitors, before the settlement of HSC in the bone marrow. Three hematopoietic waves have been described in mice. The first one is the primitive hematopoiesis initiated at embryonic day E7.5 in the yolk sac, with the generation of a mesodermal hemogenic endothelium (Figure 23).[239] From E8.5 to E10.5 is the transient hematopoiesis during which the

hemogenic endothelium give rise to erythromyeloid progenitors (EMPs: Cf1r^{+} Kit^{+} CD45^{low} AA4.1^{+}) that will colonize the fetal liver and differentiate into pre-macrophage (pMac: Cx3cr1^{+}). From the liver, EMPs and pMac will further colonize embryo's tissue in a Cx3cr1-dependant manner (Figure 23).[229] The third wave, or definitive hematopoiesis, starts at E10.5 and see hematopoietic stem cell (HSCs) emerge from the hemogenic endothelia in the aorta-gonad-mesonephros region (AGM), the vitelline and umbilical arteries, before migration to the fetal liver where they expand (Figure 23).[238] Around E17.5, HSCs migrates to the newly formed bone marrow niche.[229,234,236,238,240] During colonization of the embryos, pMac will differentiate in a tissue-specific manner to give rise to what we know as tissue-resident macrophages. The mechanisms that regulates this tissue-specific differentiation are still unclear, but some transcription factors have been linked to specific differentiation, like Id3 for Kupffer cells, Irf8 and Sall1 for microglia or Id2 and Runx3 for Langerhans cells.[229,233,240]

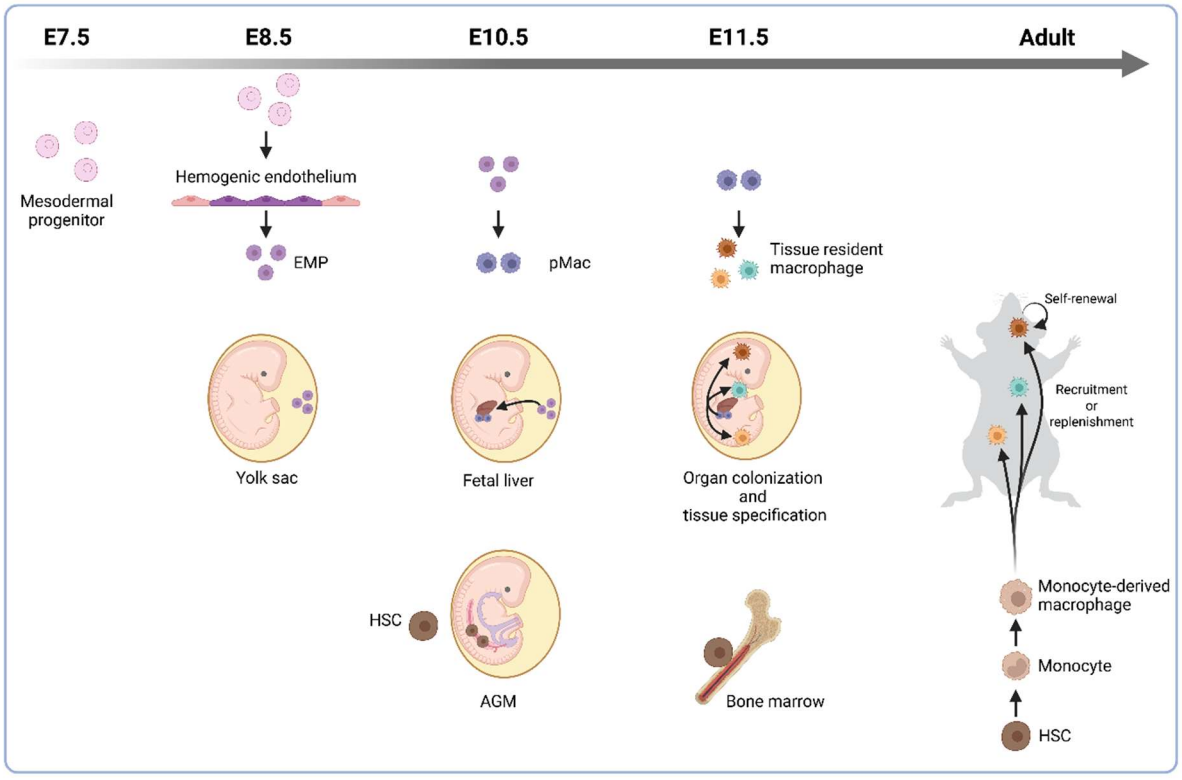

Figure 23. Developmental origin of macrophage in mice. AGM: Aorta-Gonado-Mesonephros, E: Embryonic day, EMP: Erythro-Myeloid Progenitor, HSC: Hematopoietic stem cell, pMac: Macrophage progenitor. Created with BioRender.

4.4 Cardiac resident-macrophage at steady state

The question of macrophage ontogeny in the heart has been a matter of controversy over the years. In 2013, Nakano *et al.* conducted a study to demonstrate the existence of a subset of endocardial cells expressing the transcription factor Nkx2.5 and displaying hemogenic capacity that could give rise to cardiac macrophages.[241] The same group later used lineage tracing to confirm the endocardial origin of cardiac macrophages. Using *Nfatc1*^{Cre} reporter mice, they show that 58% of F4/80^{+} macrophages in the atrioventricular cushion were Nfatc1-derived, and that the depletion of those endocardial-derived macrophages resulted in abnormal valvular development.[242] Other studies were conducted to define the mechanisms and revealed that the Nkx2.5/Notch/Retinoic acid pathway was essential.[51,243] Those study were opposed to the general consensus that myeloid cells originate from hemogenic endothelium in the yolk-sac and AGM region of the embryo.[229,232,234–238,240] In order to clarify the origin of cardiac resident macrophages, Liu *et al.* elegantly performed multiple lineage tracing experiments which demonstrated that the reporter used in previous study (i.e., *Nkx2.5* and *Nfatc1*) were not specific of endocardial cells, but could also label endothelium of the yolk-sac. Thereby, it cannot be excluded that the so-called endocardial-derived macrophages were in fact yolk-sac-derived.[244] They further used specific endocardial reporters *Mef2c* and *Npr3* and demonstrated the absence of endocardial-derived macrophages.[244]

Since the emergence of the developmental hematopoiesis concept, several studies have attached to investigate the origin of cardiac-resident macrophages (CRM).[245–249] In a study from 2014, Epelman *et al.* explored the ontogeny of CRM in mice.[245] They analyzed mouse heart at E10.5, prior to fetal liver and HSCs hematopoiesis, and revealed that primitive yolk-sac derived macrophages could already be detected.[245] They show that the vast majority of CRM are CCR2^{-} and derive from the yolk-sac and fetal liver progenitors. They are renewed through local

proliferation rather than monocyte replacement. Conversely, a small population of $CCR2^+$ CRM originate and are maintained from circulating monocytes progenitors.[245,250–252] The embryonic-derived $CCR2^-$ population can further be divided based on major histocompatibility complex class II expression into MHC-II^{high} and MHC-II^{low}.[245,248,252–254] MHC-II is the mice homolog of human leukocyte antigen-DR (HLA-DR) and is involved in antigen presentation. Furthermore, some studies showed a specific spatial distribution of these subtypes, with $CCR2^-$ MHC-II^{high} being preferentially located close to nerve bundles and endings, whereas $CCR2^-$ MHC-II^{low} are distributed around blood vessels.[252,253] Although $CCR2^-$ CRM are almost exclusively replenish by local proliferation, upon depletion or inflammation $CCR2^+$ monocytes can replace the different CRM populations of the mouse heart.[245] In human, the analysis of explanted heart confirmed the existence of $CCR2^+$ and $CCR2^-$ macrophage populations. $CCR2^-$ population represents embryonic-derived CRM with self-renewal ability, whereas the $CCR2^+$ population is monocyte-derived.[250,253,255]

CRM have plenty of functions in the developing heart as well as in the adult heart. Those functions are summarized in Figure 24. Briefly, it has been demonstrated that CRM assure the clearance of cardiomyocytes defective mitochondria via the efferocytosis receptor MER tyrosine kinase (MERTK).[256] RCM-derived amphiregulin mediates connexin 43 phosphorylation translocation in cardiomyocytes, thereby stabilizing electrical conduction.[257,258] CRM regulates cardiac growth in response to hypertensive stress through Insulin-like growth factor 1 (IGF-1).[259] Studies have also demonstrated that CRM prevents cardiac fibrosis and promotes angiogenesis (Figure 24).[253,260]

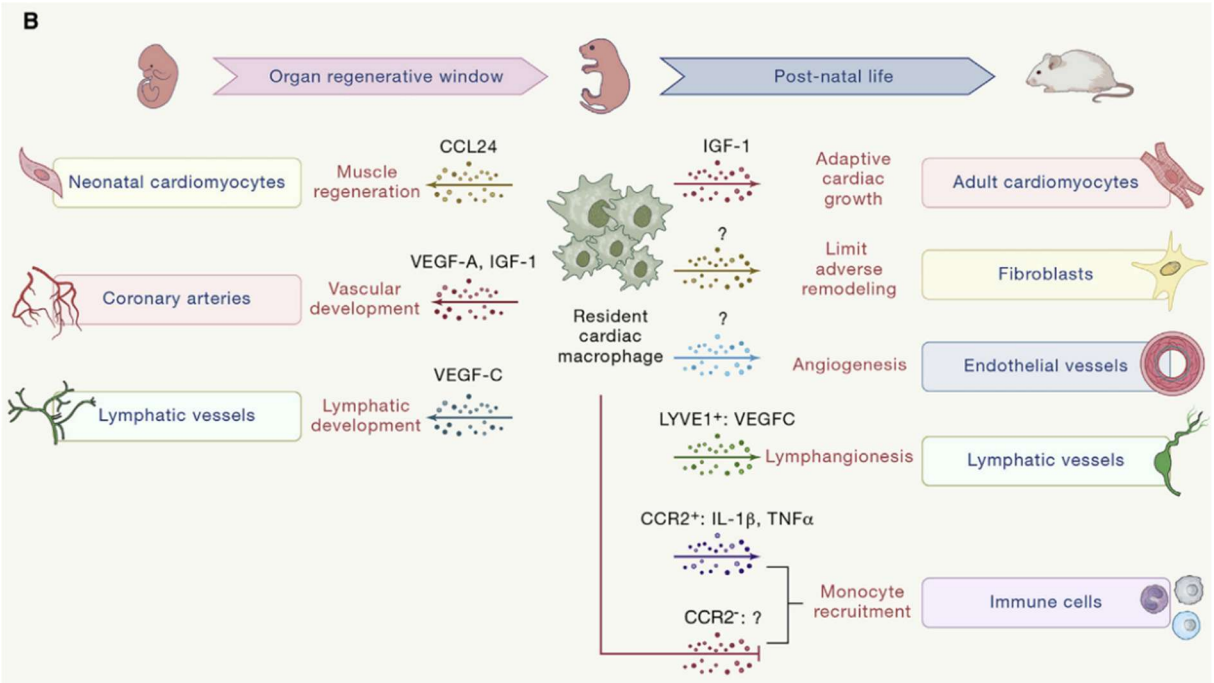

Figure 24. Cardiac resident macrophages functions. During development, CRM participates to cardiomyocytes proliferation through CCL24, vascular and lymphatic development through VEGF signaling. In adult, CRM helps to the adaptive growth of cardiomyocytes, limits the activation of cardiac fibroblasts, stimulates angiogenesis and lymphangiogenesis. Finally, CRM limit monocytes recruitment whereas it is stimulated by $CCR2^{+}$ macrophages. From Zaman and Epelman.[249]

Overall, at steady state, the heart macrophage population, which represents 5 to 10% of the cardiac cells, are distinguished based on their origin and functions.[247,255,261,262] Three distinct populations are described: $CCR2^{-}$ $MHC\text{-}II^{high}$; $CCR2^{-}$ $MHC\text{-}II^{low}$; and $CCR2^{+}$.[250] Each of these population coexist in the adult heart in specific niche, and originate from different stages of development. The respective proportion and function of each subpopulation is relatively stable at steady state, but can drastically vary upon disease or injury.

4.5 Macrophages in heart and valve diseases

Upon diseases, the macrophage niche is quickly reorganized to respond to the disturb homeostasis caused by the injury. This modification is often beneficial in the acute phase, but the long-term consequences of such a rearrangement of the macrophage niche can also have detrimental effects. The role of macrophages in response to heart injury has been extensively studied in the context of myocardial infarction (MI).[250,263–267] Although the rapid increase of macrophages after infarction has long been described, the mechanisms behind this influx were only recently been elucidated. It was shown that after MI the tissue-resident $CCR2^+$ macrophages orchestrate the recruitment of circulating monocytes through a Myeloid Differentiation primary response 88 - Monocyte Chemoattractant Protein (MYD88-MCP) pathway. On the other hand, the $CCR2^-$ macrophage population inhibits monocyte recruitment.[250] It is important to note that the $CCR2^+$ recruited macrophages are distinct from the tissue-resident $CCR2^+$ macrophages as they have different transcriptional signature.[250] In terms of consequence, the depletion of resident $CCR2^+$ macrophages leads to a reduction of the infarct size, whereas depletion of $CCR2^-$ resident macrophages increases the infarct size, confirming the different roles of macrophages depending on their origin.[250]

In valve diseases, macrophage have been mostly studied in the context of calcified aortic valve disease (CAVD), where macrophages participate to the fibrocalcific degeneration of the aortic cusps.[268–273] In the mitral valve, studies on macrophages were initially conducted on their function during mitral valve development and post-natal remodeling.[32,41,240] The study of macrophages in MVD is more recent and was limited to the Marfan syndrome-related MVD.[41,204,205] As described in the section 3.3, it was shown that during myxomatous MV degeneration of Marfan patient or Marfan mice and pig models, there is an increase of infiltrating $CCR2^+$ macrophages as well as an increase of $CCR2^-$ resident macrophages.[204] They

further crossed the Marfan Fbn1$^{C1039G/+}$ mice with CCR2$^{RFP/RFP}$ mice to generate a model of Marfan syndrome mice deficient for CCR2 in order to block the recruitment of macrophages into the MV. After immunofluorescent analysis, they conclude that the deficiency of CCR2^{+} macrophages in the MV was sufficient to prevent Marfan-related MVD progression.[204]

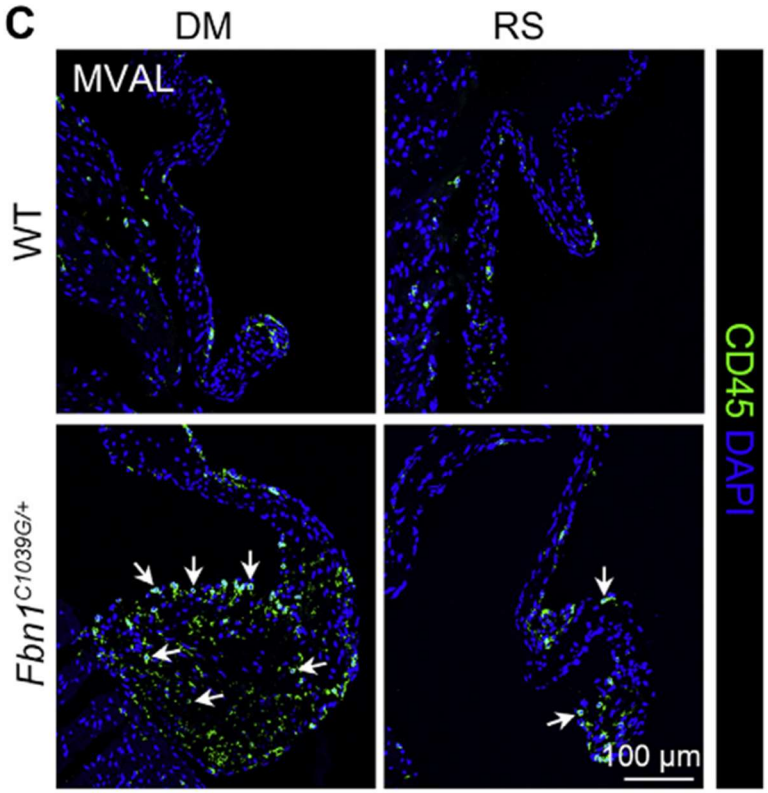

Figure 25. CCR2^{+} macrophage depletion in the Marfan mice model. CD45 staining of WT and Fbn1$^{c1039G/+}$ Marfan mice mitral valve, treated with DMSO (DM) or with CCR2 inhibitor (RS). From Xu and Yutzey.[205]

In a later study, the same group used a different strategy to limit the infiltration of circulating macrophages. They used the molecule RS504393, a selective antagonist of CCR2, to prevent recruitment of macrophages into the MV, and showed that it prevents the development and the progression of MVD (Figure 25).[205] It is important to note that Marfan-related MVD cannot recapitulate sporadic MVD phenotype. Indeed, in Marfan syndrome, caused by Fibrillin 1 mutation, the ECM is more prone to elastin fragmentation, and studies have proved that fibrillin fragment induced macrophage chemotaxis using Marfan-mice and Human aortic extract *in*

vitro.[76,274,275] Moreover, TGF-β signaling is largely increased in Marfan patient, and could also induce immune activation of the MV cells, and recruitment of circulating monocytes.[115]

In the context of non-syndromic forms of MVD, although several findings push towards the contribution of macrophages in the disease, the formal identification of increased macrophages has not yet been characterized. The first evidence come from the identification by immunofluorescence of increased $CD45^+$ and $F4/80^+$ cells in the MV of conditional endothelial Filamin A knock-out mice.[40] The second line of evidence comes from a study by *Minvielle* Moncla *et al.* who performed a mendelian randomization on large dataset including GWAS, blood proteome and genome-wide expression data to identify candidate drivers of MVP. They found 33 blood proteins enriched in immune networks associated with MVP. Additionally, by computing cytokine activity profile and using digital cell quantification, they identified a shift towards a cytokine signature that promote "M2" macrophage polarization in MVP.[276] Finally, in the previous study from our group on non-syndromic MVD, the *FLNA*-KI rat model was used for MV transcriptomic analysis.[208] 524 genes were found differentially expressed between KI and WT animals. Enrichment analysis of those differentially expressed genes highlighted 34 GO-terms. Unexpectedly, 10 of 34 GO-terms were related to chemotaxis and immune cell migration, suggesting a major role of immune cells in the pathophysiology of MVD.[208]

The literature is rather poor on the role of filamin A in macrophage, but a few studies were conducted.[176,277,278] Notably, it was shown that filamin A is required for podosome stabilization during macrophage migration in mesenchymal environment.[176] Another study revealed that Filamin A expression was increased in macrophages from advanced atherosclerotic plaques compared to intermediate stage. The inhibition or knockdown of filamin A in macrophages increased the efflux of cholesterol and lowered lipid uptake, thereby ameliorating the severity

of the plaques.[277] Specifically, the absence of filamin A in macrophages decreased their ability to migrate and proliferate, but also reduced the secretion of pro-inflammatory cytokines.[277]

II. Hypothesis and objectives

Given the previously published transcriptomic analysis of the *FLNA*-KI rat identifying chemotaxis and immune cells as a major contributor of MVD pathophysiology, we sought to investigate the role of immune cells. Additionally, previous studies conducted on Marfan-related MVD demonstrated that macrophages were increased in mice model of Marfan syndrome with myxomatous mitral valve degeneration and that the blockade of macrophage recruitment prevented the development of the pathology.

Therefore, we hypothesized that the increased immune and chemotactic signaling observed in the *FLNA*-KI rats at three weeks was caused by an increase in macrophages population, which contributed to the development or the maintenance of MVD, and could represent a new therapeutic target.

Our objectives are to confirm the presence of macrophages in the MV of *FLNA*-KI rats, and to corroborate if they also contribute to Human sporadic forms of MVD. To this aim, we did a time course analysis of the *FLNA*-KI rat model to characterize the morphological, molecular and cellular landscape of the MV from birth to the age of three weeks. We also analyzed the molecular signature of human MVD in a unique cohort of 78 samples of Human sporadic MVD.

We developed *in vitro* assay to assess the functional properties of macrophages carrying the *FLNA* mutation, and *in vivo* strategy to block macrophages recruitment to the mitral valve in order to assess the therapeutic potential of targeting macrophages.

III. Article: Macrophage recruitment as a hallmark of non-syndromic myxomatous mitral valve dystrophy

1. Introduction

Using histological, transcriptomic and cytometry analysis, we performed a time course analysis of MVD development and macrophage contribution to the pathophysiology of myxomatous mitral valve dystrophy in the *FLNA*-KI rat model. We also corroborated the involvement of macrophages in Human sporadic forms of MVD with bulk RNA-seq in a unique cohort of 78 sample collected in France and Italy. In the manuscript, we highlight a common phenotypic and molecular signature between Human sporadic MVD and *FLNA*-KI rats' MVD. We then demonstrate that as early as birth there is a molecular signature of MVD without morphological consequences in the *FLNA*-KI rat model. Leaflets remodeling is detected one week after birth and associates with evidences of chemotactic signaling without increased macrophage proportion. Finally, at the age of three weeks, *FLNA*-KI rat displays large remodeling of the mitral valve leaflet, with increase proportion of macrophages.

Overall, our results demonstrate the gradual development of MVD in the *FLNA*-KI rat model. Extracellular matrix homeostasis disturbance is detectable at birth, quickly followed by endothelial activation. This leads to remodeling of the MV by the age of one week, also marked by induction of chemotactic signaling. This will in turn induce recruitment of macrophages in the MV as detected at three weeks, comparable to the phenotype observed in Human end-stage sporadic MVD sample.

2. Manuscript

The following manuscript is currently under revision for publication in *Cardiovascular Research*, a journal of the European Society of Cardiology.

Macrophage Recruitment is a hallmark of Non-syndromic Mitral Valve Dystrophy

Benjamin Le Vely,[1,2#] Constance Delwarde,[1#] Claire Toquet,[1] Pascal Aumond,[1] Nelli Blank-Stein,[2] Emilie Charon,[1] Séverine Rémy,[3] Ignacio Anegon,[3] Veronika A. Myasoedova,[4] Vincenza Valerio,[4] Paolo Poggio,[4,5] Solena Le Scouarnec,[1] Jean-Jacques Schott,[1] Thierry Le Tourneau,[1] Jean Merot,[1] Elvira Mass,[2*] Romain Capoulade,[1*]

[1]Nantes Université, CHU Nantes, CNRS, INSERM, l'institut du thorax, F-44000 Nantes, France
[2]Developmental Biology of the Immune System, Life & Medical Sciences (LIMES) Institute, University of Bonn; 53115 Bonn, Germany
[3]INSERM UMR 1064-CR2TI, Transgenic Rats ImmunoPhenomic, Nantes, France
[4]Centro Cardiologico Monzino IRCCS, 20138 Milan, Italy
[5]Department of Biomedical, Surgical and Dental Sciences, University of Milan, 20122 Milan, Italy

[#]: first authors contributed equally
*: senior authors contributed equally

Correspondence:
Romain Capoulade, PhD
L'institut du thorax, Inserm U1087/CNRS U6291
IRS-UN, 8 quai Moncousu, BP 70721
44007 Nantes Cedex 1
Email : romain.capoulade@univ-nantes.fr

Short title: Macrophage Recruitment in MVD

Category: Original article

Total word count: 9270

ABSTRACT

Aims: Mitral valve dystrophy (MVD) is a progressive cardiac disease characterized by extracellular matrix remodeling, leaflet thickening, and proteoglycan accumulation. Despite its significant contribution to cardiovascular morbidity and mortality, the underlying pathophysiological mechanisms involved in its development and progression remain unclear. Recent investigations have revealed a genetic component to the disease, such as mutations in the *FLNA* gene, and suggested potential involvement of immune cells in the pathogenesis of MVD. In this study, we investigated the role of macrophages in MVD using a large collection of human non-syndromic MVD samples and a unique animal model, the Filamin-A knock-in (KI) rat.

Methods and Results: Transciptomic analysis of 78 human non-syndromic MVD samples revealed significant enrichment of pathways associated with immune activation and macrophage recruitment. Comparative analyses between human and rat MVD identified shared molecular signatures, validating the Filamin-A KI rat model for studying human MVD pathophysiology. Analyses of wild-type (WT) and KI rat MVs demontrated a gradual activation of valvular cells from birth, which translated into phenotypic MV remodeling by postnatal day 7. These early events were associated with the development of a pro-inflammatory valvular environment, despite no initial increase in myeloid cells. The subsequent accumulation of macrophages in the already remodeled MV leaflets indicated the initiation of an active recruitment process, likely involved in the progression of non-syndromic MVD.

Conclusion: This study highlights the central role of chemotaxis and macrophage recruitment and activation in the pathophysiological processes leading to non-syndromic myxomatous MVD. Macrophage invovlement emerges as a hallmark of non-syndromic MVD, a disease previously described as non-inflammatory, and opens new avenues to identify potential therapeutic targets to mitigate disease progression.

TRANSLATIONAL PERSPECTIVE

The pathophysiological mechanisms driving non-syndromic mitral valve dystrophy (MVD), the most common cause of mitral valve prolapse, remain poorly understood. Traditionally considered a non-inflammatory condition, MVD has not previosly been associated with immun cell involvement. Here, we identify for the first time a central role for macrophages in the pathological processes of non-syndromic MVD. Macrophage activation and recruitment emerge as hallmark features of the disease, supporting their contribution in the progression of valve remodeling. These findings shift the current paradigm and open new avenues for therapeutic exploration, particularly in a condition where treatement optons remain limited to invasive surgical interventions.

INTRODUCTION

Mitral valve dystrophy (MVD) is one of the most common valvular heart diseases affecting 2 to 5% of the general population.[1] Myxomatous MVD, characterized by elongated and thickened MV leaflets coupled with an accumulation of proteoglycans, is the main etiology observed in patients with primary mitral regurgitation.[2] Despite its prevalence and significant contribution to cardiovascular morbidity and mortality, the pathophysiological mechanisms underlying MVD remain poorly understood, leaving open-heart MV surgery as the only therapeutic option for patients with severe and symptomatic forms.[3,4]

The MV is a complex tissue composed of an extracellular matrix (ECM) organized in three layers and populated by valvular interstitial cells (VICs), which maintain valve homeostasis, and valvular endothelial cells (VECs), which line the valve surface.[5] Recently, the presence of immune cells has been highlighted in both healthy and myxomatous valves, with macrophages emerging as a particularly prominent population.[6–11] As also reported for VICs and VECs, the immune cell population displays significant heterogeneity within the valve.[12] This heterogeneity may be attributed to their distinct origins – either from an embryonic source or from bone marrow-derived monocytes[7,13,14] - and/or to the influence of the valve micro-environment on their phenotype and activation state.

Although the role of macrophages during valvulogenesis has been well described, little is known about the function of these “resident” immune cells after birth.[7,8,13,15] At birth, tissue-resident macrophages in most organs are derived from the yolk sac,[14] but under inflammatory conditions, this population is complemented or replaced by “recruited" monocyte-derived macrophages.[7] Macrophages have been implicated as key contributors to the pathophysiological processes underlying various valvular disorders in both human and murine models.[6,7,9,16] However, it remains unclear whether and how macrophages, during disease onset and progression, are shaped by their developmental origin.

The analysis of knock-out mouse models exhibiting myxomatous-like MVD showed a consistent increase in macrophages within the valves.[9,17] In Marfan syndrome, a rare connective tissue disorder

characterized by elastin fragmentation and the development of myxomatous MVD in around 50% of the affected patients, studies have demonstrated that depletion of monocytes protects against myxomatous MVD progression.[18,19] Notably, low molecular weight elastin-derived peptides, which are released in Marfan syndrome, act as potent chemoattractant *in vivo*.[20–22] This mechanism, combined with altered Transforming Growth Factor-β (TGF-β) signaling, likely leads to the recruitment of monocyte-derived macrophages and the development of syndromic myxomatous MVD.[23] However, most myxomatous MVD cases are non-syndromic and exhibit lower TGF-β activation and elastin fragmentation compared to Marfan syndrome. Therefore, the specific role of macrophages in initiating or advancing non-syndromic MVD remains unclear. Since non-syndromic cases represent the majority of MVD patients, further studies are now essential to determine whether targeting macrophages could serve as a promising therapeutic strategy for this common pathology.

We recently generated the first rat model for non-syndromic myxomatous MVD: the Filamin-A (FlnA) knock-in (KI) rat.[24] Transcriptomic analysis performed at postnatal day 21 (D21) revealed multiple pathophysiological processes involved in the MV disease processes, including ECM remodeling, response to stress, endothelial to mesenchymal transition, and a central role for immune cells. Indeed, 30% of the Gene Ontology-terms associated with differentially expressed genes between KI and wild-type (WT) rats referred to the involvement of immune cells in the MVD pathophysiology.[24]

In the current study, we aimed to evaluate the contribution of myeloid cells, particularly macrophages, in the development of non-syndromic MVD. To achieve this, we analyzed a unique collection of human sporadic myxomatous MV samples alongside with our FlnA-P637Q KI rat model of non-syndromic MVD. Transcriptomic analysis revealed activation of inflammation and immune cell chemotaxis signaling pathways, as well as increased macrophage numbers in diseased tissue. These findings were consistent in both human “end-stage” MVD samples and during the developmental phases of MVD in our rat model, underscoring a key role of macrophages in the pathophysiology of non-syndromic myxomatous MVD.

METHODS

Human mitral valve RNA-seq

Resected MV leaflets from open heart surgery performed in patients with isolated non-syndromic myxomatous MV prolapse at the Nantes University Hospital (Nantes, France) and the Centro Cardiologico Monzino (Milan, Italy) were snap-frozen or collected in RNA Later (Thermo Fisher, AM7020) for 24h, and stored in -80°C before RNA extraction. The study complies with the Declaration of Helsinki and was approved by the local ethical committees (Nantes: N°215/2013; Milan: CCM-3122014). All patients signed written informed consent.

Frozen MV samples were crushed on dry ice. 50 mg of MV powder was used for RNA extraction with miRNeasy kit (Quiagen, 217084) per manufacturer's protocol. Quality control of RNA was performed on Bioanalyzer (Agilent, USA), and the 78 samples with RIN>6.5 were used to prepare the library with Illumina Stranded mRNA Prep, Ligation kit (Illumina, USA) following the manufacturer's protocol. Libraries were validated using both the Qubit Fluorometer and the Fragment Analyzer (Agilent, USA). Sequencing was performed on a Novaseq 6000 sequencer (Illumina, USA). Sequenced reads were demultiplexed using bcl2fastq2 software (Illumina, USA) and QC were performed using FastQC pipeline. The primary analysis was done with prinseq, cutadapt, and multiqc tools. Reads were then aligned using STAR on GRCH38 Human genome. Finally, the expression matrix was built with htseq-Count.

Due to the limited access to human control MV and the lack of available transcriptomic data in the literature, we conducted a 3-step analysis (Figure 1a). Firstly, we ranked the 36 652 genes based on their normalized expression level across the 78 samples, and selected the 2000 genes with the highest expression profile: the over-representation analysis (ORA) was performed on those 2000 genes with MsigDB.[25] Secondly, we run the xCell deconvolution algorithm[26] on normalized expression data to estimate the core enrichment in immune cells for each sample. Finally, to compare the molecular signature of human MVD and rat FLNA-KI MVD, we used our previously published RNA-seq data of MV

from 3-week-old FLNA-KI rats.[24] We firstly mapped rat genes to the Human gene ID using biomaRt,[27] and applied the same method to extract the 2000 highly expressed genes from the rat MV. ORA was conducted with MsigDB on the common genes found in both human MVD and rat FLNA-KI datasets.

Human mitral valve histological staining and immunostaining

One additional human MV was collected in Nantes University Hospital at the time of MV replacement for significant MV regurgitation associated with non-syndromic MV prolapse (ethical committee: N°215/2013). The patient signed informed consent. As a control, and following the signed family agreement, the MV from a patient referred for sudden cardiac death at the "Centre de référence des maladies rythmiques et cardiaques" of the Nantes University Hospital, was collected. Both samples were fixed in 10% formalin (Sigma-Aldrich, HT501320) for 48h. Paraffin-embedded slides were cut and stained with Hematoxylin Eosin Saffron (HES) to assess MV morphology. Immunohistochemistry analyses were performed using antibodies against CD68 (pan-macrophages; M0876, DakoCytomation) (Supplementary Table S1).

FlnA-P637Q Knock-In rat model

The rat model used in this study has been previously described.[24] Briefly, Sprague-Dawley FlnA-P637Q Knock-In (KI) rats were engineered using CRISPR/Cas9 method.[28] All rat experiments were carried out following European Union Directive 2010/63/EU about the protection of animals used for scientific purposes and were authorized by the French Ministry of Higher Education and Research after approval by the Ethics Committee on Animal Experimentation from the Région Pays de la Loire (approval numbers: APAFIS 33433 & 44870).

In the present study, newborn (D0), 2-day-old (D2), 7-day-old (D7) and 3-week-old (D21) KI and WT rats were analyzed by investigators blinded to the animals' genotype. Rats were anesthetized with

isoflurane (Iso-Vet 100%, Piramal; induction at 4% and maintenance at 2%). Immediately after the euthanasia by cervical dislocation, the chest was opened, and the heart was harvested and placed in ice-cold PBS.

Flow cytometry

Flow cytometry was performed at D7 and D21. Anterior and posterior MV leaflets were dissected from at least 7 littermate rats for each genotype and were pooled in 1X HBSS (Sigma, H1641), 2% FBS (Biosera, FB-1200) to generate one biological sample. MVs were digested using a solution of 1X HBSS, 1.2U/mL Dispase II (Sigma, D4693) and 2mg/mL Collagenase IV (Worthington, LS004188) for 45 min at 37°C under agitation. Cells were filtered on a 40 µm cell strainer before 2 washing cycles in HBSS, 2% FBS with centrifugation cycles (4°C for 5' at 400 x g). Fc Block (Purified Rat Anti-Mouse CD16/CD32 (Mouse BD Fc Block™), 10µg/mL) was added to the cells to limit non-specific staining, and then isolated cells were stained with antibodies (Supplementary Table S1) for 1h at 4°C on a rotating wheel. Cells were finally washed 3 times in FACS Buffer (PBS, FBS 2%, EDTA 1mM) (centrifugation cycles at 4°C for 5', 400 x g), before adding DAPI to assess viability. To compensate for fluorescence spectral overlap, controls were prepared using Ultracom eBeads Plus (Invitrogen, 01-3333-42), for each antibody of the panel, according to the manufacturer's protocols.

Flow cytometry was conducted using a Symphony A5.2 Flow Cytometer (BD Biosciences). FCS 3.0 files were processed using BD FACSDiva™ v8.5 software. For flow cytometry analyses, cells were gated using FSC-A vs SSC-A, then cell doublets were gated out using FSC-A vs FSC-H followed by DAPI staining exclusion to identify viable (i.e. $DAPI^-$) single cells (Supplementary figure S1). To quantify the proportion of hematopoietic cells in MV, the viable single cells were gated on CD45 expression. $CD45^+$ cells were further gated on CD11b and CD206 expression to identify myeloid cells. Negative cells for CD206 and CD11b were considered as non-myeloid $CD45^+$ cells. The CD45 negative cells were then gated on CD31 for VECs. The rest of the cells, negative for all markers, were considered as VICs. Indeed, no specific

marker is currently available to identify and quantify rat VICs by flow cytometry. The analyses of flow cytometry were performed on FlowJo Software (Tree Star, Ashland, USA). Flow cytometry was performed on 6 WT and 6 KI biological replicates at D21, and 10 WT and 9 KI at D7.

Histological staining and immunofluorescence of rat mitral valves

Following the previously published protocol for histological staining,[24] hearts from D0, D2 and D7 were fixed in 10% formalin (Sigma-Aldrich, HT501320) for 24h, dehydrated, cleared in xylene and embedded in paraffin. 3 µm thick slides were sectioned using a microtome and serial slides were stained. Hematoxylin Phloxine Saffron (HPS: Hematoxylin cp813, Diapath; Phloxine pb-p-25, Biognost; Saffron 27481.105, VWR) and Alcian Blue (c0053, Diapath; pH2.5) staining were performed. The slides were examined under light microscopy and scanned using Hamamatsu NanoZoomerS360. As previously defined,[24] several histological features (i.e. leaflet thickness, free edge and medial part thicknesses, endothelial cell turgescence, leaflet immaturity, proteoglycan content) were used to qualitatively recognize myxomatous MVD. The histological score, presented in Supplementary Table S2, was built to assess the remodeling of the MV at D0 and D2 on 12 WT and 12 KI animals. 16 WT and 15 KI animals were also evaluated at D7. The content in proteoglycans was quantified by Alcian Blue using QuPath software, as previously published.[24] Briefly, the anterior and posterior MV leaflets were segmented and colour deconvolution was applied to quantify the Alcian blue positive area.

For immunofluorescence staining, serial frozen OCT-embedded slides were brought to room temperature and fixed before antigen retrieval in Citrate buffer pH 6.2, and then saturated in 2% BSA (bovine serum albumin, Sigma-Aldrich, A7030). Primary antibodies were used to identify macrophages (i.e. $CD206^{+}$), hematopoietic stem cells (i.e. $CD45^{+}$) and VECs (i.e. $CD31^{+}$) (see the complete list of antibodies, references and dilutions in Supplementary Table S1). All primary antibodies were incubated at 4°C overnight. Appropriate secondary antibodies were incubated for 1h at room temperature before

nuclei were stained with 1µg/mL Hoechst. All images were captured using ECLIPSE Ti2 microscope (Nikon).

RT-qPCR

WT and KI MV leaflets were dissected, snap-frozen and stored at -80°C before RNA extraction using the miRNeasy mini kit (Qiagen, 217084), as previously described.[24] Briefly, quality control was performed using the NanoDrop (ThermoFisher) with a 260/280 ratio of 1.8-2.2 being acceptable. cDNA transcription was conducted using the High-Capacity cDNA Reverse Transcription Kit (Applied Biosystems, 4368814) per manufacturer's protocol. cDNA was stored at -20°C until amplification by real-time semi-quantitative PCR (qPCR). Specific primers targeting relevant genes involved in the pathophysiological pathways, as identified in our previous study,[24] were designed using Primer3Plus and included *Ccl7*, *Esm1*, *Has1*, *Hyal1*, *Tnfsf18,* and *Gapdh* as the housekeeping gene (Supplementary Table S3). The qPCR reaction was performed using the Power SYBR green PCR master mix (Applied Biosystems, 4367659) on QuantStudio 5 Real-Time PCR System (Applied Biosystems, A28140). Melting curve (95°C for 15 sec and 60°C for 15 sec) was performed at the end of the last cycle to assess the amplification specificity. Results of gene expression were processed under DA2 v2.6 software. Ct raw data were adjusted between runs with an interplate calibrator. For each marker, delta Ct was calculated on the housekeeping gene (i.e. *Gapdh*). Log2 transformation was applied to transform the data to a linear scale.

RNA-seq of mitral valves in rats

Anterior and posterior MV leaflets from 6 WT and 6 KI rats were dissected, snap-frozen and stored at -80°C before RNA extraction using the miRNeasy mini kit (Qiagen, 217084) per manufacturer's protocol. RNA samples were quantified using a Qubit Fluorometer (Thermo Fisher Scientific, USA) and

qualified using a BioAnalyzer (Agilent, USA). Libraries were prepared using the Illumina Stranded mRNA Prep, Ligation kit (Illumina, USA) following the manufacturer's protocol, with a modification after the PCR step where all samples were purified twice with AMPure beads (Beckman Coulter, A63880) to remove small fragments. Libraries were validated using both the Qubit Fluorometer and the Fragment Analyzer (Agilent, USA). Sequencing was performed with a P2 100 cycles kit on a NextSeq 2000 sequencer (Illumina, USA).

The RNA-seq analysis was performed with Sequana 0.14.[29,30] We used the RNA-seq pipeline: https://github.com/sequana/sequana_rnaseq built on top of Snakemake 7.8.5.[31] Briefly, reads were trimmed from adapters using Fastp 0.20.1, then mapped to the Rattus norvegicus genome assembly from Ensembl (mRatBN7_2_dna_sm_toplevel_109) using STAR 2.7.8a.[32,33] FeatureCounts 2.0.1 was used to produce the count matrix, assigning reads to features using corresponding annotation v109 from Ensembl with strand-specificity information.[34] Quality control statistics were summarized using MultiQC 1.11.[35] Statistical analysis on the count matrix was performed to identify differentially expressed genes (DEGs). Differential expression testing was conducted using DESeq2 library 1.30.0 scripts.[36] DEGs were selected with a p-value <0.05 and Fold Change (FC) >1.2 or FC <0.8. Finally, gene set enrichment analysis was performed using ClusterProfiler and mSigDB. Significant Gene Ontology (GO)-terms (p<0.05) were then grouped under metaclusters, as previously described.[24]

Statistics

Data are presented as means ± SEM or median (interquartile range, IQR), as appropriate. The Mann-Whitney test has been used to assess the difference in cellular proportion and the relative transcript expression between WT and KI animals. Data were analyzed using GraphPrism software, v8. A p-value <0.05 was considered significant.

Data availability

The data supporting the findings of this study are available from the corresponding author upon reasonable request.

RESULTS

Transcriptomic profiling of human "end-stage" non-syndromic MVD reveals immune cell involvement in disease processes

To investigate which cellular and molecular alterations are induced upon MVD, we performed bulk RNA-seq analysis on 78 human MVs collected from isolated non-syndromic MVD patients (Figure 1a). They presented classical clinical features for patients undergoing MV surgery for sporadic MVD (Supplementary Table S4): the mean age was 61 ± 11 years, 77% were male, and 51% presented hypertension, 22% dyslipidemia, and 5% diabetes. There was no specific transcriptomic signature observed between males and females or between samples from France and Italy (Supplementary Figure S2).

We extracted the 2000 top expressed genes, which included many genes associated with ECM remodeling (*FN1*, *VIM*, *COL1A1*, *VCAN*, *POSTN*), TGF-β signaling (*LTBP2*, *LTBP1*), and immune cells (*C7*, *MMP2*, *CD81*, *ITGB1*) (Figure 1b). Interestingly, among those highly expressed genes, several have been previously linked to MVD, such as *FLNA*, *FBN1*, and *TNS1* (Figure 1b). ORA of these 2000 genes resulted in 95 GO Biological Processes and 6 KEGG pathways significantly enriched (Supplementary Table S5). The enriched GO terms referred to cell activation, adhesion, migration, and response to TGF-β, as well as to cytoskeleton organization and ECM receptor interaction (Figure 1c). Interestingly, *MMP2*, *ITGB1,* and *CXCL12,* genes belonging to the term "Leukocyte transendothelial migration", were also enriched in MVD samples (Figure 1d and Supplementary Table S5), suggesting that immune cell infiltration may play a role in disease pathophysiology. To assess which cell types potentially contribute to MVD, we

performed a deconvolution analysis using XCell.[26] The enrichment score showed that macrophage-specific genes are the main contributors to the MVD transcriptional signature (Figure 1e), indicating the relevance of this immune cell type in the pathophysiology of human "end-stage" MVD. Other immune cells, such as megakaryocytes, monocytes, and dendritic cells, were also identified with lower enrichment scores (Figure 1e).

We further used immunohistochemistry to assess the presence and localization of macrophages in human MV from patients with non-syndromic MVD associated with severe mitral regurgitation requiring MV replacement surgery. This was compared to healthy control valves (Figure 1f). In the diseased specimen, we observed classical features of myxomatous MVD, including elongated and thickened MVs, disruption of the layered organization of the leaflet's structure, and myxomatous deposits. These pathological changes were associated with a higher abundance of $CD68^+$ macrophages, which infiltrated the complete leaflet, while macrophages were confined to the outer layers in control MV (Figure 1f).

Next, we used the FlnA KI rat model to determine whether the observed immune-related signatures in human MVD are species-specific or represent a common hallmark of MVD. To this end, we compared the 2000 top expressed genes from 78 human MVD samples with those from the dataset of D21 KI rat MVs.[24] Rat genes were first mapped to their human orthologues, then ranked based on expression level, and the top 2000 genes were selected for comparison. 951 out of 2000 top expressed genes (47.5%) were shared between human and rat MVD (Figure 1g). ORA identified shared pathways between human and rat MVD, including cell adhesion, cell activation, ECM remodeling, cytoskeleton organization, and leukocyte migration (Figure 1g).

Altogether, these findings underscore an important immune component in the pathophysiological traits of human non-syndromic MVD, including signs of leukocyte recruitment and ectopic localization of $CD68^+$ cells within the valve leaflets, and point to macrophages as potential contributors. They further emphasize the translational relevance of our rat model to study human MVD pathophysiology.

Increased abundance and altered distribution of macrophages in MV of KI rats mirror human MVD

To investigate the cellular distribution of immune and non-immune cells in MVD on a single-cell level, we developed a flow cytometry panel to quantify the different cell subtypes within MVs from D21 rats (Figure 2a and Supplementary Figure S1). Consistent with previous studies[8], VICs were the predominant cell population, with a moderate but significant decrease in their proportion in KI MV (81.9% ± 2.2% in WT *versus* 78.5% ± 2.5% in KI; p=0.02; Figure 2c). $CD31^+$ VECs represented the second-largest population, showing no significant difference between WT and KI rats (9.7% ± 0.8% *versus* 8.7% ± 1.7%, respectively; p=0.75; Figure 2c).

In contrast, the proportion of $CD45^+$ immune cells was significantly higher in KI MVs compared to WT (12.8% ± 2.3% *versus* 8.4% ± 2.1% respectively, p=0.002; Figure 2b and 2c). The $CD45^+$ population represented predominantly myeloid cells with ~95% of cells co-expressing the myeloid/macrophage cell markers CD11b and/or CD206 in both WT and KI animals (Figure 2d). Specifically, the $CD45^+$ $CD206^+$ $CD11b^+$ myeloid cell population was significantly increased in KI MV (8.0% ± 1.2% *versus* 5.7% ± 1.6% in WT; p=0.001) as well as the $CD45^+$ $CD11b^+$ $CD206^-$ population (4.0% ± 1.5% *versus* 2.2% ± 1.4% in WT; p=0.01; Figure 2d). Meanwhile, non-myeloid $CD45^+$cells (i.e. $CD45^+$ $CD11b^-$ $CD206^-$) were present in small amounts (<0.6%) and showed no difference between genotypes (Figure 2d).

To validate our findings, we performed immunofluorescence staining using markers for leukocytes (CD45) and macrophages (CD206) on serial sections. The overlap of CD45 and CD206 signals confirmed that most $CD45^+$ cells were indeed $CD206^+$ macrophages (Figure 2e). An increased number of both $CD45^+$ leukocytes and $CD206^+$ cells was visible in KI animals. Interestingly, the distribution of these cells differed between WT and KI animals. In both genotypes, $CD45^+$ and $CD206^+$ cells are located in the sub-endothelial atrialis layer and the medial part of the leaflet. However, in KI animals, these cells more frequently invaded the inner tissue, similar to the observations reported in human MVD. Noteworthy,

macrophages were also observed on the ventricular side of KI MV leaflets, a MV leaflet area of turbulent shear stress and increased mechanical stress.

Overall, flow cytometry and immunofluorescent analysis revealed a significant increase and altered distribution of macrophages in MV of D21 KI rats compared to WT, concordant with transcriptomic and histological findings in human MVD.

Early onset of valve remodeling and endothelial activation precedes macrophage recruitment during the progression of MVD

To evaluate the time course of the development of MVD and decipher whether the increased proportion of macrophages observed in diseased MV from both rats and humans was the cause or the consequence of MVD, MV leaflet remodeling, molecular signature, and macrophage recruitment were assessed at D0, D2 and D7 in KI and WT animals.

At both D0 and D2, histological analysis revealed similar MV morphology in WT and KI (Figure 3a and 3b). The overall structure of the KI and WT MV leaflets was disorganized and immature, with minimal deposits of collagen and proteoglycan, as shown by HPS and Alcian Blue staining, respectively. The evaluation of the leaflet's remodeling of serial sections revealed diverse and heterogeneous morphological features across the entire MV, both in WT and KI (Supplementary Figure S3). The leaflet's cellularity appeared to be increased compared to the more mature stages (i.e. D21) (Figure 3a and 3b). Additionally, VECs presented a turgescent phenotype, indicative of endothelial cell activation. This activation was specific to VECs and was not observed in endothelial cells surrounding the myocardium (Figure 3a and 3b), suggesting a MV-specific endothelial activation.

Although no consistent differential histological features were detected at D0 and D2, we investigated whether genes upregulated in D21 KI MVs[24] were already elevated at birth. The ECM remodeling marker *Has1* was significantly upregulated in KI compared to WT at both D0 and D2, as assessed by RT-qPCR (Figure 3c). In contrast, *Hyal1*, another ECM remodeling marker, showed no difference at

these early time points (Figure 3c). The endothelial activation marker *Esm1* showed a trend toward increased expression at D0 and became significantly upregulated at D2 (Figure 3d). Finally, we observed no difference in the expression of pro-inflammatory markers, such as *Ccl7* and *Tnfsf18*, at D0. However, *Tnfsf18* was significantly upregulated in KI MVs at D2 (Figure 3e). In summary, these gene expression findings, in combination with the histological assessment, highlight the potential role for postnatal mechanical stresses on the valvular cell activation, and an early onset of a pro-inflammatory valvular micro-environment.

We continued our longitudinal analyses at D7, where macroscopic evaluation revealed morphological alterations in both the anterior and posterior MV leaflets in KI animals. These leaflets appeared opaque and redundant compared to those of WT animals (Figure 4a). Histological analysis confirmed that KI animals display thicker MVs with prevailing proteoglycan content, a hallmark of myxomatous MVD (Figure 4b). We evaluated MVD at D7 using qualitative and semi-quantitative histological criteria (Supplementary Table S2). Compared to WT, KI MVs presented a higher incidence of leaflet thickening (80% of KI *versus* 37% of WT animals; data not shown), particularly in the medial region and the free edge of the leaflets. Additionally, turgescent VECs were frequently observed in KI MVs (red box), while WT MVs displayed normal morphology (blue box) (Figure 4b). Although MV remodeling was heterogeneous among KI rats, these animals exhibited a significantly higher histological score compared to WT (Figure 4c). Proteoglycan content analysis showed a trend towards increased Alcian Blue staining in KI MVs (Figure 4d), which was significant for the anterior leaflet (Figure 4e) but not the posterior leaflet (Figure 4f). Consistent with the presence of MVD, molecular markers of MVD were differentially expressed in KI MVs compared to WT (Supplementary Figure S4).

Based on the phenotypic and molecular evidence of MVD at D7 in KI animals, we performed flow cytometry experiments using the same strategy as applied at D21 (Supplementary Figure S1) to determine the proportion of different cell subtypes within MV tissue (Figure 4g-i). As opposed to the findings at D21, we did not observe any significant differences in the proportions of cells (i.e. VICs,

VECs and $CD45^+$ cells) between KI and WT animals (Figure 4h). The proportions of $CD45^+$ immune cells in general and of myeloid cells ($CD45^+$ $CD11b^+$ and/or $CD206^+$) were similar between KI and WT MVs at D7 (Figure 4i). The localization of immune cells ($CD45^+$ and $CD206^+$) within the MV tissue was also similar between genotypes (Figure 4j). These cells were preferentially located in the sub-endothelial atrialis layer, particularly in the medial region and the free edge of both leaflets.

Overall, these results highlight the progressive development of the pathophysiological processes leading to MVD. Activation of the disease-related signaling pathways begins gradually from birth, resulting in a morphologically detectable MVD at D7, which exhibits the same phenotypic traits observed at D21. However, at this early stage, there is no myeloid cell accumulation into the diseased MV, suggesting that macrophage recruitment occurs after the development of MVD.

Early transcriptomic changes reveal ECM remodeling and pro-inflammatory signaling in KI MVs

To determine the main mechanisms underlying MV remodeling observed as early as D7, we performed RNA-seq analysis on MVs from 6 WT and 6 KI (Figure 5a). This analysis revealed a total of 2250 DEGs, with 678 upregulated and 1572 downregulated. Gene Set Enrichment Analysis of these DEGs identified 173 significantly enriched GO terms (p-value <0.05; Supplementary Table S6), which were further grouped into metaclusters (MCs) (Figure 5b-e). As expected at this earlier time point, we found 35 GO terms related to "Morphogenesis and development" (MC1, Figure 5b). MC2 encompassed "Cytoskeleton and extracellular matrix", and was generated based on 15 GO terms related to actin and microtubules dynamics and ECM organization (Figure 5c). Genes such as *Has1*, *Wnt11*, *Serpinb2*, *Pdgfb* and *Itgb3* were differentially expressed in this MC. The third MC, called "Chemotaxis and cytokines", comprised 10 GO terms related to immune cell chemotaxis, migration and cytokine activity (MC3, Figure 5d). Among the DEGs in MC3, we identified several genes involved in chemotaxis such as *Itgb1, Itga1, Tnfsf18, Cx3cr1, Il1b,* and *Icam1* (Figure 5f). MC4, called "Valvular cells activation and differentiation", included 52 GO-terms related to cellular activation, differentiation, proliferation,

adhesion, migration, with genes such as *Has1*, *Spp1*, *Edn1*, *Acta2* and *Tgfb2* being differentially expressed (Figure 5e). Altogether, the transcriptomic data show a dysregulation of the ECM organization coupled to cellular activation processes. This analysis also points to the emergence of a pro-inflammatory valvular micro-environment, which may contribute to the recruitment and accumulation of monocyte-derived macrophages occurring between D7 and D21.

Finally, we investigated potential pathways that may drive monocyte recruitment during the first weeks of age by comparing DEGs at D7 and D21 (from our previous analysis[24]). This analysis identified 82 common DEGs (Figure 5g). ORA of those genes pointed out the consistent activation of signaling pathways related to immune cell migration and chemotaxis (*Ccl7, Tnfsf18, Tgfbr1, Slit2, Csfr2b*). Interestingly, growth factor and BMP signaling pathways, which were consistently described as key players in the ECM remodeling leading to MVD, were also steadily modulated between these timepoints (Figure 5h).

Overall, the transcriptomic analysis reveals hallmarks of early MVD pathogenesis, including activation of signaling pathways involved in cytoskeleton dynamics, ECM remodeling, and valvular cell differentiation and activation. Interestingly, KI MVs exhibit a pro-inflammatory microenvironment, similar to that observed in human “end-stage” disease, which may contribute to ECM remodeling and promote macrophage recruitment and accumulation that likely occurs between D7 and D21 in rats.

DISCISSION

This study provides the first evidence of the central contribution of chemotaxis and macrophage recruitment and activation in the pathophysiological processes leading to human non-syndromic MVD. Based on the first transcriptomic analysis of a large collection of human non-syndromic MVD, we confirmed the activation of ECM remodeling, cytoskeleton organization, and TGF-β/BMP signaling pathways in the pathophysiology, and also highlighted a significant contribution of immune cells,

particularly macrophages, in this process. Interestingly, the MVD molecular signatures from human "end-stage" disease were also consistently reported over different early time-points in the FlnA-P637Q KI rat model of non-syndromic MVD. This common transcriptomic signature between human and KI rat MVD confirms the relevance of the FlnA-P637Q rat model to study the kinetics of the pathophysiological mechanisms leading to MVD. In newborn and D2 KI rats, we identified the molecular signature of MVD, which did not yet translate to morphological MV remodeling. At D7, the phenotypic and molecular screening revealed the presence of MVD associated with a pro-inflammatory microenvironment but without an increase in myeloid cells. Finally, at D21, we reported an abundance of myeloid cells in MV from KI rat. These findings highlight the gradual activation of the pathophysiological mechanisms associated with MVD following birth, which will later lead to a morphologically detectable MVD. Our results also support the role of myeloid cell recruitment, and specifically macrophages, that invaded the already remodeled MV leaflets, in the maintenance and/or progression of non-syndromic MVD, highlighting potential therapeutic targets to treat patients diagnosed with MVD.

Different cell populations were described in healthy and pathological MV tissues, each of them participating in the development, maturation and homeostasis of the valve.[7,13,15,37,38] Myxomatous MVD is mainly characterized by ECM remodeling with accumulation of proteoglycans, and until recently, most of the studies were focused on VICs, the fibroblast-like cells responsible for ECM production, to unravel the pathophysiological mechanisms leading to MVD. However, recent data emerged regarding the potential role of myeloid cells, and especially macrophages, in the development of myxomatous valve disorders and syndromic MVD,[6,7,15,17,18,39] although the sporadic form of MVD has always been considered as a non-inflammatory disease. By taking advantage of the transcriptomic analysis performed on a unique collection of human non-syndromic myxomatous MVD, we challenged this concept and confirmed an activation of leukocyte chemotaxis-related pathways conjointly with macrophage activation and accumulation at the end-stage of MVD. Together with a recent Mendelian randomization study integrating multi-omics data,[40] as well as previously published data in mice

462 models of bone marrow transplants and Marfan-related syndromic myxomatous MVD,[6,9,17,18,41] these
463 findings support the substantial contribution of macrophages and immune responses in the processes
464 leading to MVD.

465 The FlnA-P637Q rat model offers a unique opportunity to study the kinetics of the development of
466 MVD and activation/accumulation of macrophages. We observed a 2-fold increase in the proportion
467 of macrophages in myxomatous MVD from KI rats compared to controls at D21, with an ectopic
468 location of these cells invading the diseased tissue. This particular topography was also reported in
469 human “end-stage” disease, reinforcing the suitability of the rat model. The MV remodeling observed
470 in the context of non-syndromic MVD is characterized by important changes in the composition of the
471 ECM that likely modify the cellular sensing of mechanical stresses within the MV tissue. Interestingly,
472 it has been recently shown that dynamic forces related to fibroblast activation and ECM remodeling
473 act as a critical attractant signal for macrophages.[42–44] Moreover, hyaluronic acid binding proteins have
474 been implicated in triggering immune responses.[45,46] Our study reveals a dysregulation of the
475 hyaluronan synthesis and degradation pathway in KI MVs, characterized by upregulation of the
476 synthase *Has1* and downregulation of the hyaluronidase *Hyal1*. Together with the extensive Alcian
477 blue staining detected in KI valves, we thus postulate that the deregulation of valvular hyaluronan
478 homeostasis, as a marker of VIC activation, contributes to ECM remodeling and increased tissue-
479 specific mechanical stress, thereby providing a favorable context for monocyte and macrophage
480 attraction and activation in non-syndromic MVD.

481 Analysis of the early developmental disease stages in the FlnA-P637Q rat model shows a molecular
482 activation of VICs and VECs from birth onward that leads to morphologically observable MVD as early
483 as D7, with similar features to those observed at D21.[24] However, there was no difference in the
484 proportion of macrophages in the MV of these juvenile D7 rats, suggesting that the accumulation of
485 macrophages in MVD occurs between D7 and D21, and then more likely contributes to the
486 maintenance and/or progression of the disease, instead of its initiation. These findings are in line with

recently published data on Marfan-related syndromic MVD, where myeloid cell recruitment follows valve remodeling,[7] and where deficiency in recruited macrophages limited the progression of Marfan-related myxomatous MV disease.[18] However, the transposition of findings from Marfan syndrome-related MVD to the more common sporadic form of MVD remains limited, as Marfan syndrome is primarily characterized by elastin fragmentation,[47] which is known to act as a chemoattractant and may thus serve as the main trigger of macrophage recruitment in this context.[20–22] In non-syndromic MVD, where elastin fragmentation is less prominent, alternative mechanisms beyond elastin-mediated chemoattraction are likely to contribute to the pathophysiological process.

In our study, we reported a gradual activation of VECs coupled with the establishment of a pro-inflammatory valvular micro-environment, two potential contributing processes to macrophage recruitment. VEC activation, associated with an increased expression of endothelial cell adhesion molecules, such as *ICAM1*, has long been implicated in circulating monocyte recruitment in the context of other valve diseases.[48,49] Remarkably, *Icam1* was upregulated in KI MV as compared to WT at D7, supporting the pivotal role of VEC activation in both monocyte recruitment and the crosstalk with valve interstitial cells and macrophages during MVD development. The presence of a pro-inflammatory microenvironment in the absence of macrophage accumulation further supports the local activation of tissue-resident macrophages within the diseased valve, which may in turn promote additional macrophage recruitment via the release of chemoattractant cytokines such as *Ccl7*. The specific contribution of each mechanism and their potential crosstalk remains to be elucidated and will provide essential insights for therapeutic strategies targeting non-syndromic myxomatous MVD. By distinguishing the mechanisms involved in the initiation versus progression of the disease, we aim to refine the identification of optimal therapeutic targets for this frequent and life-threatening condition.

The present study has some limitations. First, the macroscopic evaluation of MV at D0 and D2 revealed heterogeneous and variable leaflet remodeling, which is likely reflective of the physiological immaturity and transitional remodeling processes occurring at these early postnatal stages. While

advanced imaging approaches, such as 3D rendering of the entire MV leaflets, could potentially improve discrimination between healthy and diseased valves, the rapid hemodynamic changes following birth, particularly the onset of systemic circulation, substantially alter the mechanical environment surrounding the MV. These biomechanical shifts likely contribute to the structural reorganization of the leaflets and may account for the disorganized morphology observed at early time points. Second, an inherent limitation of flow cytometry is the dependence on predefined antibody panels. In our case, this restricted the identification of all cellular subpopulations within the valve tissue. Although single-cell RNA-seq approaches would provide deeper insights into the cellular landscape and heterogeneity, such analyses were beyond the scope of the current study. Given the available tools for the rat model and in line with our previous work and published findings, we focused on the role of macrophages in MVD pathophysiology.[7,17,18,24,40]

In conclusion, by analyzing the first human MV transcriptome alongside a translationally relevant FlnA-P637Q KI rat model of non-syndromic myxomatous MVD, we identify a previously unrecognized contribution of macrophages to the pathophysiological processes underlying this disease. Our findings demonstrate that the gradual postnatal activation of disease-associated pathways leads to morphological manifestations of MVD within days after birth, followed by macrophage recruitment, which likely contributes to disease maintenance and/or progression. Although further work is needed to elucidate the underlying cellular crosstalk, our data point to monocyte-derived macrophages as potential therapeutic targets in non-syndromic myxomatous MVD.

Funding: The present study has received funding from the European Union's Horizon 2020 research and innovation program under the Marie Sklodowska-Curie grant agreement No. 846291, from the French Society of Cardiology under the "Alain Castaigne" scientific prize, both awarded to RC. The study has also received funding from the French Federation of Cardiology under the "dotation" grant 2023 awarded to RC and the "impulsion" grant 2023 awarded to JM. RC is also supported by a "Connect Talent" research chair from Région Pays de la Loire and Nantes Métropole. EM is funded by the Deutsche Forschungsgemeinschaft (DFG, German Research Foundation) under Germany's Excellence Strategy – EXC2151 – 390873048, SFB1454 (Project-ID 432325352), FOR5547 (Project-ID 503306912), FOR5775 (Project-ID 533863915), and by the European Research Council (ERC) under the European Union's Horizon 2020 research and innovation program (Grant Agreement No. 851257). BLV received a PhD scholarship from the Graduate Program InnoCARE of Nantes Université and from the Deutscher Akademischer Austauschdienst (DAAD, German Academic Exchange Service).

Author contribution: BLV, CD, JM, EM and RC contributed to the conception and experimental design of the study. BLV, CD, CT, PA, NBS, EC, JM, EM, and RC collected the data and participated in their analysis. SR and IA generated the rat model. VAM, VV, PP, SLS, JJS and TLT participated in the collection of human samples. BLV and CD drafted the original version of the manuscript. EM and RC reviewed, validated and approved the final version. BLV and CD contributed equally to this work. EM and RC provided equal supervision of the study. All authors critically reviewed the manuscript and contributed to editing the final version.

Acknowledgments: We thank the Cytocell cytometry facility in Nantes for their expert technical assistance. We acknowledge the IBISA MicroPICell facility (Biogenouest), a member of the national infrastructure France-Bioimaging supported by the French national research agency (ANR-10-INBS-04). We are most grateful to the Genomics Core Facility GenoA, member of Biogenouest and France

Genomique and to the Bioinformatics Core Facility BiRD, member of Biogenouest and Institut Français de Bioinformatique (IFB) (ANR-11-INBS-0013), as well as the Biomics Core Facility from Institut Pasteur (Paris, France) for the use of their resources and their technical support. We also acknowledge the Therassay and the UTE facilities of the Structure Fédérative de Recherche François Bonamy (Nantes, France) for technical assistance.

Conflict of Interest: None declared.

REFERENCES

1. Nkomo VT, Gardin JM, Skelton TN, Gottdiener JS, Scott CG, Enriquez-Sarano M. Burden of valvular heart diseases: a population-based study. *The Lancet* 2006;**368**:1005–1011.

2. Tsao CW, Aday AW, Almarzooq ZI, Alonso A, Beaton AZ, Bittencourt MS, Boehme AK, Buxton AE, Carson AP, Commodore-Mensah Y, Elkind MSV, Evenson KR, Eze-Nliam C, Ferguson JF, Generoso G, Ho JE, Kalani R, Khan SS, Kissela BM, Knutson KL, Levine DA, Lewis TT, Liu J, Loop MS, Ma J, Mussolino ME, Navaneethan SD, Perak AM, Poudel R, Rezk-Hanna M, Roth GA, Schroeder EB, Shah SH, Thacker EL, VanWagner LB, Virani SS, Voecks JH, Wang N-Y, Yaffe K, Martin SS. Heart Disease and Stroke Statistics-2022 Update: A Report From the American Heart Association. *Circulation* 2022;**145**:e153–e639.

3. Otto CM, Nishimura RA, Bonow RO, Carabello BA, Erwin JP, Gentile F, Jneid H, Krieger EV, Mack M, McLeod C, O'Gara PT, Rigolin VH, Sundt TM, Thompson A, Toly C. 2020 ACC/AHA Guideline for the Management of Patients With Valvular Heart Disease: A Report of the American College of Cardiology/American Heart Association Joint Committee on Clinical Practice Guidelines. *Circulation* 2021;**143**:e72–e227.

4. Praz F, Borger MA, Lanz J, Marin-Cuartas M, Abreu A, Adamo M, Ajmone Marsan N, Barili F, Bonaros N, Cosyns B, De Paulis R, Gamra H, Jahangiri M, Jeppsson A, Klautz RJM, Mores B, Pérez-David E, Pöss J, Prendergast BD, Rocca B, Rossello X, Suzuki M, Thiele H, Tribouilloy CM, Wojakowski W, ESC/EACTS Scientific Document Group, Vahanian A, Mestres C-A, Abid L, Aktaa S, Akowuah EF, Arbelo E, Asselbergs FW, Barbato E, Boriani G, Brida M, Buccheri S, Byrne RA, Chioncel O, Conradi L, De Bonis M, Delgado V, Franzone A, Haugaa KH, Heidecker B, Ibanez B, Iung B, James S, Køber L, Koskinas KC, Landmesser U, Lip GYH, McEvoy JW, Meltzer G, Messika-Zeitoun D, Mihaylova B, Mindham R, Moelgaard I, Nielsen JC, Owens G, Pasquet AA, Pilgrim T, Prescott E, Quintana E, Rudolph V, Sadaba R, Sannino A, Tanner FC, Urena M, Vaartjes I, Vrints C, Wahba A, Walther T, Witkowski A, Zeppenfeld K, Shuka N, Kichou B, Chilingaryan AL, Bartko PE, Samadov F, Van De Heyning CM, Kusljugic Z, Kinova E, Bulum J, Eftychiou C, Linkova H, Fosbøl E, Bahaa H, Truusalu J, Piuhola J, Donal E, Petriashvili S, Rudolph TK, Drakopoulou M, Kertész A, Guðmundsson H, Cole B, Carasso S, Navazio A, Sugralimova M, Bajraktari G, Kerimkulova A, Elgdhafi EO, Glaveckaite S, Lebrun F, Demarco DC, Lisii DM, Streukens S, Antova E, Dalen H, Kukulski T, Gavina C, Popescu BA, Bini R, Ivanov I, Hudec M, Bunc M, Bermejo TJ, Meurling CJC, Jeger R, Abid L, Degertekin MM, Nesukay EG, Garbi M, Mullabayeva G, Grabenwoeger M, Eynden FV, Vojacek J, Vincentelli A, Falk V, Dedeilias P, Parolari A, Braun J, Nikolic A, Ellensen VS, Sousa-Uva M, Micovic S, Legarra JJ, Ferrari E, Moorjani N. 2025 ESC/EACTS Guidelines for the management of valvular heart disease. *European Heart Journal* 2025:ehaf194.

5. Delwarde C, Capoulade R, Mérot J, Le Scouarnec S, Bouatia-Naji N, Yu M, Huttin O, Selton-Suty C, Sellal J-M, Piriou N, Schott J-J, Dina C, Le Tourneau T. Genetics and pathophysiology of mitral valve prolapse. *Front Cardiovasc Med* 2023;**10**:1077788.

6. Visconti RP, Ebihara Y, LaRue AC, Fleming PA, McQuinn TC, Masuya M, Minamiguchi H, Markwald RR, Ogawa M, Drake CJ. An In Vivo Analysis of Hematopoietic Stem Cell Potential: Hematopoietic Origin of Cardiac Valve Interstitial Cells. *Circulation Research* 2006;**98**:690–696.

7. Hulin A, Anstine LJ, Kim AJ, Potter SJ, DeFalco T, Lincoln J, Yutzey KE. Macrophage transitions in heart valve development and myxomatous valve disease. *Arterioscler Thromb Vasc Biol* 2018;**38**:636–644.

8. Hulin A, Hortells L, Gomez-Stallons MV, O'Donnell A, Chetal K, Adam M, Lancellotti P, Oury C, Potter SS, Salomonis N, Yutzey KE. Maturation of heart valve cell populations during postnatal remodeling. *Development* 2019;**146**:dev173047.

9. Hulin A, Moore V, James JM, Yutzey KE. Loss of Axin2 results in impaired heart valve maturation and subsequent myxomatous valve disease. *Cardiovasc Res* 2017;**113**:40–51.

10. Thalji NM, Hagler MA, Zhang H, Casaclang-Verzosa G, Nair AA, Suri RM, Miller JD. Nonbiased Molecular Screening Identifies Novel Molecular Regulators of Fibrogenic and Proliferative Signaling in Myxomatous Mitral Valve Disease. *Circ Cardiovasc Genet* 2015;**8**:516–528.

11. Geirsson A, Singh M, Ali R, Abbas H, Li W, Sanchez JA, Hashim S, Tellides G. Modulation of Transforming Growth Factor- Signaling and Extracellular Matrix Production in Myxomatous Mitral Valves by Angiotensin II Receptor Blockers. *Circulation* 2012;**126**:S189–S197.

12. Lavine KJ, Pinto AR, Epelman S, Kopecky BJ, Clemente-Casares X, Godwin J, Rosenthal N, Kovacic JC. The Macrophage in Cardiac Homeostasis and Disease: JACC Macrophage in CVD Series (Part 4). *J Am Coll Cardiol* 2018;**72**:2213–2230.

13. Liu K, Jin H, Tang M, Zhang S, Tian X, Zhang M, Han X, Liu X, Tang J, Pu W, Li Y, He L, Yang Z, Lui KO, Zhou B. Lineage tracing clarifies the cellular origin of tissue-resident macrophages in the developing heart. *J Cell Biol* 2022;**221**:e202108093.

14. Mass E, Nimmerjahn F, Kierdorf K, Schlitzer A. Tissue-specific macrophages: how they develop and choreograph tissue biology. *Nat Rev Immunol* 2023;**23**:563–579.

15. Shigeta A, Huang V, Zuo J, Besada R, Nakashima Y, Lu Y, Ding Y, Pellegrini M, Kulkarni RP, Hsiai T, Deb A, Zhou B, Nakano H, Nakano A. Endocardially Derived Macrophages Are Essential for Valvular Remodeling. *Developmental Cell* 2019;**48**:617-630.e3.

16. Bischoff J, Casanovas G, Wylie-Sears J, Kim D-H, Bartko PE, Guerrero JL, Dal-Bianco JP, Beaudoin J, Garcia ML, Sullivan SM, Seybolt MM, Morris BA, Keegan J, Irvin WS, Aikawa E, Levine RA. CD45 Expression in Mitral Valve Endothelial Cells After Myocardial Infarction. *Circ Res* 2016;**119**:1215–1225.

17. Sauls, K. *et al.* Increased Infiltration of Extra-Cardiac Cells in Myxomatous Valve Disease. *J Cardiovas Dev Dis* **2**, 200–213 (2015).

18. Kim AJ, Xu N, Umeyama K, Hulin A, Ponny SR, Vagnozzi RJ, Green EA, Hanson P, McManus BM, Nagashima H, Yutzey KE. Deficiency of Circulating Monocytes Ameliorates the Progression of Myxomatous Valve Degeneration in Marfan Syndrome. *Circulation* 2020;**141**:132–146.

19. Xu N, Yutzey KE. Therapeutic CCR2 Blockade Prevents Inflammation and Alleviates Myxomatous Valve Disease in Marfan Syndrome. *JACC: Basic Trans Sci* 2022;**7**:1143–1157.

20. Guo G, Booms P, Halushka M, Dietz HC, Ney A, Stricker S, Hecht J, Mundlos S, Robinson PN. Induction of Macrophage Chemotaxis by Aortic Extracts of the mgR Marfan Mouse Model and a GxxPG-Containing Fibrillin-1 Fragment. *Circulation* 2006;**114**:1855–1862.

21. Guo G, Gehle P, Doelken S, Martin-Ventura JL, Von Kodolitsch Y, Hetzer R, Robinson PN. Induction of Macrophage Chemotaxis by Aortic Extracts from Patients with Marfan Syndrome Is Related to Elastin Binding Protein. Ushio-Fukai M, ed. *PLoS ONE* 2011;**6**:e20138.

22. Radonic T, De Witte P, Groenink M, De Waard V, Lutter R, Van Eijk M, Jansen M, Timmermans J, Kempers M, Scholte AJ, Hilhorst-Hofstee Y, Van Den Berg MP, Van Tintelen JP, Pals G, Baars MJH, Mulder BJM, Zwinderman AH. Inflammation Aggravates Disease Severity in Marfan Syndrome Patients. Ahuja SK, ed. *PLoS ONE* 2012;**7**:e32963.

23. Gao F, Chen Q, Mori M, Li S, Ferrari G, Krane M, Fan R, Tellides G, Liu Y, Geirsson A. Integrin-mediated mTOR signaling drives TGF-β overactivity and myxomatous mitral valve degeneration in hypomorphic fibrillin-1 mice. *J Clin Invest* 2025:e183558.

24. Delwarde C, Toquet C, Aumond P, Kayvanjoo AH, Foucal A, Le Vely B, Baudic M, Lauzier B, Blandin S, Véziers J, Paul-Gilloteaux P, Lecointe S, Baron E, Massaiu I, Poggio P, Rémy S, Anegon I, Le Marec H, Monassier L, Schott J-J, Mass E, Barc J, Le Tourneau T, Merot J, Capoulade R. Multimodality imaging and transcriptomics to phenotype mitral valve dystrophy in a unique knock-in Filamin-A rat model. *Cardiovasc Res* 2023;**119**:759–771.

25. Subramanian A, Tamayo P, Mootha VK, Mukherjee S, Ebert BL, Gillette MA, Paulovich A, Pomeroy SL, Golub TR, Lander ES, Mesirov JP. Gene set enrichment analysis: A knowledge-based approach for interpreting genome-wide expression profiles. *Proc Natl Acad Sci USA* 2005;**102**:15545–15550.

26. Aran D, Hu Z, Butte AJ. xCell: digitally portraying the tissue cellular heterogeneity landscape. *Genome Biol* 2017;**18**:220.

27. Durinck S, Spellman PT, Birney E, Huber W. Mapping identifiers for the integration of genomic datasets with the R/Bioconductor package biomaRt. *Nat Protoc* 2009;**4**:1184–1191.

28. Remy S, Chenouard V, Tesson L, Usal C, Ménoret S, Brusselle L, Heslan J-M, Nguyen TH, Bellien J, Merot J, De Cian A, Giovannangeli C, Concordet J-P, Anegon I. Generation of gene-edited rats by delivery of CRISPR/Cas9 protein and donor DNA into intact zygotes using electroporation. *Sci Rep* 2017;**7**:16554.

29. Cokelaer T, Desvillechabrol D, Legendre R, Cardon M. 'Sequana': a Set of Snakemake NGS pipelines. *JOSS* 2017;**2**:352.

30. Desvillechabrol D, Legendre R, Rioualen C, Bouchier C, Van Helden J, Kennedy S, Cokelaer T. Sequanix: a dynamic graphical interface for Snakemake workflows. Hancock J, ed. *Bioinformatics* 2018;**34**:1934–1936.

31. Köster J, Rahmann S. Snakemake—a scalable bioinformatics workflow engine. *Bioinformatics* 2012;**28**:2520–2522.

32. Chen S, Zhou Y, Chen Y, Gu J. fastp: an ultra-fast all-in-one FASTQ preprocessor. *Bioinformatics* 2018;**34**:i884–i890.

33. Dobin A, Davis CA, Schlesinger F, Drenkow J, Zaleski C, Jha S, Batut P, Chaisson M, Gingeras TR. STAR: ultrafast universal RNA-seq aligner. *Bioinformatics* 2013;**29**:15–21.

34. Liao Y, Smyth GK, Shi W. featureCounts: an efficient general purpose program for assigning sequence reads to genomic features. *Bioinformatics* 2014;**30**:923–930.

35. Ewels P, Magnusson M, Lundin S, Käller M. MultiQC: summarize analysis results for multiple tools and samples in a single report. *Bioinformatics* 2016;**32**:3047–3048.

685 36. Love MI, Huber W, Anders S. Moderated estimation of fold change and dispersion for RNA-seq
686 data with DESeq2. *Genome Biol* 2014;**15**:550.

687 37. Nakano H, Liu X, Arshi A, Nakashima Y, Handel B van, Sasidharan R, Harmon AW, Shin J-H,
688 Schwartz RJ, Conway SJ, Harvey RP, Pashmforoush M, Mikkola HKA, Nakano A. Haemogenic
689 endocardium contributes to transient definitive haematopoiesis. *Nat Commun* 2013;**4**:1564.

690 38. Yzaguirre AD, Speck NA. Insights into blood cell formation from hemogenic endothelium in lesser-
691 known anatomic sites. *Dev Dyn* 2016;**245**:1011–1028.

692 39. Dal-Bianco JP, Aikawa E, Bischoff J, Guerrero JL, Hjortnaes J, Beaudoin J, Szymanski C, Bartko PE,
693 Seybolt MM, Handschumacher MD, Sullivan S, Garcia ML, Mauskapf A, Titus JS, Wylie-Sears J,
694 Irvin WS, Chaput M, Messas E, Hagège AA, Carpentier A, Levine RA. Myocardial Infarction Alters
695 Adaptation of the Tethered Mitral Valve. *J Am Coll Cardiol* 2016;**67**:275–287.

696 40. Minvielle Moncla L-H, Briend M, Sokhna Sylla M, Mathieu S, Rufiange A, Bossé Y, Mathieu P.
697 Mendelian randomization reveals interactions of the blood proteome and immunome in mitral
698 valve prolapse. *Commun Med* 2024;**4**:108.

699 30. Kim, A. J., Xu, N. & Yutzey, K. E. Macrophage lineages in heart valve development and disease.
700 *Cardiovas Res.* **117**, 663–673 (2021).

701 42. Adlerz KM, Aranda-Espinoza H, Hayenga HN. Substrate elasticity regulates the behavior of human
702 monocyte-derived macrophages. *Eur Biophys J* 2016;**45**:301–309.

703 43. Pakshir P, Alizadehgiashi M, Wong B, Coelho NM, Chen X, Gong Z, Shenoy VB, McCulloch CA, Hinz
704 B. Dynamic fibroblast contractions attract remote macrophages in fibrillar collagen matrix. *Nat*
705 *Commun* 2019;**10**:1850.

706 44. Charras G, Sahai E. Physical influences of the extracellular environment on cell migration. *Nat*
707 *Rev Mol Cell Biol* 2014;**15**:813–824.

708 45. Proudfoot AEI, Handel TM, Johnson Z, Lau EK, LiWang P, Clark-Lewis I, Borlat F, Wells TNC, Kosco-
709 Vilbois MH. Glycosaminoglycan binding and oligomerization are essential for the in vivo activity
710 of certain chemokines. *Proc Natl Acad Sci U S A* 2003;**100**:1885–1890.

711 46. Gray AL, Pun N, Ridley AJL, Dyer DP. Role of extracellular matrix proteoglycans in immune cell
712 recruitment. *Int J Experimental Path* 2022;**103**:34–43.

713 47. Milewicz DM, Braverman AC, De Backer J, Morris SA, Boileau C, Maumenee IH, Jondeau G,
714 Evangelista A, Pyeritz RE. Marfan syndrome. *Nat Rev Dis Primers* 2021;**7**:1–24.

715 48. Levine RA, Hagége AA, Judge DP, Padala M, Dal-Bianco JP, Aikawa E, Beaudoin J, Bischoff J,
716 Bouatia-Naji N, Bruneval P, Butcher JT, Carpentier A, Chaput M, Chester AH, Clusel C, Delling FN,
717 Dietz HC, Dina C, Durst R, Fernandez-Friera L, Handschumacher MD, Jensen MO, Jeunemaitre XP,
718 Marec HL, Tourneau TL, Markwald RR, Mérot J, Messas E, Milan DP, Neri T, Norris RA, Peal D,
719 Perrocheau M, Probst V, Pucéat M, Rosenthal N, Solis J, Schott J-J, Schwammenthal E,
720 Slaugenhaupt SA, Song J-K, Yacoub MH. Mitral valve disease—morphology and mechanisms. *Nat*
721 *Rev Cardiol* 2015;**12**:689–710.

722 38. Delwarde, C. *et al.* Genetics and pathophysiology of mitral valve prolapse. *Front. Cardiovasc.*
723 *Med.* **10**, (2023).

724

FIGURE LEGENDS

Figure 1: Transcriptomic analysis of human end-stage non-syndromic MVD. a. Analysis workflow of 78 human MVD samples. **b.** Violin plot showing the expression level of 18 genes among the list of the most 2000 expressed genes. The numbers in brackets correspond to the position of the gene on the ranked gene list. **c.** GSEA of Gene-Ontology Biological Process (GOBP) and KEGG pathways identified based on the top 2000 ranked genes expression. **d.** Enrichplot of the immune KEGG pathway. **e.** Deconvolution of the expression data using xCell showing the enrichment score of 17 immune cell types. **f.** Human control MV (n=1) and non-syndromic MVD (n=1) analysis: HES and CD68 staining showed ECM remodeling and an increase in macrophage signal in MVD as compared to the control valve. Scale bars are 2.5 mm, 500 µm or 100µm. **g.** Comparative analysis of the top 2000 most expressed genes in human MVD and *FLNA*-KI rat model. The 951 common genes were analyzed with GSEA. The dotplot represents the most relevant and significant GO terms. HES: Hematoxylin Eosin Saffron, KI: Knock-In, MV: Mitral Valve, MVD: Mitral Valve Dystrophy.

Figure 2: Identification of cell populations in the mitral valve and their location in 21-day-old KI and WT animals. a. Workflow of the experiments indicating markers used for the identification of cell types. **b.** Gating strategy for cell sorting and cell number analysis to determine their relative proportions within the MV tissue. Live single cells were gated on CD45 expression for hematopoietic lineage. $CD45^+$ cells were then gated with CD11b and CD206 to identify myeloid cells. $CD45^-$ cells were gated with CD31 to identify VECs. The negative cells for all markers were considered as VICs. **c.** Histogram showing the relative proportion of VICs, VECs and $CD45^+$ cells in MV from KI and WT 21-day-old rats (n=6 for WT and KI). **d.** Barplot representation of the $CD45^+$ cells showing increased proportion of myeloid cells ($CD45^+$ $CD206^+$ and/or $CD11b^+$, n=6 individual experiments for WT and KI, performed with a pool of 7 to 10 rat's MV from the same litter). **e.** Immunostainings of $CD45^+$ and $CD206^+$ cells in WT and KI MV showing that leukocytes/macrophages lined up in the sub-endothelial atrial layer in WT

750 animals, whereas they were present more diffusely in KI animals. A 20x magnification was applied to
751 the posterior leaflet. Scale bars are 500 µm or 100 µm. *: p<0.05, **: p<0.01 from Mann-Whitney test.
752 KI: Knock-In, LA: Left Atrium, LV: Left Ventricle; VECs: Valvular Endothelial Cells; VICs: Valvular
753 Interstitial Cells; WT: Wild-Type.

754

755 **Figure 3: Histological and molecular evaluation of WT and KI mitral valves at D2 and D0. a.** Newborn
756 (D0) histological evaluation based on Hematoxylin Phloxine Saffron (HPS, left) and Alcian Blue (right)
757 staining in serial MV sections for WT (top) and KI (bottom) animals. **b.** 2-day-old (D2) histology
758 evaluation based on HPS (left) and Alcian Blue (right) staining in serial MV sections for WT (top) and KI
759 (bottom) animals. Images are representative of 12 WT and 12 KI animals, at D0 and D2. Scale bar = 250
760 µm and 50µm. **c.** Fold-changes of the gene expression levels between KI and WT for the extracellular
761 matrix-related genes *Has1* and *Hyal1*, at D0 and D2. **d.** Fold-changes of the gene expression levels
762 between KI and WT for the endothelium activation-related gene *Esm1*, at D0 and D2. **e.** Fold-changes
763 of the gene expression levels between KI and WT for the inflammation-related genes *Ccl7* and *Tnfsf18*,
764 at D0 and D2. n = 10-22 rat's MV. *: p<0.05, **: p<0.01, ***: p<0.001 from Mann-Whitney test. KI:
765 Knock-In; WT: Wild-Type.

766

767 **Figure 4: Phenotyping of WT and KI mitral valves at D7. a.** Representative images of the mitral valve
768 in WT and KI animals, showing the thickening of both anterior and posterior leaflets in KI animals
769 compared to WT. Scale bars are 500µm **b.** Standard histological evaluation based on HPS and Alcian
770 Blue staining of WT and KI MV. Magnification of regions of interest shows flat endothelial cells in WT
771 (blue box) and turgescent endothelial cells in KI (red box). Images are representative of 16 WT and 15
772 KI animals. Scale bars are 250 µm and 15µm. **c.** Histological score to grade MV remodeling (n=16 for
773 WT and n=15 for KI, all biological replicates). **d-f.** Quantification of the proteoglycans content
774 estimated by the proportion of Alcian Blue in the whole MV (**d**), and in the anterior (**e**) or posterior

leaflet (**f**) (n=13 for WT and n=12 for KI, all biological replicates). **g.** Gating of hematopoietic cells with CD45 expression and sub-gating for myeloid cells with CD11b and CD206 expression. **h.** Relative proportion of VICs, VECs, and $CD45^+$ cells in MV from 7-day-old rats. n=10 for KI and n=9 for WT. **i.** Barplot representation of the $CD45^+$ cells based on CD11b and CD206 expression (n=10 individual experiments for WT and n=9 for KI, each experiment was performed with a pool of 7 to 10 rat's MV from the same litter). **j.** Immunostainings of $CD45^+$, $CD206^+$ and $CD31^+$ cells in WT and KI mitral valve. Scale bars are 200 µm or 100 µm. *: $p<0.05$, ***: $p<0.001$ from Mann-Whitney test. Ant: Anterior leaflet; KI: Knock-In; LA: Left Atrium, LV: Left Ventricle; Post: Posterior leaflet; VECs: Valvular Endothelial Cells; VICs: Valvular Interstitial Cells; WT: Wild-Type.

Figure 5: Transcriptomic analysis of WT and KI mitral valves at D7. a. Schematic representation of the analysis. 6 WT and 6 KI MV were sequenced, resulting in the identification of 2250 DEGs. **b-e**. Gene Set Enrichment Analysis (GSEA) identified 173 enriched GO terms that were further used to build Metaclusters (MC). Dot plots are representative of the GO terms in the corresponding metacluster. **f.** Heatmap of representative genes from MC3 showing upregulation of chemotaxis and cytokine related genes in KI animals. **g.** Venn diagram of the KI vs WT DEGs at D7 and D21. **h.** GSEA of the overlapping 82 DEGs at both D7 and D21. DEG: Differentially Expressed Gene, GO: Gene Ontology, KI: Knock-In, MC: Metacluster, MV: Mitral Valve, WT: Wild-Type.

FIGURE 1

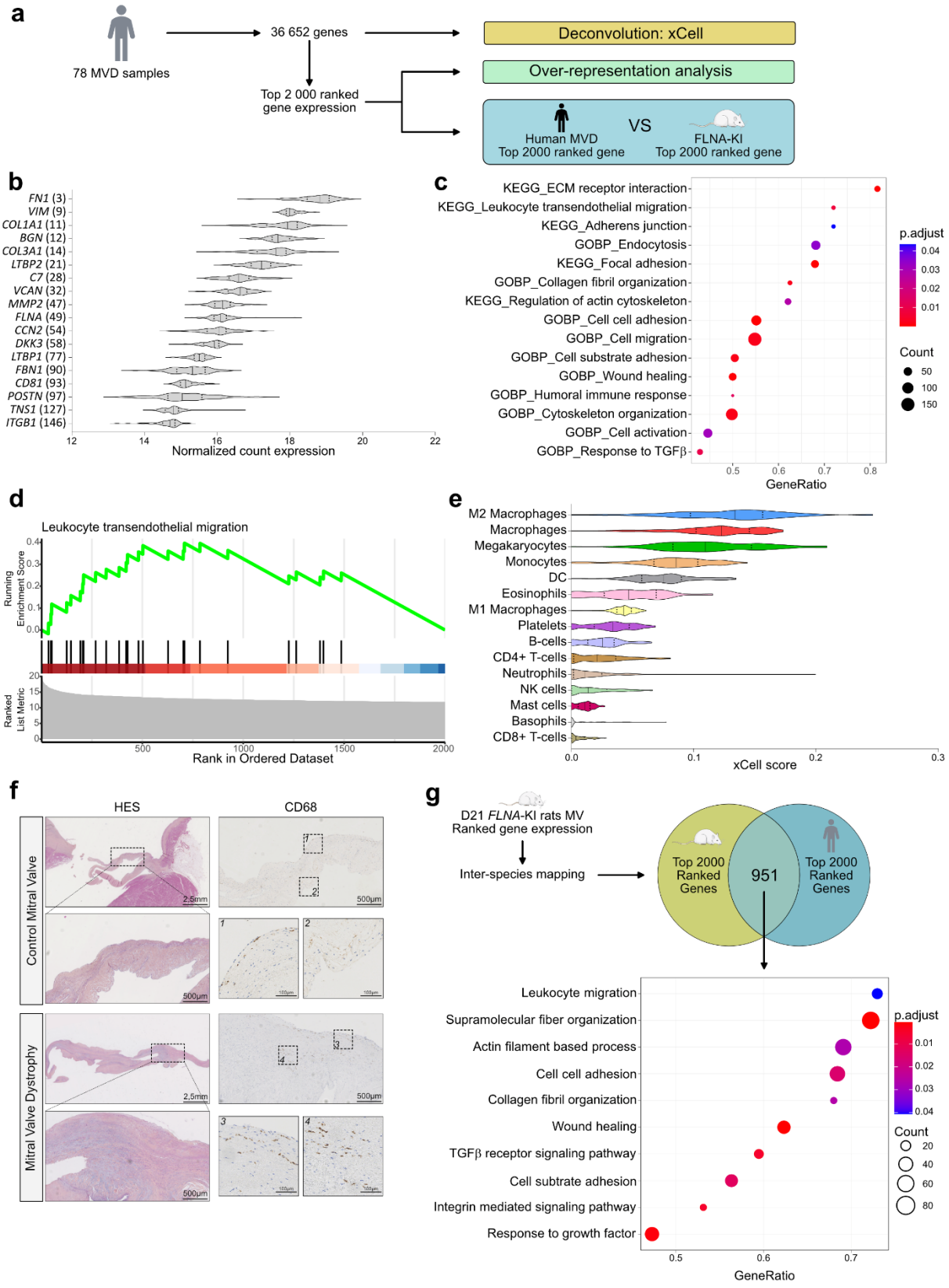
a
78 MVD samples
36 652 genes
Top 2 000 ranked gene expression
Deconvolution: xCell
Over-representation analysis
Human MVD Top 2000 ranked gene
VS
FLNA-KI Top 2000 ranked gene
b
FN1 (3)
VIM (9)
COL1A1 (11)
BGN (12)
COL3A1 (14)
LTBP2 (21)
C7 (28)
VCAN (32)
MMP2 (47)
FLNA (49)
CCN2 (54)
DKK3 (58)
LTBP1 (77)
FBN1 (90)
CD81 (93)
POSTN (97)
TNS1 (127)
ITGB1 (146)
Normalized count expression
c
KEGG_ECM receptor interaction
KEGG_Leukocyte transendothelial migration
KEGG_Adherens junction
GOBP_Endocytosis
KEGG_Focal adhesion
GOBP_Collagen fibril organization
KEGG_Regulation of actin cytoskeleton
GOBP_Cell cell adhesion
GOBP_Cell migration
GOBP_Cell substrate adhesion
GOBP_Wound healing
GOBP_Humoral immune response
GOBP_Cytoskeleton organization
GOBP_Cell activation
GOBP_Response to TGFβ
GeneRatio
p.adjust
Count
d
Leukocyte transendothelial migration
Running Enrichment Score
Ranked List Metric
Rank in Ordered Dataset
e
M2 Macrophages
Macrophages
Megakaryocytes
Monocytes
DC
Eosinophils
M1 Macrophages
Platelets
B-cells
CD4+ T-cells
Neutrophils
NK cells
Mast cells
Basophils
CD8+ T-cells
xCell score
f
HES
CD68
Control Mitral Valve
Mitral Valve Dystrophy
g
D21 FLNA-KI rats MV Ranked gene expression
Inter-species mapping
Top 2000 Ranked Genes
951
Top 2000 Ranked Genes
Leukocyte migration
Supramolecular fiber organization
Actin filament based process
Cell cell adhesion
Collagen fibril organization
Wound healing
TGFβ receptor signaling pathway
Cell subtrate adhesion
Integrin mediated signaling pathway
Response to growth factor
GeneRatio
p.adjust
Count

FIGURE 2

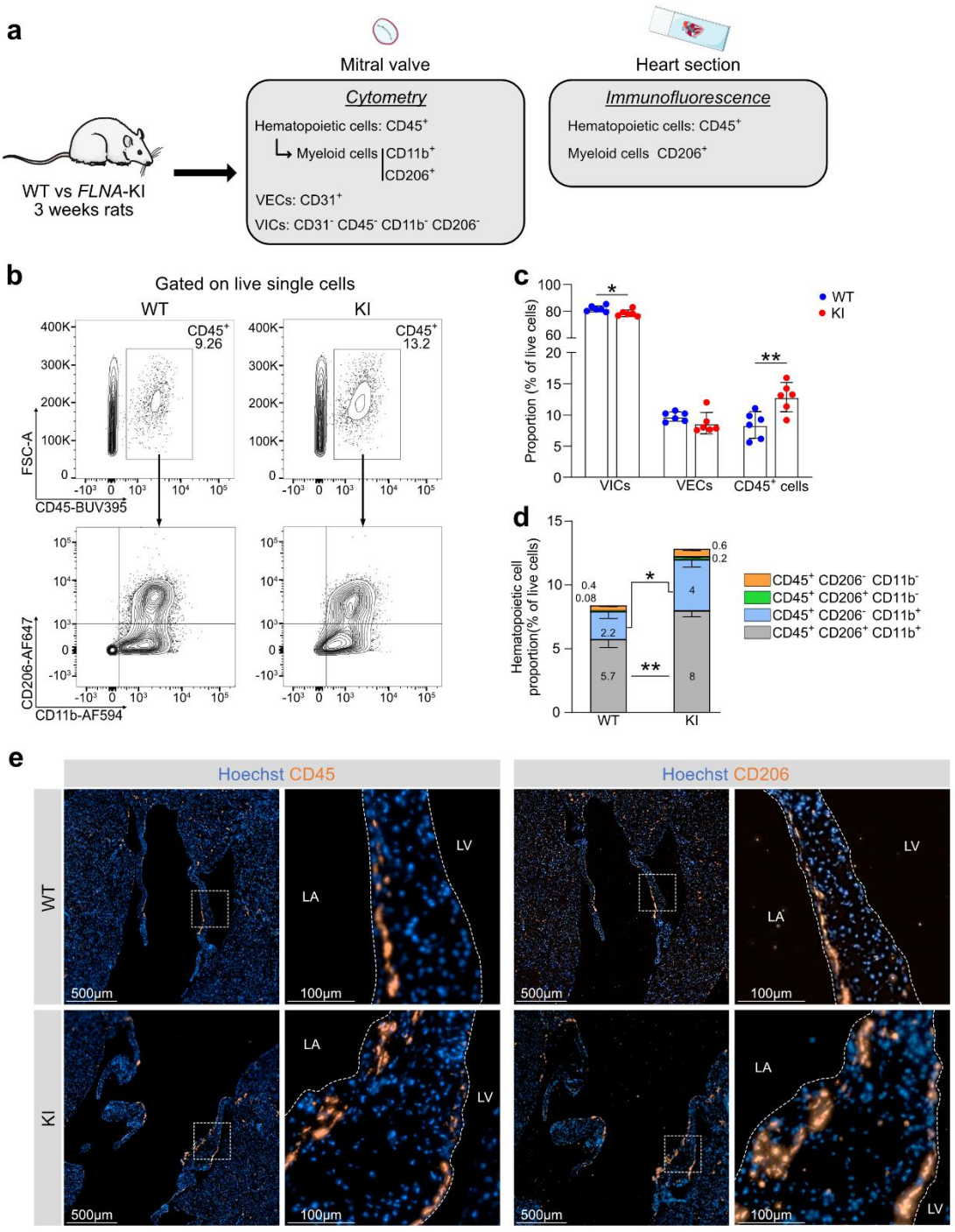
a
Mitral valve
Heart section
Cytometry
Hematopoietic cells: CD45+
Myeloid cells CD11b+ CD206+
VECs: CD31+
VICs: CD31- CD45- CD11b- CD206-
Immunofluorescence
Hematopoietic cells: CD45+
Myeloid cells CD206+
WT vs FLNA-KI
3 weeks rats
b
Gated on live single cells
WT
KI
CD45+ 9.26
CD45+ 13.2
FSC-A
CD45-BUV395
CD206-AF647
CD11b-AF594
c
Proportion (% of live cells)
WT
KI
VICs
VECs
CD45+ cells
d
Hematopoietic cell proportion(% of live cells)
CD45+ CD206- CD11b-
CD45+ CD206+ CD11b-
CD45+ CD206- CD11b+
CD45+ CD206+ CD11b+
e
Hoechst CD45
Hoechst CD206
WT
KI
LV
LA
500µm
100µm

FIGURE 3

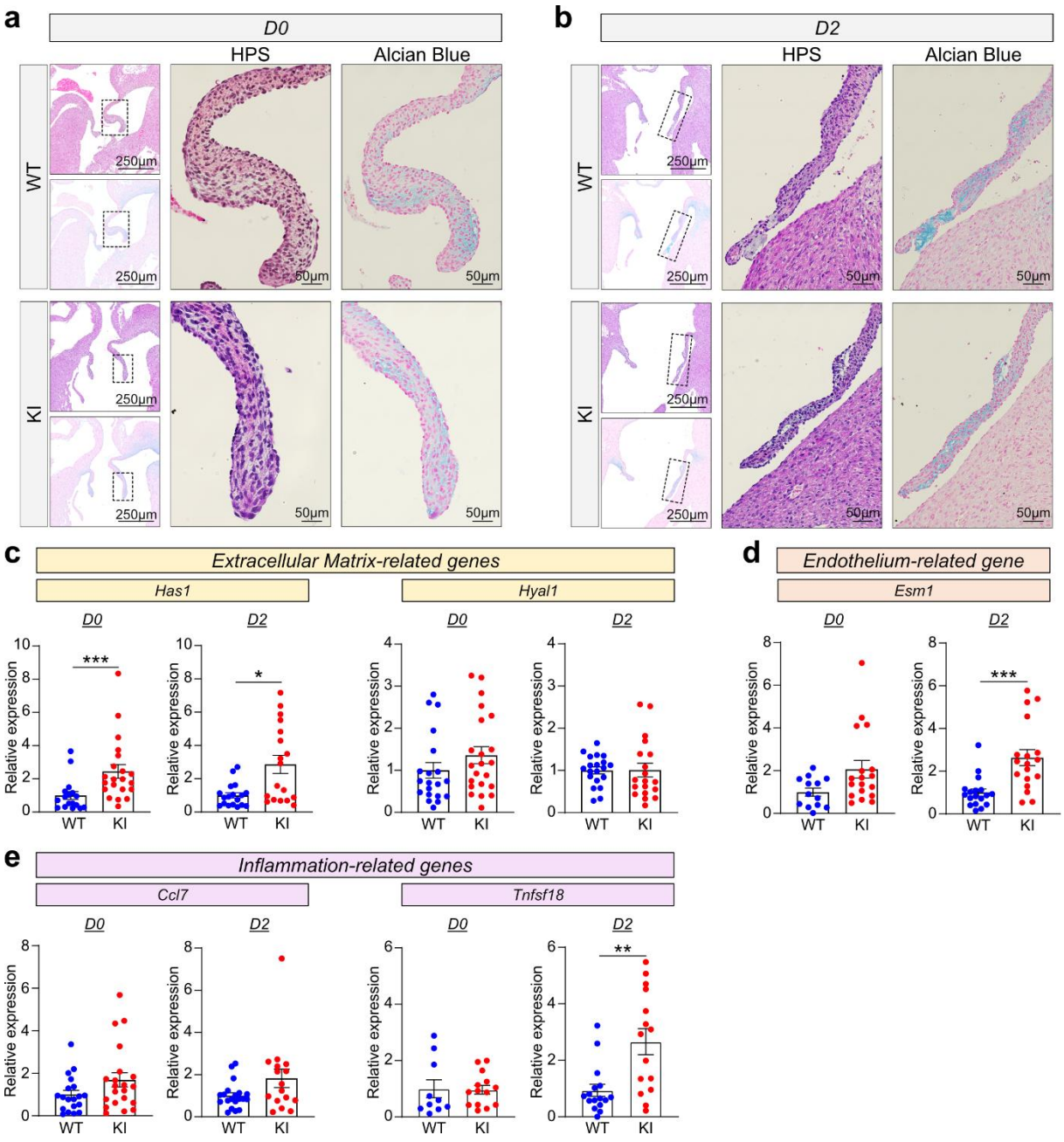
a
D0
HPS
Alcian Blue
WT
KI
250µm
50µm
b
D2
HPS
Alcian Blue
WT
KI
250µm
50µm
c
Extracellular Matrix-related genes
Has1
Hyal1
D0
D2
Relative expression
WT
KI
***
*
d
Endothelium-related gene
Esm1
***
e
Inflammation-related genes
Ccl7
Tnfsf18
**

FIGURE 4

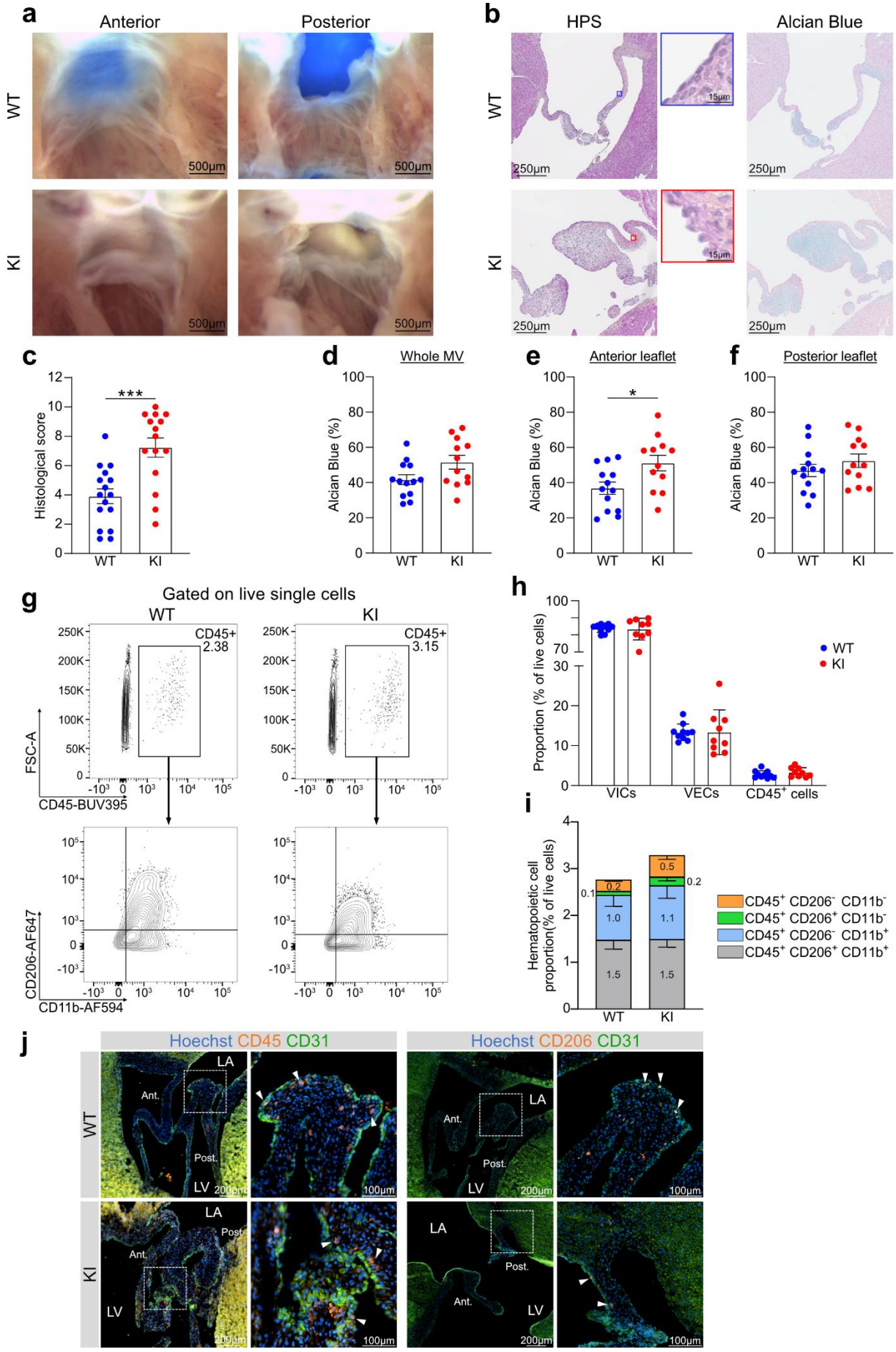
a
Anterior
Posterior
WT
KI
500µm
b
HPS
Alcian Blue
15µm
250µm
c
Histological score
***
WT
KI
d
Whole MV
Alcian Blue (%)
e
Anterior leaflet
*
f
Posterior leaflet
g
Gated on live single cells
CD45+ 2.38
CD45+ 3.15
FSC-A
CD45-BUV395
CD206-AF647
CD11b-AF594
h
Proportion (% of live cells)
VICs
VECs
CD45+ cells
i
Hematopoietic cell proportion(% of live cells)
CD45+ CD206- CD11b-
CD45+ CD206+ CD11b-
CD45+ CD206- CD11b+
CD45+ CD206+ CD11b+
j
Hoechst CD45 CD31
Hoechst CD206 CD31
LA
Ant.
Post.
LV
200µm
100µm

800

FIGURE 5

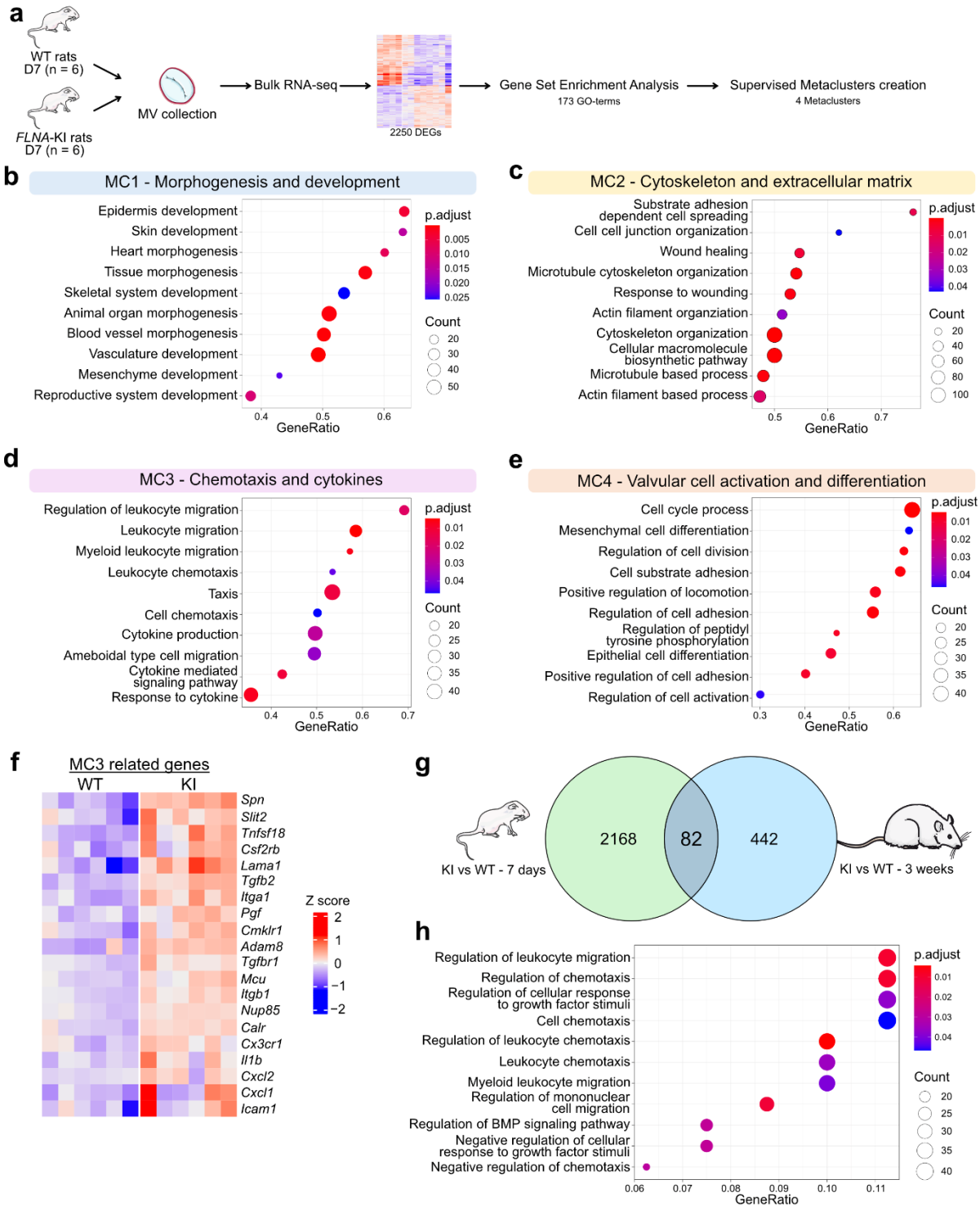

801

802

803 **GRAPHICAL ABSTRACT**

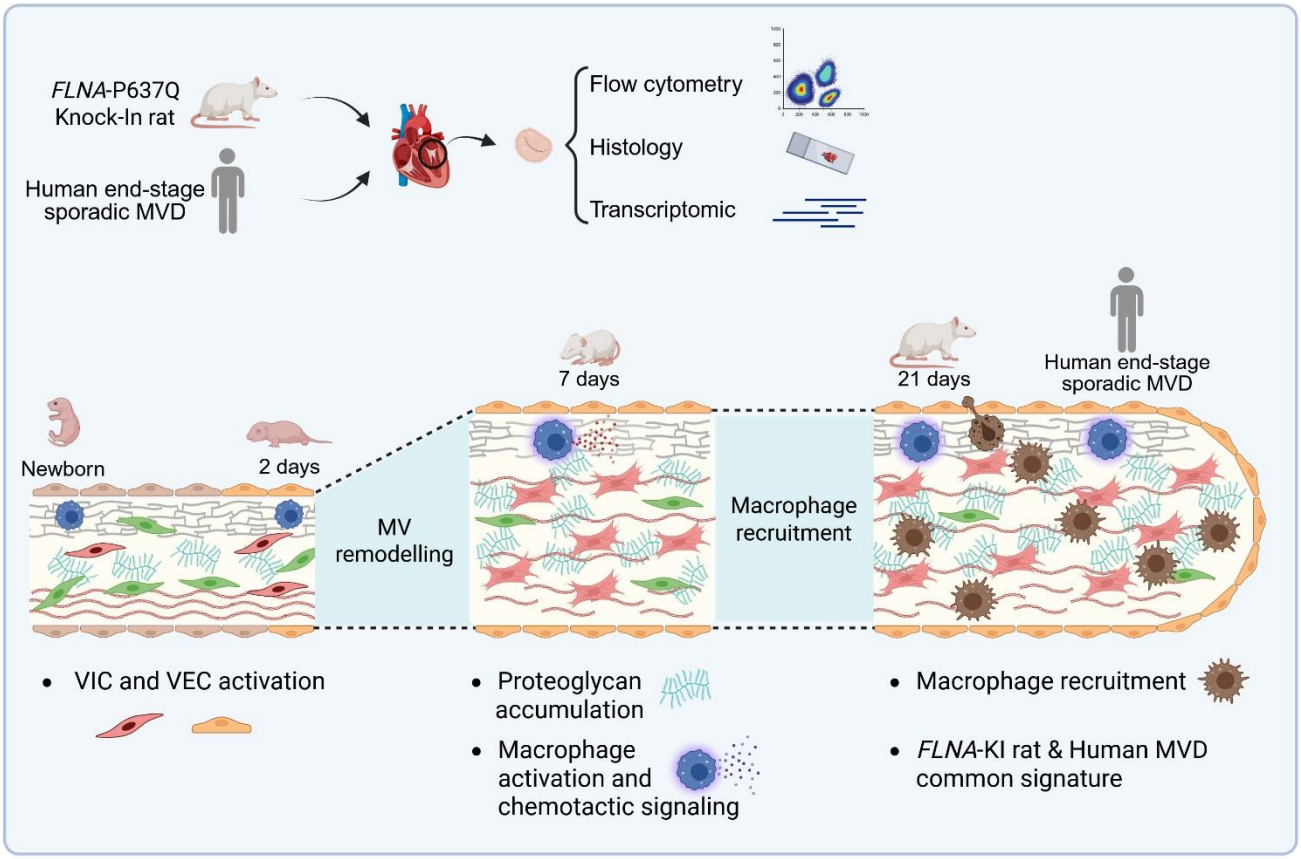

804

SUPPLEMENTARY MATERIALS FOR

Macrophage Recruitment is a hallmark of Non-syndromic Mitral Valve Dystrophy

Benjamin Le Vely,[#] Constance Delwarde,[#] Claire Toquet, Pascal Aumond, Nelli Blank-Stein, Emilie Charon, Séverine Rémy, Ignacio Anegon, Veronika A. Myasoedova, Vincenza Valerio, Paolo Poggio, Solena Le Scouarnec, Jean-Jacques Schott, Thierry Le Tourneau, Jean Merot, Elvira Mass,* Romain Capoulade,*

SUPPLEMENTARY TABLE S1: List of Antibodies

Application	Antibody	Reference	Concentration (µg/ml)	Fluorophore	Clone	Isotype	Excitation laser
Flow Cytometry	**CD45**	BD Bioscience 740258	2	BUV395	30-F11	IgG2b,κ	UV (355 nm, 100mW)
Flow Cytometry	**CD206**	Santa cruz sc-58986	1,5	AF647	15-2	IgG1,κ	R (637 nm, 140mW)
Flow Cytometry	**CD31**	Novus NB100-64796PE	1	PE	TLD-3A12	IgG1	YG (561 nm, 200mW)
Flow Cytometry	**CD11b**	Novus NB100-65284AF594	1	AF594	OX-42	IgG2a	YG (561 nm, 200mW)
IHC	**CD68**	DakoCytomation M0876	1/200				
IF	**CD206**	ProteinTech, 60143-1-Ig	1/10000				
IF	**CD45**	Gift from TRIP platform	1/200				
IF	**CD31**	Novus, Nß100-2284	1/100				
IF	**Goat anti-Mouse**	ThermoFisher, A10037	1/1000				
IF	**Goat anti-Rabbit**	ThermoFisher, A21206	1/1000				

Legend: Antibodies used for flow cytometry, immunofluorescence (IF) and immunohistochemistry (IHC) experiments.

SUPPLEMENTARY TABLE S2: Histological Criteria used for the Grading of Myxomatous MVD at D7

Criteria	Grading
Thickened anterior leaflet	0 / 0.5 / 1
Thickened posterior leaflet	0 / 0.5 / 1
Thickened free edge	0 / 0.5 / 1
Thickened medial part	0 / 0.5 / 1
Remodeled tricuspid valve	0 / 0.5 / 1
Leaflet redundancy	0 / 0.5 / 1
Turgescent or proliferative zone	0 / 0.5 / 1
Immature anterior leaflet	0 / 0.5 / 1
Immature posterior leaflet	0 / 0.5 / 1
Presence of collagen	0 / 0.5 / 1
Diffuse Alcian Blue staining	0 / 0.5 / 1

Legend: Histological criteria used to characterize mitral valve phenotype in 7-day-old rats. Phenotype was graded as absent (0), intermediate phenotype (0.5) and present (1).

SUPPLEMENTARY TABLE S3: Sequences of the primers used for molecular phenotyping of the Mitral Valve

Gene	Forward	Reverse
Ccl7	GTGTCCCTGGGAAGCTGTTA	CACAGACTTCCATGCCCTTT
Esm1	TGATTTCGGTGACGAGTTTG	AAGGGGAAGTCCAGACACCT
Gapdh	TCATACTTGGCAGGTTTCTCC	CTGAACGGGAAGCTCACTG
Has1	GGGCGTCTCTGAATAGCATC	CATGGGCTACGCTACCAAGT
Hyal1	ATGTGCCCATAATGCCCTAC	AGCTCCTCCAGGGGTAGAAG
Tnfsf18	ACACACGTGTCCCCGAGATA	TTCTTCCATCTGCTCCCCAC

Legend: Sequences of the primers used in qPCR.

SUPPLEMENTARY TABLE S4: Characteristics of the Patients

Variables	n=78
Clinical	
Age, years	61 ±11
Male gender, %	77%
Height, cm	173 ±9
Weight, kg	74 ±13
Body surface area, m^2	1.88 ±0.19
Body mass index, $kg.m^{-2}$	25 ±3.4
Sinus rhythm, %	90%
History of hypertension, %	51%
Systolic blood pressure, mm Hg	126 ±11
Diastolic blood pressure, mm Hg	74 ±8
Diabetes, %	5%
Dyslipidemia, %	22%
History of smoking, %	37%
Doppler-echocardiographic data	
LV end diastolic diameter, mm	58 ±8
LV end systolic diameter, mm	38 ±6
LV ejection fraction, %	64 ±7
Severity of MR	
Moderate-to-severe, %	9%
Severe, %	91%
Etiology of MVD	
Isolated P2, %	44%
Bileafets, %	56%

Legend: LV: left ventricle, MV: mitral valve, MVD: mitral valve dystrophy, MR: mitral regurgitation. Values are mean ±SD or percentage.

SUPPLEMENTARY TABLE S5: List of GSEA Biological Process and KEGG pathways obtained from the 2000 most expressed genes in the human RNA-seq data

Complete list of the GO-terms and the 2000 ranked gene list is presented in the attached Excel file called “Extended data from Human MVD RNA-seq”.

SUPPLEMENTARY TABLE S6: List of GSEA Biological Process obtained from Rat RNA-seq data at D7

Complete list of the GO-terms is presented in the attached Excel file called “Extended data from Rat MV RNA-seq at D7”

SUPPLEMENTARY FIGURE S1

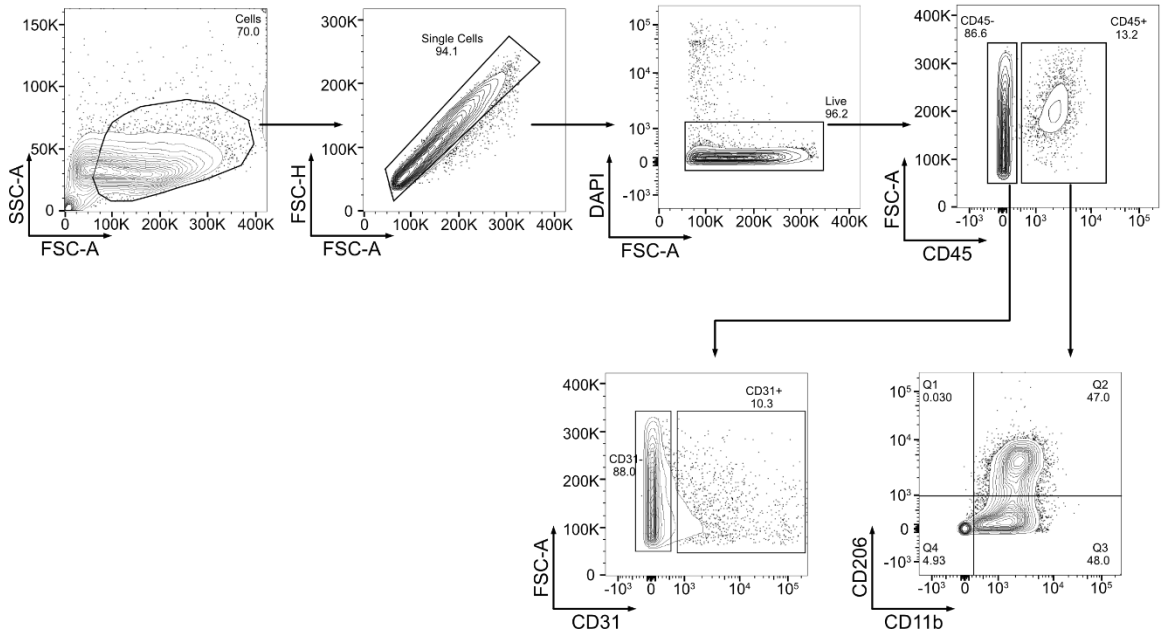

Legend: Gating strategy for flow cytometry analysis of D21 and D7 mitral valve from WT and KI rats.

SUPPLEMENTARY FIGURE S2

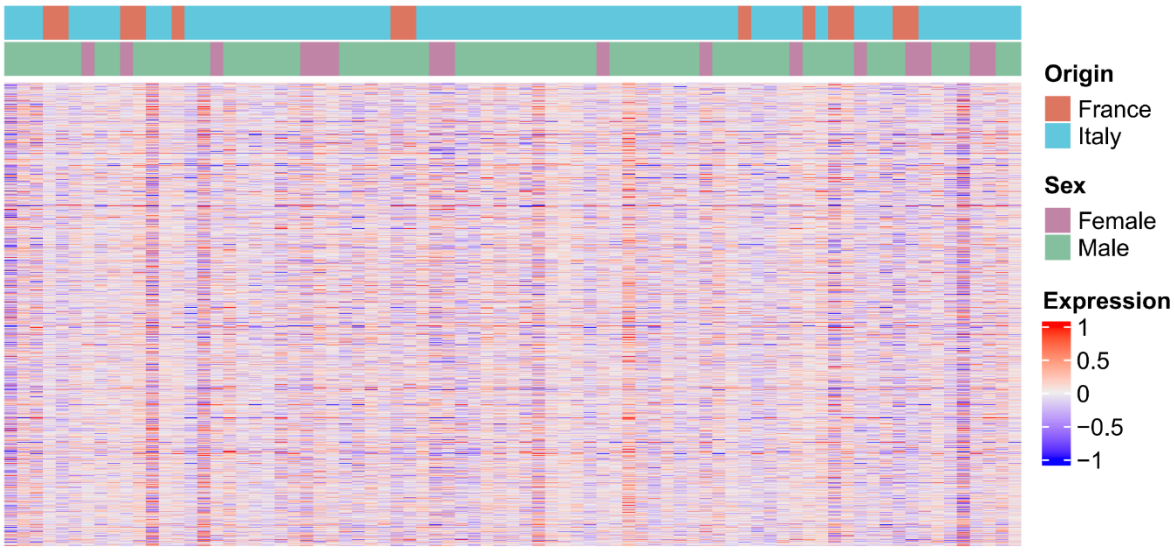

Legend: Heatmap of the top 2000 highly expressed genes across the 78 samples of human MVD. Origin of the tissue as well as sex of the patients had no impact on the clustering of these samples.

SUPPLEMENTARY FIGURE S3

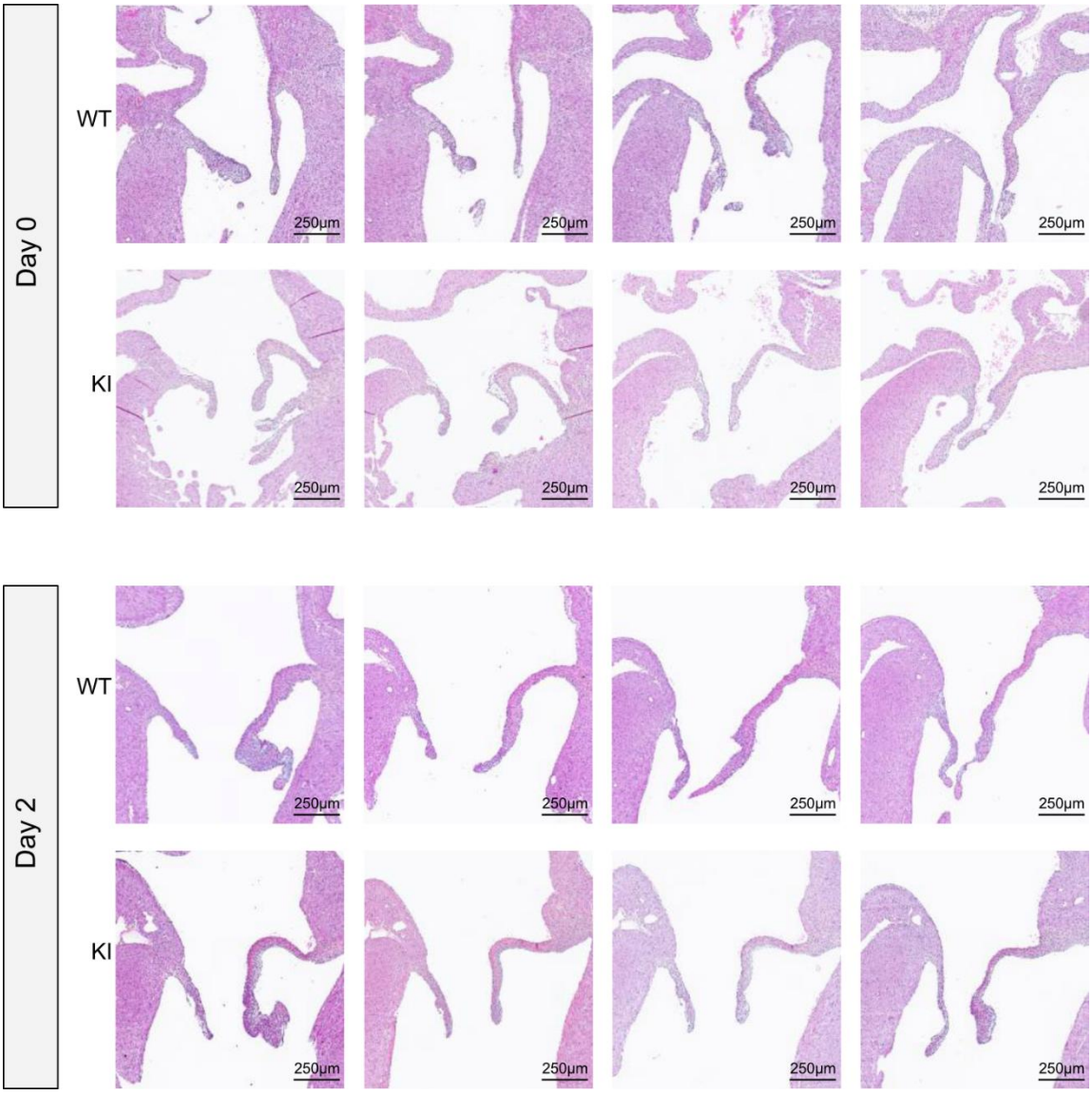

Legend: Overall immaturity of the MV structure was assessed through serial HPS staining at D0 and D2 in WT and KI rat MV sections. Representative images show the heterogeneous structure of MV leaflets along the different sections varying from thickened to thin leaflets. Scale bar 250µm

SUPPLEMENTARY FIGURE S4

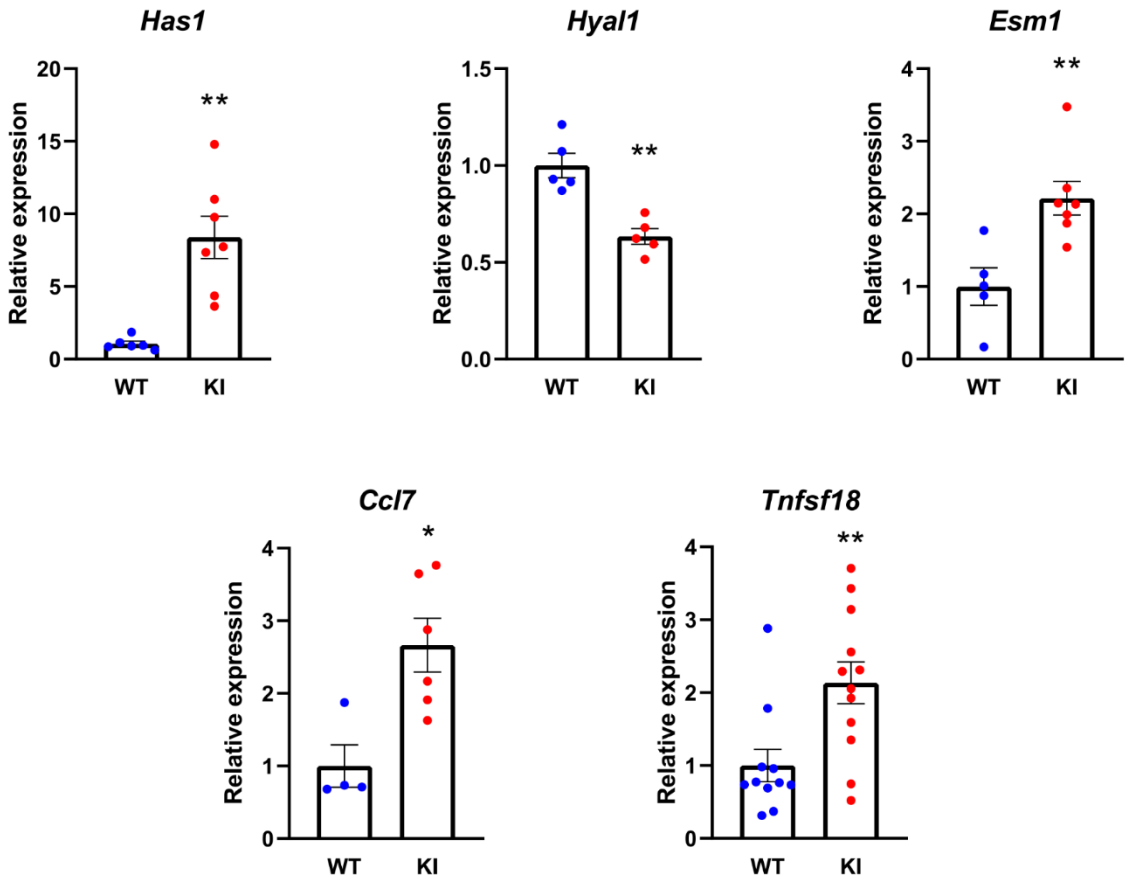

Legend: Fold-change of the gene expression levels between KI and WT MV at D7 by RT-qPCR (n=5 to 12MV). * p<0.05 vs WT, Mann-Whitney test.

IV. Complementary studies

1. Single nuclei transcriptomic of *FLNA*-KI rat's mitral valve

1.1 Introduction

The previous work demonstrated the dynamic contribution of macrophages in the pathophysiology of MVD. We demonstrated that extracellular matrix remodeling occurred within 7 days post-natal, and that macrophage expansion was secondary to this remodeling. One limit of the study is that we couldn't precisely discriminate macrophage phenotype or origin due to the limited panel of flow cytometry antibody available for rat markers. Therefore, in order to better decipher the cellular landscape, determine the origin of chemotactic signaling at 7 days, and identify the interactions between macrophage and the other cell types during MVD, we conducted a single nuclei RNA-seq analysis. Two timepoints were selected and analyzed: post-natal day 7 (D7), in which the MV is remodeled without increased macrophage proportion, and day 21 (D21), in which there is increased macrophage proportion associated to the remodeling of the MV leaflet.

1.2 Materials and methods

1.2.1 Mitral valve and nuclei isolation

Anterior and posterior MV leaflets from 5 to 10 littermates WT and KI rats were dissected, pooled and snap-frozen. For nuclei isolation, 500µL of ice-cold homemade lysis buffer (10mM Tris-HCl, 10mM KCl, 1mM $MgCl_2$, 250mM Sucrose, 0.1% Triton X100, 1mM DTT, 1µM flavopiridol, and 0.2U/µL RNase inhibitor) was added to the frozen sample. The lysis buffer containing the tissue was transferred to a Dounce homogenizer and disrupted approximately 30 times. The homogenate was transferred in a 1% bovine serum albumin (BSA)-coated tube and 1mL of lysis buffer was added. After 10 minutes incubation on ice, the homogenate was filtered through a 70µm strainer and centrifuge at 500g at 4°C for 5 minutes. The pellet was then resuspended in 1.5mL of lysis buffer and incubated 5 minutes on ice before being centrifuge again. Finally, the pellet was resuspended in 500µL of resuspension buffer (PBS, 1% BSA, 1µM flavopiridol, and 0.2U/mL RNase inhibitor) and filtered through a 20µm strainer. After centrifugation the nuclei pellet was resuspended in 100µL resuspension buffer and nuclei were counted and quality checked.

1.2.2 cDNA library preparation and sequencing

The experiment was performed with the Chromium GEM-X Single Cell 3' Reagents kits v4 from 10X genomics, following manufacturer's protocol. Briefly, Gel Beads-in-Emulsion (GEMs) were generated and barcoded in using the GEM-X chip and the Chromium X series instrument. 14500 nuclei per conditions were loaded in order to target a recovery of 10000 nuclei. Reverse transcription, cleanup, cDNA amplification and library construction were

conducted following the standard protocol from 10X genomics. Quality controls of the library were performed using Agilent High sensitivity D5000 Screentape for Tapestation and Qubit assay was done to determine the concentration of the library. Sequencing was performed at the EMBL genomics core facility GeneCore on a NextSeq 2000 sequencing system (Illumina) using a P3 flowcell (Illumina). Alignments of the sequencing data to the rat genome assembly (mRatBN7.2) was performed by the core facility.

1.2.3 Data analysis

Aligned data were processed using Python and the Scanpy package.[279] Quality checks were performed and cells with less than 200 or more than 5000 genes were removed. Cells with more than 0.5% of mitochondrial genes or more than 2% of ribosomal genes were also removed. Doublet detection and removal was performed with Scrublet algorithm using default parameters.[280] Following data cleanup, principal component analysis (PCA) and dimension reduction was performed and data were visualized with uniform manifold approximation and projection (UMAP). Dotplot of the 13 clusters specific markers was generated. One cluster of cardiomyocytes (*Ryr2*, *Tnnt2*) and 2 clusters of proliferation (*Mki67, Top2a*) were removed from analysis. 2 clusters with less than 150 cells were also removed. After cluster quality check, 2 clusters were also excluded due to poor quality as the clusters had no specific markers and much lower genes expressed per cell than the average of all other clusters. The remaining seven clusters were annotated based on key markers of the cell types expected to be present in the tissue: VECs, VICs, and macrophages. For differentially expressed genes (DEGs) analysis, subsets of cell type were created for each timepoint, and KI vs WT DEG analysis was performed. Gene ontology (GO-terms) enrichment analysis was then performed with the significant DEGs (padj < 0.05 and $0.3 <$ Log2FoldChange < -0.3) using GProfiler.[281] For

interaction analysis, D7 and D21 dataset were processed separately. Python dataset were exported for R, and CellChat V2.0.0 package was used on each dataset.[282,283]

1.3 Results

After nuclei isolation and sequencing (Figure 26a), a total of 36 498 cells and 25 629 genes were used as input data. After quality control and data cleaning, 23 398 cells and 18 541 genes were kept for analysis. Dimension reduction was performed and a UMAP was used to visualize the 7 clusters (Figure 26b). Interestingly, none of the clusters seemed to be specific to the *FLNA*-KI genotype, but some clusters appeared to be timepoint specific. Notably, clusters 0 and 4 were almost exclusive of D7 samples, and clusters 1 and 3 were specific of D21 samples (Figure 26c-f). For cell type annotation, a panel of key specific markers of endothelial cells, interstitial cells, and macrophages was designed and expression across clusters was assessed (Figure 26g). Clusters 2, 3 and 4 had a high expression of endothelial genes *Pecam1* (CD31), *Cdh5* (Vascular endothelial cadherin), *Vwf* (Von Willebrand Factor), *Nos3* (Endothelial nitric oxide synthase), and *Ptprb* (Vascular endothelial protein tyrosine phosphatase), and were classified as VECs. Clusters 0, 1 and 5 had high expression of ECM genes such as *Col1a1* (Collagen type I alpha 1 chain), *Col1a2* (Collagen type I alpha 2 chain), *Adamts19* (A disintegrin and metalloproteinase with thrombospondin motifs 19), *Postn* (Periostin), and *Bgn* (Biglycan) and were labelled as VICs. As for cluster 6, it had high expression of *Ptprc* (CD45), *Mrc1* (CD206), *Il6r* (Interleukin 6 receptor), *P2ry12* (Purinergic receptor P2Y G protein coupled 12), and hematopoietic marker *Lyn*, and was thus classified as macrophages (Macs) (Figure 26g).

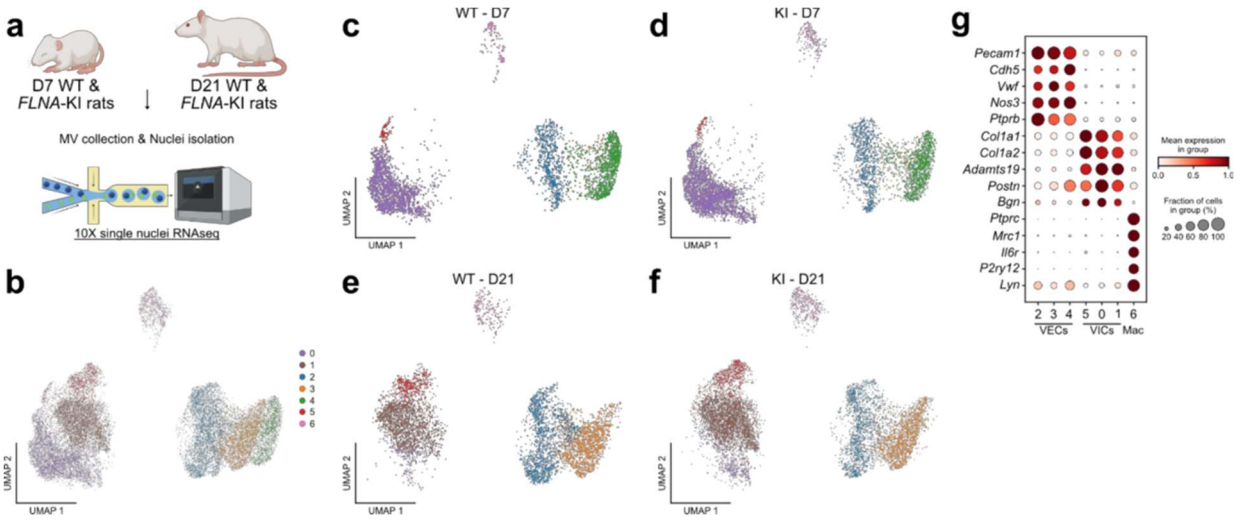

Figure 26. snRNA-seq analysis of D7 and D21 KI and WT mitral valve. a: Experimental setup of the experiment. **b:** UMAP of the four samples depicting the seven clusters. **c-f:** UMAP of individual samples of WT (c and e) and KI (d and f) at D7 (c and d) and D21 (e and f). **g:** Dotplot of specific endothelial, interstitial and macrophage genes showing clusters identity.

Following clusters annotation, VECs, VICs and Macs were subsetted to look for clusters differences and identify the different cell state. Then, we computed for differentially expressed genes between KI and WT samples at both timepoints. Genes were considered differentially expressed between genotype when adjusted p-value was below 0.05 and Log2FoldChange was over 0.3 or below -0.3. Upregulated DEGs were then used for an enrichment analysis using Gene-Ontology biological process (GO-BP).

Compared to the other VECs clusters, VEC-4 exhibit high expression of immature or developmental endothelial gene like *Tie1* (Tyrosine kinase with immunoglobulin like and EGF like domains-1), *Kdr* (Vascular endothelial growth factor receptor-2), *Nrp1* (Neuropilin-1), *Postn*, and *Foxp2* (Forkhead box P2) (Figure 27b). Combined with the fact that this cluster is specific of D7 samples, VEC-4 was labelled as Early-VECs (Figure 27c, d). Cluster VEC-3 was present only at D21 (Figure 27f, g) and had expression of classical endothelial marker *Ednrb* (Endothelin receptor type B), *Tek* (Angiopoietin-1 receptor/Tie2), *Pecam1* (CD31) and was

labelled as homeostasis VECs (Figure 27b). Finally, the cluster VEC-2 was annotated as activated VECs because of its high expression of proteoglycan gene *Vcan* (Versican), adhesion molecules *Icam1* (Intercellular adhesion molecule-1), *Vcam1* (Vascular cell adhesion molecule-1), and *Esam* (Endothelial cell adhesion molecule) (Figure 27b). Interestingly, this cluster also had strong expression of the MVP-associated gene *Lmcd1* (Figure 27a, b). We found 187 upregulated genes in VEC-2 and 108 in VEC-4 at D7 (Figure 27e). KI cells in VEC-4 had enriched pathways such as 'Macromolecule localization', 'Vascular process in circulatory system', 'Circulatory system process', 'Regulation of cell adhesion'. In contrast KI cells in activated VECs cluster 2 had enriched pathways like 'Extracellular matrix organization', 'Response to wounding', 'Cell surface receptor signaling pathway', 'Response to growth factor'. Interestingly, two immune pathways were also enriched in KI VEC-2: 'Response to cytokine' and 'Cellular response to cytokine stimulus'. This is consistent with our previous bulk RNA-seq analysis of D7 KI MV which demonstrated increased immune and chemotactic signature in KI MV compared to WT (Figure 27e). For D21 timepoint, we found 349 upregulated genes in VEC-2 and 158 in VEC-3 at D21 (Figure 27h). Interestingly, the immune activation of KI VECs is persistent over time, as immune pathways 'Lymphocyte activation' and 'Immune system process' are enriched in KI VEC-2 at D21. We also found enrichment of pathways like 'Response to stress' or 'Cell activation', indicating that this cluster of VECs is highly activated in KI MV. Finally, KI VEC-3 had enriched pathways related to extracellular matrix organization, suggesting a supporting role of VEC in the remodeling of the ECM observed in *FLNA*-KI MV (Figure 27h).

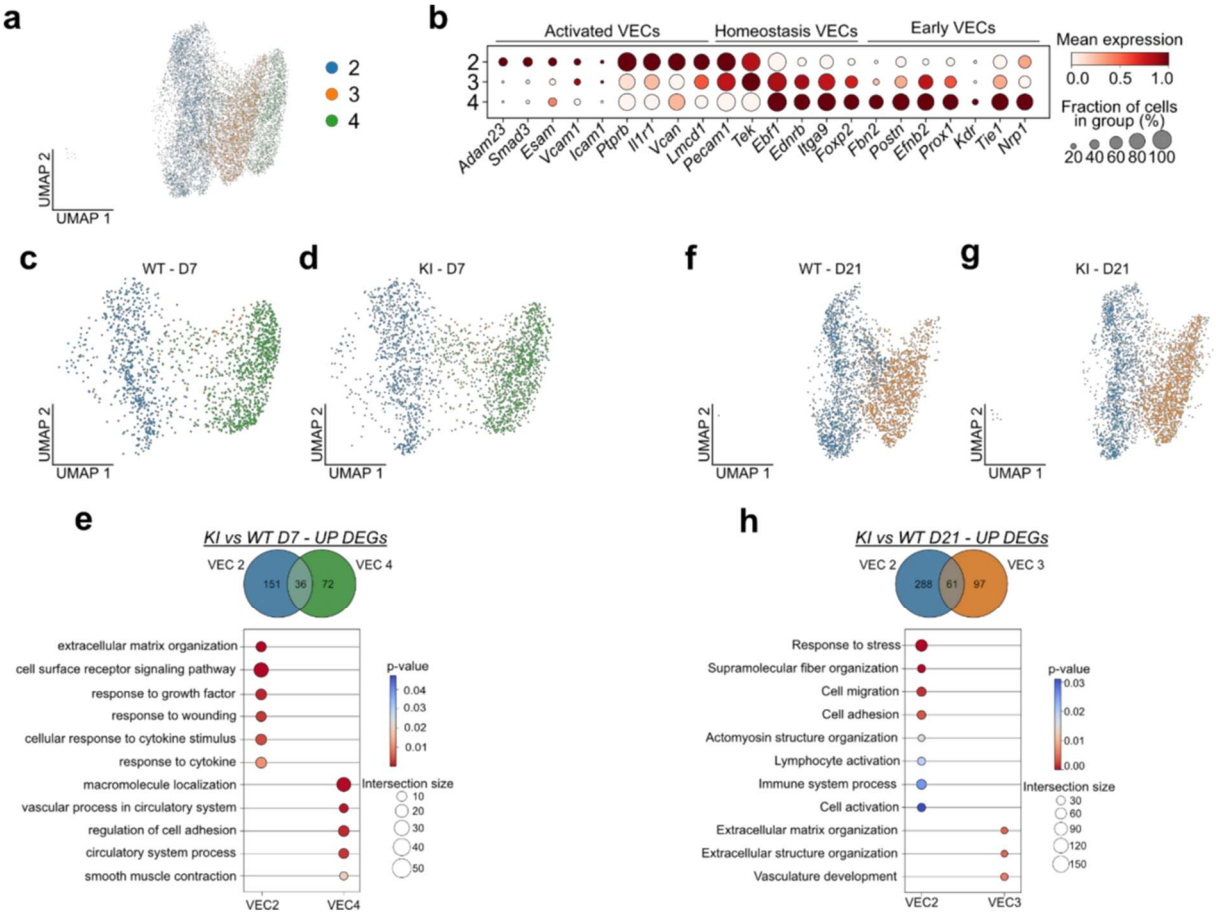

Figure 27. Valvular endothelial cells subset analysis. a: UMAP of VECs subset. **b:** Dotplot of VECs clusters specific markers. **c-d:** UMAP of D7 samples showing WT (**c**) and KI (**d**) clusters. **e:** Venn diagram representing the number of upregulated DEGs between KI and WT cells of each cluster. The Dotplot below shows the top GO-term associated to each cluster. **f-g:** UMAP of D21 samples showing WT (**f**) and KI (**g**) clusters. **h:** Venn diagram representing the number of upregulated DEGs between KI and WT cells of each cluster. The Dotplot below shows the top GO-term associated to each cluster.

The same approach was applied on VICs clusters, and the three clusters were identified as Early-VICs for cluster VIC-0, pro-inflammatory VICs for cluster VIC-1, and remodeling VICs for VIC-5 due to expression of ECM gene (Figure 28a, b). At D7, 192 DEGs were found in the KI cluster VIC-0 and those genes were enriched in pathways like 'Cell proliferation', 'Cell migration', 'Cell adhesion', 'Extracellular matrix', 'Actin filament-based process', indicating an already disturbed cellular and ECM homeostasis at D7 (Figure 28c-e). At D21, there was 104 upregulated DEGs in VIC-0, 430 in VIC-1 and 209 in VIC-5. Enrichment

analysis revealed pathways like ‘Smooth muscle contraction’, ‘Tissue morphogenesis’, and ‘Response to wounding’ for KI VIC-0 (Figure 28f-h). For VIC-1, enriched pathways were ‘Cell-matrix adhesion’, ‘Chemotaxis’, ‘Immune system process’, ‘Leukocyte migration’, consistent with the inflammatory VICs annotation. Regarding VIC-5, pathways enriched in KI sample were related to ‘Cell-cell adhesion’, ‘Membrane organization’, or ‘Regulation of macromolecule metabolic process’, confirming their role in the remodeling of the MV (Figure 28f-h).

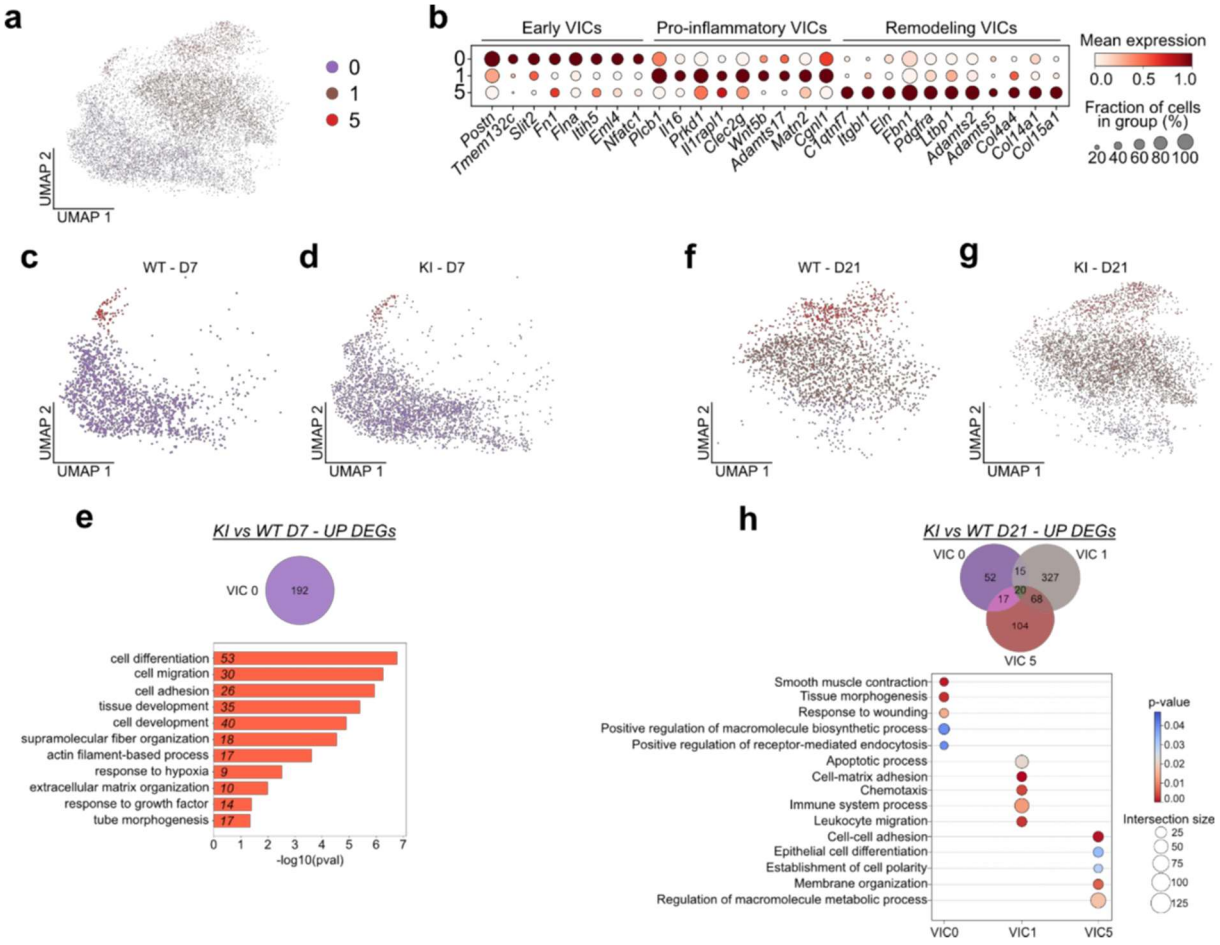

Figure 28. Valvular interstitial cells subset analysis. a: UMAP of VICs subset. **b:** Dotplot of VICs clusters specific markers. **c-d:** UMAP of D7 samples showing WT (**c**) and KI (**d**) clusters. **e:** Venn diagram representing the number of upregulated DEGs between KI and WT cells of each cluster. The Dotplot below shows the top GO-term associated to each cluster. **f-g:** UMAP of D21 samples showing WT (**f**) and KI (**g**) clusters. **h:** Venn diagram representing the number of upregulated DEGs between KI and WT cells of each cluster. The Dotplot below shows the top GO-term associated to each cluster.

As the initial clusterisation grouped all macrophages in a single cluster, we decided to subcluster the macrophages to have a better look at their diversity. Sub-clusterisation identified 3 different sub-population of macrophages (Figure 29a). Macrophage sub-cluster Mac6-1 had very high expression of *Mrc1*, *Csf1r* (Colony stimulating factor 1 receptor), and *Tnfrsf11a* (TNF receptor superfamily member 11a/Receptor Activator of NF-KB), suggestive of resident macrophages (Figure 29b). The sub-population Mac6-2 strongly expressed *Timd4* (T cell immunoglobulin and mucin domain containing 4), *Cx3cr1* (C-X3-C motif chemokine receptor 1), and *Ccr2* which indicate that they are monocyte-derived. They were also positive for *Vcan*, and *Tgfb1* suggesting a pro-remodeling phenotype (Figure 29b). Finally, the last population: Mac6-3, was classified as pro-inflammatory as they highly expressed *S100a8*, *S100a9*, *Il1b* (Interleukine-1 beta), *Fcgr1a* (Fc gamma receptor Ia). They also expressed *Ccr2* indicating that they are monocyte-derived (Figure 29b). Although cell proportion is not quantitative in single nuclei experiment, it is interesting to note that the monocyte-derived Mac6-2 subcluster proportion was increased in KI condition at both D7 and D21 timepoint, which would be consistent with our hypothesis of peripheral macrophage recruitment in the KI MV (Figure 29c).

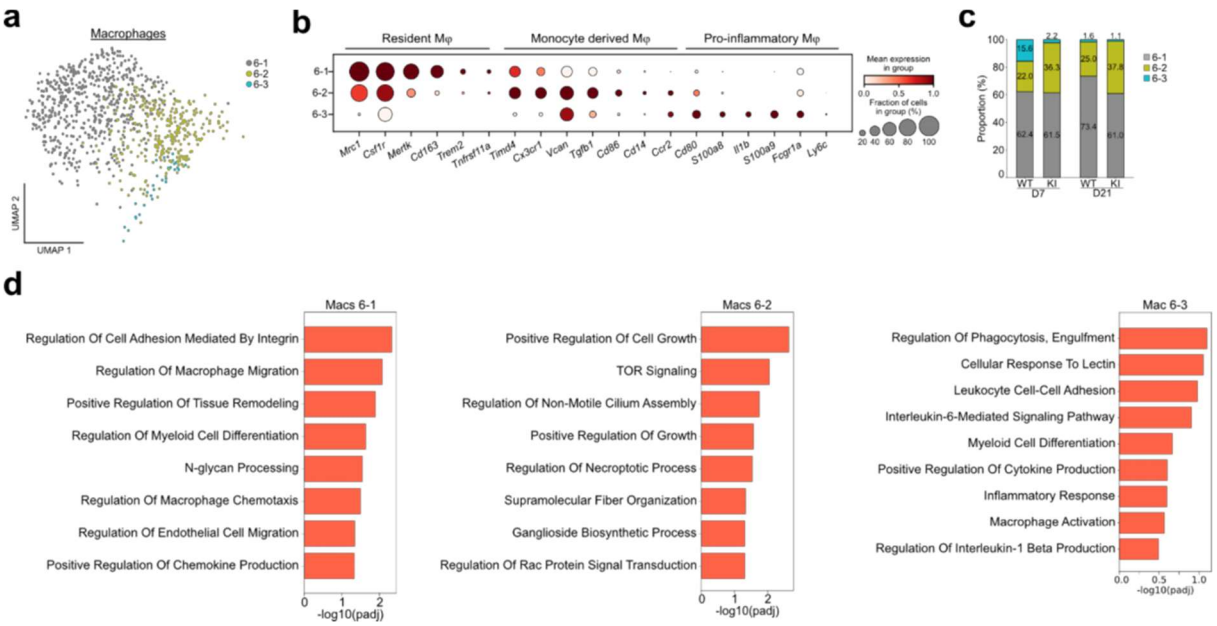

Figure 29. Macrophage subclusterisation. a: UMAP of macrophage subclusters. **b:** Dotplot of macrophage subclusters markers. **c:** Proportion of macrophage subcluster across the samples. **d:** Barplot of the top GO-term identified by ranked-gene enrichment analysis on each macrophage subclusters.

Differential expression analysis revealed only 1 DEG at D7 in Mac 6-1 (*Wwp1*), and 8 DEGs at D21 in Mac 6-1 (*Mrc1*, *Fkbp5*, *Slc10a6*, *Ahnak*, *Xdh*, *Fcho2*, *Atf6*, *Vim*), indicating that KI macrophages are overall similar to WT despite the *FLNA* mutation. To determine the phenotype of the macrophage sub-population, we performed an over-representation analysis based on ranked gene expression for each sub-cluster (Figure 29d). Consistently with the classification as tissue-resident macrophages, we identified that Mac 6-1 was involved in cell adhesion mediated by integrin, macrophage migration, regulation of tissue remodeling, macrophage chemotaxis. Mac 6-2 was involved in pathways regulating cell growth, TOR and Rac signaling, supramolecular fiber assembly and ganglioside biosynthetic pathway, consistent with a pro-remodeling phenotype. Finally, the pro-inflammatory Mac 6-3 was enriched for pathways like phagocytosis, leukocyte adhesion, myeloid cell differentiation, inflammatory response, Il1 production and Il6 pathway, as well as macrophage activation (Figure 29d).

In a last effort to understand how VICs, VECs, and macrophages can interact to promote disease development and progression, we conducted an interaction analysis using CellChat (Figure 30). This algorithm predicts interaction between clusters based on expression level of ligand-receptor pairs. The analysis was performed separately for D7 and D21 datasets.

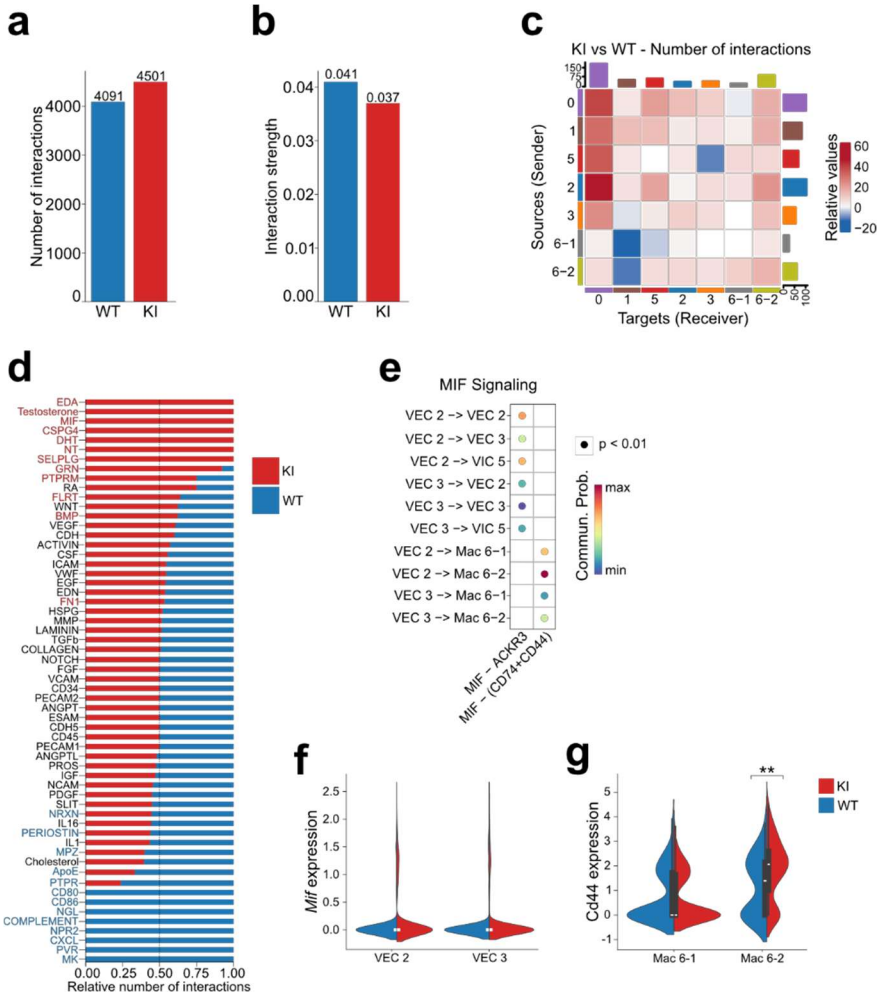

Figure 30. CellChat analysis of D21 WT and KI-MV. a: Number of interactions inferred by CellChat in WT and KI samples at D21. **b:** Interaction strength inferred by CellChat in WT and KI samples at D21. **c:** Heatmap of KI vs WT number of interactions between the clusters. Red square indicates increase number of interactions between source and target in KI, and blue indicates reduced number of interactions in KI. **d:** RankNet plot showing the relative contribution of signaling pathways to the global communication network in KI (red) and WT (blue). Pathways with name in red or blue means significantly enriched in KI or WT respectively. **e:** Bubbleplot of the MIF signaling pathway in KI. **f:** Violin plot of MIF expression in WT and KI VECs clusters. **g:** Violin plot of CD44 expression in WT and KI macrophage subclusters

For D21, the algorithm computed more interactions for KI compared to WT (4501 for KI vs 4091 for WT), however the interaction strength was slightly lower for KI (0.037 vs 0.041) (Figure 30a, b). Going into detail about the outgoing and incoming interactions, the main sources of interaction are clusters of activated VEC-2, and clusters VIC-0 and VIC-1 (Figure 30c). The main targets of these interactions are clusters VIC-0 and monocyte-derived macrophage cluster Mac 6-2. Interaction pathways were then ranked using RankNet function of CellChat to identify which pathways are significantly enriched in KI MV (Figure 30d). We kept only pathways that were significantly enriched in terms of interaction number and strength. We found 12 pathways enriched in KI sample: EDA (Ectodysplasin A), Testosterone, MIF (Macrophage migration inhibitory factor), CSPG4 (Chondroitin sulfate proteoglycan 4), DHT (Dihydrotestosterone), NT (Neurotrophin), SELPLG (Selectin P ligand), GRN (Granulin), PTPRM (Protein tyrosine phosphatase receptor type M), FLRT (Fibronectin leucine rich transmembrane protein), BMP (Bone morphogenetic protein), FN1 (Fibronectin 1).

We focused on the pathways involved in macrophages function and MV remodeling. Thus, we decided to decipher the interactions regarding MIF signaling pathway (Figure 30e). MIF interaction was inferred in KI-D21 sample but not in WT. Two pairs of ligand-receptor are present in this pathway: MIF-atypical chemokine receptor 3 (ACKR3) between VEC-2/VEC-3 as source of interaction and VEC-2/VEC-3/VIC-5 as targets. More interestingly, there was an interaction from VEC-2 and VEC-3 towards Mac 6-1 and Mac 6-2 involving ligand MIF and (CD74+CD44) receptor (Figure 30e). We then went back to the expression data to see if the ligand or receptor are overexpressed in KI clusters. We found that MIF ligand was not differentially expressed across VECs clusters, but CD44, a hyaluronan receptor was overexpressed in KI monocyte-derived macrophages (Figure 30f, g).

1.4 Conclusion

The single nuclei RNA-seq experiment allow us to better understand the cellular landscape of the diseased MV, and the dynamic of interactions occurring between the different cell types present in the MV. We first highlighted that both WT and *FLNA*-KI MV had the same clusterisation at both timepoint, indicating that the genotype does not affect the cellular identity of the MV. However, there was some differences between the timepoints, consistent with previous reports showing the dynamic cellular modification happening after birth during the maturation of the MV.[32,41] Although we did not find different cluster between genotypes, differential expression analysis revealed differences between the *FLNA*-KI and WT cells. For every cluster, KI-cells had generally a more "active" phenotype compared to WT. As such we identified that immune activation starts at D7 in VECs, and persist over time in VECs. This immune activation is also detected in VICs clusters at D21 only. Those results consolidate our previous findings in which we had describe a chemotactic environment at D7 persistent at D21 but associated to an increase in macrophage proportion. We can now postulate that the chemotactic environment detected at D7 is related to VECs activation, and as pathology progress the VICs also starts to upregulate immune pathways contributing to MVD maintenance.

Unlike VICs and VECs, macrophages from *FLNA*-KI MV were not different from WT, suggesting that the *FLNA* mutation does not modify macrophages phenotype. For the first time, we were able to decipher the different subpopulation of macrophages based on markers expression. Those results would benefit to be validated *in vivo*, by evaluating the origin of macrophages using lineage tracing, and quantify precisely the proportion of each subpopulation by flow cytometry. Unfortunately, such experiments are difficult to perform on rat model due to the limited number of lineage tracing tools and antibody availability. Finally, the interaction

analysis revealed some pathways in KI samples that are not inferred in WT. Among them, the MIF pathway is of particular interest. MIF interaction was inferred in KI samples at D21 between VECs and macrophages. Specifically, the interaction inferred is between MIF send by VECs, towards the (CD74+CD44) receptors on macrophages. The CD74 is a receptor involved in the antigen presentation, and the CD44 is a hyaluronan receptor. CD74 was not differentially expressed between KI and WT macrophage at D21 (Data not shown), but CD44 overexpression in KI was confirmed in the subcluster of monocyte-derived macrophage Mac 6-2. This is of particular interest, as we have previously showed an upregulation of *Has1* in the *FLNA*-KI MV that indicate an increase of hyaluronic acid in the diseased MV. The composition of the ECM could modify the expression pattern of macrophages surface receptors and thus induce different interaction with the other cell types of the valve.

2 Depletion of macrophage with CCR2 inhibitors

2.1 Introduction

Based on our observation that the *FLNA*-KI rat presented accumulation of macrophages in the MV occurring between D7 and D21, we sought to prevent the recruitment of macrophages in the MV to modulate the evolution of MVD. To this aim, we used the selective CCR2 inhibitor RS504393, previously used in the Marfan-syndrome related MVD to reverse development of the disease.[205] We treated *FLNA*-KI rats from D7 to D21 with a daily dose of CCR2 inhibitors and analyzed the development of MVD and macrophage population in the tissue.

2.2 Materials and methods

2.2.1 Animals

A total of 64 animals from 4 WT and 4 KI litters were used for the experiment. For each litter, 4 rats were randomly assigned to the vehicle group and 4 to the treatment group. WT and *FLNA*-KI rats were daily treated with either DMSO or 2mg/kg RS504393 (Tocris) via intraperitoneal injection from D7 to D21. Animal's weight was measured every day to follow weight gain and to determine the dose of treatment. Blood samples were performed every five days. An echocardiography was performed at D13 and D21. At the final timepoint (D21), rats were anesthetized using 5% isoflurane, and euthanized by cervical dislocation. The chest was rapidly open to harvest the heart and place it in ice-cold PBS. Hearts were then either placed in formalin for histology, or dissected to collect the MV leaflets that were snap-frozen for molecular analysis.

2.2.2 Blood counts

To collect blood, 1.5mL tubes were coated with heparin. The tip of rat tails was cut and massaged to collect a blood drop. Tubes were briefly centrifuged for homogenization. 15µL of blood was necessary for blood count using the hematocytometer Element HT5 analyzer (ScilVet).

2.2.3 Histology

Hearts were rinsed in ice-cold PBS and fixed in 10% formalin for 24 hours. Hearts were then dehydrated, cleared in xylene and embedded in paraffin. 3µm sections were cut with a microtome and serial slides were stained with hematoxylin phloxin saffron (HPS) and Alcian blue. Stained sections were observed by a pathologist blinded for the treatment group. The proteoglycan content was analyzed using QuPath software to quantify the proportion of Alcian blue in the MV anterior and posterior leaflets. Briefly, the leaflets were segmented and color deconvolution was applied to quantify the Alcian blue positive area. For immunofluorescence staining, paraffin-embedded sections were deparaffinized before antigen retrieval in citrate buffer (pH6) and saturation with 5% BSA (bovine serum albumin, Sigma-Aldrich, A7030). Primary antibody against CD45 (Abcam ab10558, 1/1000) and CD206 (Ptglab 60143, 1/10000) were incubated overnight at 4°C followed by appropriate secondary antibody for 2 hours at room temperature. Nuclei were stained using 1µg/mL Hoechst and images were captured using Nikon ECLIPSE Ti2 microscope.

2.3 Results

Blood samples were taken at D21 and analyzed on a hematocytometer (Figure 31). Although there was a trend in slightly higher number of circulating leukocytes in KI rats, no significant differences were observed, and the treatment with CCR2 inhibitor had no effect on the total number of circulating leukocytes (Figure 31a). In the DMSO treated groups, the number of circulating monocytes was significantly higher in KI rats compared to WT (Figure 31b). However, the treatment with CCR2 inhibitors had no effect on the level of circulating monocytes both in WT and KI animals (Figure 31b). Finally, genotype and treatment with RS504393 had no effect on lymphocytes and neutrophils counts (Figure 31c, d).

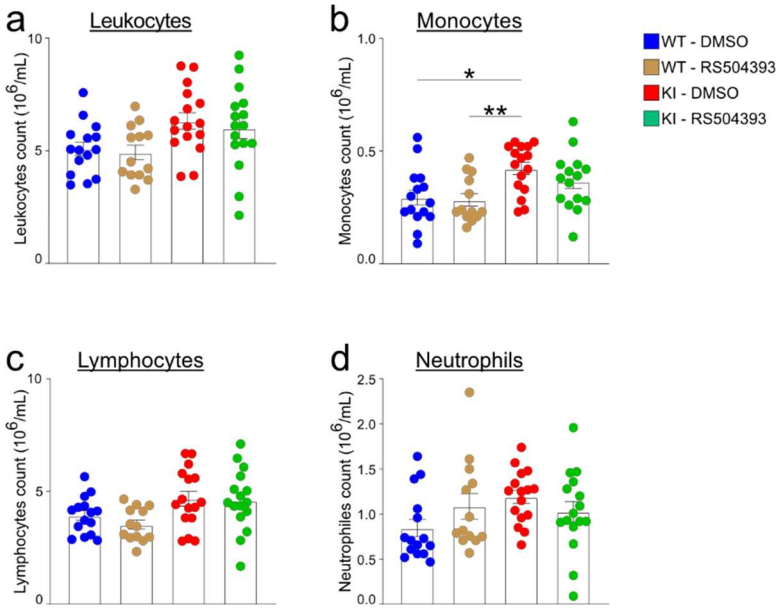

Figure 31. Blood cell counts of D21 WT and KI rats. Leukocytes (**a**), monocytes (**b**), lymphocytes (**c**) and neutrophils (**d**) counts measured by hemocytometer. * $p<0.05$, ** $p<0.01$ using the non-parametric Kruskal-Wallis test.

We then sought to determine if the treatment prevented the development of MVD or reduced the number of macrophages in the MV leaflets. We first focused our analysis on KI rats as we didn't expect that CRR2 inhibition will have an effect on WT MV morphology. We stained

serial slides of KI MV using HPS for global morphology assessment and Alcian Blue to assess proteoglycan content (Figure 32). HPS staining evaluation showed no difference between DMSO-treated and RS504393-treated KI rats (Figure 32a). This was confirmed by the quantification of Alcian blue content that revealed no differences in both leaflets (Figure 32b, c). Macrophages were stained by immunofluorescence with CD45 and CD206 antibody (Figure 32d). The number of macrophages in the MV was then evaluated using Fiji software. Unexpectedly, no difference was observed regarding the number of CD45 or CD206 macrophages in the MV of treated KI rats (Figure 32e, f).

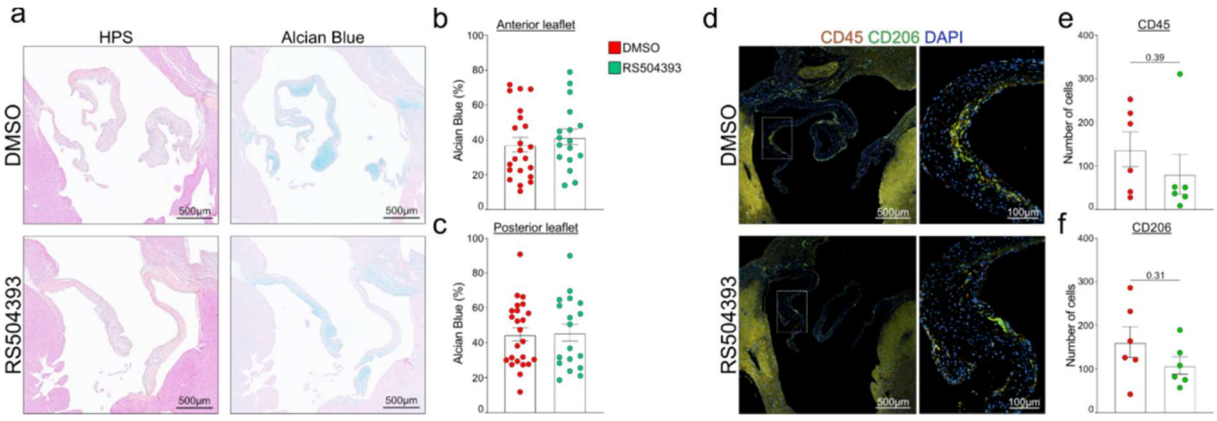

Figure 32. Histological analysis of KI rat's MV. a: HPS (left panel) and Alcian blue (right panel) of KI MV treated with DMSO (top panel) or RS504393 (bottom panel). **b:** Quantification of Alcian blue staining in the anterior leaflet of the MV (n = 17 to 24 sections representing 7 DMSO and 5 RS504393 treated rats). **c:** Quantification of Alcian blue staining in the posterior leaflet. **d:** Immunofluorescence images of CD45 and CD206 staining in KI MV treated with DMSO or RS504393. Dotted squares are zoomed in the right panel. Scale bar = 500 or 100µm. **e-f:** Number of CD45 (**e**) and CD206 (**f**) positive cells per MV (n = 6 MV for each group). Indicated p-values were obtained by non-parametric Mann-Whitney test.

2.4 Conclusion

Overall, the results indicate that CCR2 inhibition between D7 and D21 did not reduced macrophage number in the MV, nor reduced the extent of MV remodeling in the *FLNA*-KI rat. Despite a trend towards a reduction of $CD45^{+}$ cells in the MV of KI rats treated with RS504393,

no significant differences were observed. This result is contradictory with previous study conducted on Marfan-mice and using the same molecule at the same dosage (2mg/kg/day). However, in the Marfan-mice model, macrophage recruitment in the MV occurs between 1 and 2 months of age, which was the window of treatment chosen in their study. Thereby, the Marfan-mice were treated at an older age and for a longer period than in our experiment, which could explain, at least in part, the differences observed with our *FLNA*-KI rat model). New strategies to prevent the recruitment of macrophages in the MV could be considered. The best option for efficiently target macrophage recruitment would be to use genetically engineered models, but genetic models available for cross-breeding our rat model is limited. Indeed, there is no *CCR2*-KO rat model. There is a *CSF1R*-KO rat model, but the genetic background of this model is Dark Agouti rat, whereas our *FLNA*-KI rat is Sprague-Dawley. Thereby it would require a long backcross to allow for cross-breeding in order to generate a *FLNA*-KI *CCR2*-KO rat model.

To overcome this limitation, our group is currently generating a new mouse model carrying the *FLNA*-P637Q mutation. This new model will need phenotyping to confirm the presence of MVD, and will then be of particular interest to study macrophages population, using genetic depletion of macrophages, or macrophage lineage tracing.

3 *In vitro* macrophage and VIC functional evaluation

3.1 Introduction

Macrophages plays an important role in MV development and homeostasis, but also in MVD pathophysiology as previously demonstrated. As professional phagocyte, they assure the clearance of apoptotic cells and ECM debris. Phagocytosis is a complex and dynamic process involving the actin cytoskeleton to form filopodia, and phagosomes. It is possible that the P637Q mutation in *FLNA* gene could alter the ability of macrophages to perform phagocytosis or other functions. Thereby, we attached to measure the phagocytic ability of *FLNA*-KI macrophages.

Macrophage recruitment in the tissue is a process called extravasation. It implies expression of adhesion molecules at the surface of endothelial cells to induce binding of circulation monocytes to the endothelium. Then monocytes extravasate through the endothelium and differentiate into macrophages in the tissue, where they also create intercellular adhesion with the interstitial cells. As our previous findings demonstrate a chemotactic signaling by VECs at D7 and by VECs and VICs at D21, we tried to determine how this translated in terms of cells interactions. To this aim we developed a monocyte adhesion assay using a non-adherent monocyte cell line, and rats' primary culture of VICs.

3.2 Materials and methods

3.2.1 Primary culture of Valvular Interstitial Cells

WT and KI rats were anesthetized with 5% isoflurane before being euthanized by cervical dislocation. Chest was open and the heart was harvested and placed in ice-cold PBS. The mitral valve leaflets were carefully dissected and placed in cold 1X Hank's Balanced Salt Solution (HBSS) culture media. To recover sufficient number of cells, 7 littermates MV were pooled. Tissue was rapidly processed for cell isolation. HBSS media was replaced by digestion buffer containing 2mg/mL Collagenase type 4 (Worthington Biochemical) and 1.2U/mL Dispase II (Sigma-Aldrich) and incubated at 37°C for 10 min with gentle agitation. The digestion media was carefully transferred in 15mL tube and kept on ice to block enzymatic activity. Fresh digestion buffer was then added for a new cycle of digestion. A total of four cycle was necessary to completely digest the MV leaflets. Once digestion completed, the tubes containing the cell suspension was centrifuged at 400g for 5 minutes at room temperature. Supernatant was discarded and fresh culture media (DMEM 1g/L glucose, containing 2% FCS, 1% penicillin/streptomycin, 5.5µg/mL insulin and 10ng/mL FGF-2) was added to the cell pellet. Cells were resuspended, counted and seeded at the appropriate density on collagen coated plates. VICs were used at passage 1.

3.2.2 Primary culture of peritoneal macrophages

Three weeks old WT and KI rats were injected intraperitoneally with 100mL/kg of fluid thioglycolate medium (Millipore, STBMFTM12). After 3 days, rats were anesthetized with isoflurane and euthanized by cervical dislocation. The abdominal skin was immediately cut to

expose the peritoneal cavity. 20mL of sterile PBS was injected into the peritoneum with a 23G needle. The peritoneal lavage was then collected using a 18G needle and transferred in a 50mL tube. Peritoneal lavage was centrifuged at 400g for 5 minutes. Cells were resuspended in RPMI 10% FCS, 1% penicillin/streptomycin, counted and seeded at the appropriate density.

3.2.3 Phagocytosis assay

For phagocytosis assay, peritoneal macrophages were grown in RPMI 10% FCS media. The pHrodo BioParticles phagocytosis kit (ThermoFisher, P35360) was used for the experiment per manufacturer's protocol. Briefly, *E. Coli* particles were mixed with RPMI media and added on top of the peritoneal macrophages. The pHrodo particles have the advantage to become fluorescent only at acid pH, once it is internalized in the phagolysosome. Hence, the amount of fluorescence is directly linked to the quantity of particles that have been phagocyted. The plate was immediately placed on a Leica DMI 6000B microscope with a temperature and CO_2 controller, for time-lapse imaging of the phagocytosis. Images were taken every 2 minutes for 2 hours. Fluorescence analysis was performed with Fiji software.

3.2.4 Monocyte adhesion assay

A total of 40 000 VICs per well were seeded on a 24 well plates. Once the VICs monolayer reached confluency, VICs were treated with 10ng/mL recombinant-TNFα for 3 hours. Human monocytic THP1 cells were resuspended in RPMI media without FCS and with 10nM Chloromethyl fluorodiacetate (CMFDA) green cell tracker (ThermoFisher, C2925) and incubated at 37°C for 30 minutes. THP1 cells were then centrifuged and resuspended in RPMI 10% FCS at 400 000 cells/mL. VICs media was discarded and VICs were washed before adding

500µL of the THP1 suspension was added on top of the VICs monolayer (200 000 THP1 for 40 000 VICs). The plate was incubated for 2 hours at 37°C. After 2 hours, media was discarded and the wells were rinsed three times with PBS to remove non-adherent THP1 cells. Cells were the fixed using 4% paraformaldehyde (PFA) for 10 minutes, and nuclei were stained using 1µg/mL Hoechst for 1 minutes. Images were acquired with a Nikon ECLIPSE Ti2 microscope and the number of THP1 cells attached to the VICs was determined using Fiji software by calculating the ratio of THP1 cells on VICs. The number of VICs was determined using the nuclear Hoechst staining, and THP1 monocytes using CMFDA cell tracker staining.

3.3 Results

As it was shown that KO of Filamin A was detrimental on macrophage function (see section 4.5), we sought to determine if the Filamin A P637Q mutation could also affect macrophages core function. To test this hypothesis, we assessed the phagocytic capacity of *FLNA*-KI macrophages (Figure 33). We performed a 2 hours time-lapse imaging of phagocytic macrophages and measured the fluorescent area (Figure 33a). Our analysis revealed no differences of phagocytic capacity between WT and *FLNA*-KI peritoneal macrophages (Figure 33b).

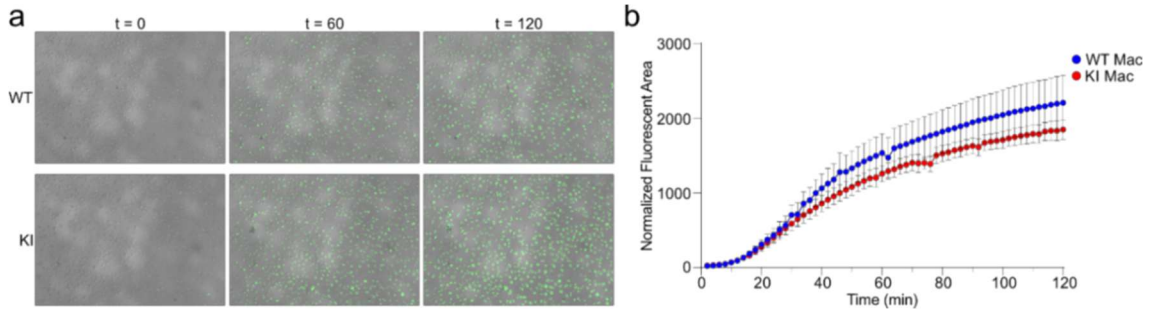

Figure 33. Phagocytosis assay of peritoneal macrophages. a: Representative images of phagocytic macrophages after 0-, 60- and 120-min of coculture with pHrodo-labeled E. Coli particles. **b:** Quantification of the fluorescent area normalized by the number of macrophages. (n = 3 biological replicates).

As Filamin A is an actin-binding protein, a mutation could particularly affect cytoskeleton dynamic, which in the case of phagocytosis, could alter filopodia formation and slow the internalization of the particles. To test the rate of particle internalization, we added the pHrodo bioparticles on top of the peritoneal macrophages and immediately place the cells on ice to let particles bind to their phagocytic receptors without being internalized. We then washed away all non-attached particles, and placed the plate at 37°C. We captured the fluorescence with Nikon ECLIPSE Ti2 microscope every 5 minutes for 30 minutes (Figure 34a). This experiment revealed that the internalization of phagocyted particles is not altered in *FLNA* P637Q macrophages (Figure 34b).

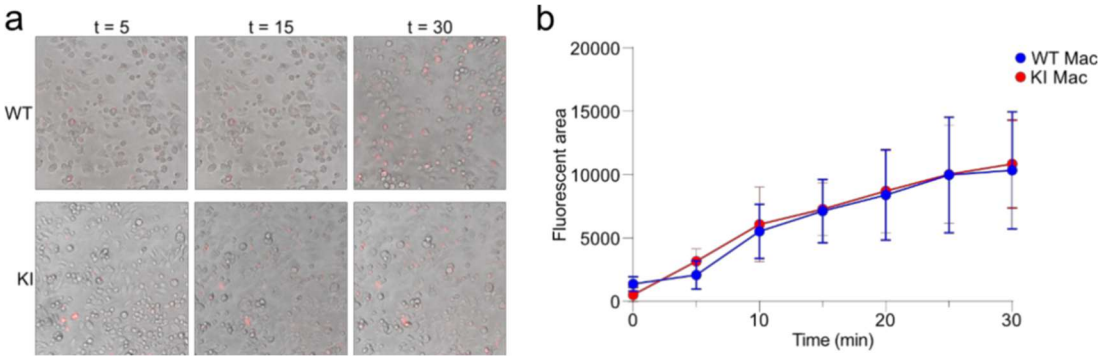

Figure 34. Particle internalization assay. a: Representative images of E. Coli particles internalization by WT and KI peritoneal macrophages after 5-, 15- and 30-min. To assess for internalization only, particles were left to bind to their receptors for 15 minutes at 4°C. **b:** Quantification of the fluorescent area in the field. (n=3 technical replicates)

Our preliminary results seem to indicate that the increase of macrophage proportion in *FLNA*-KI MV is related to a recruitment of circulating monocytes, we sought to determine if monocytes were more prone to attach to KI VICs rather than WT VICs in normal or pro-inflammatory condition (Figure 35). We found that after two hours of coculture, there was an increased number of attached monocytes to the layer of KI VICs compared to WT VICs (Figure 35a, b). As expected, the pre-stimulation of VICs with the pro-inflammatory cytokine TNF-α increased the number of monocytes attached to VICs, with a trend for exacerbated effect on KI VICs (Figure 35c, d).

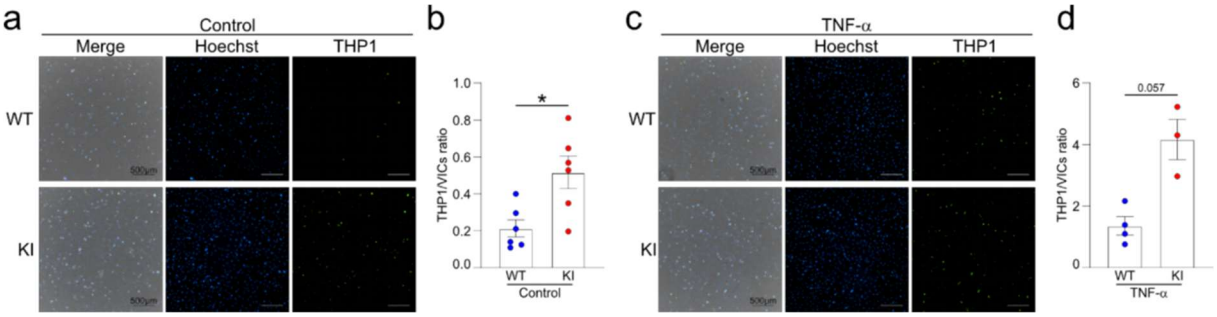

Figure 35. Adhesion assay of monocytes on WT and KI VICs. a: Adhesion assay of monocytes on WT and KI VICs in control conditions. Images were taken after 2 hours of adhesion. Attached monocytes were counted and normalized to number of VICs on the field. **b:** Adhesion assay of monocytes on WT and KI VICs primed with TNF-α for x hours before assay. Images were taken after 2 hours of adhesion and attached monocytes were counted and normalized to number of VICs on the field. Image analysis was performed using ImageJ.

3.4 Conclusion

Although some literature indicate that a Filamin A KO impairs macrophages functions[176,277,284], our preliminary results indicate that the P637Q Filamin A mutation did not affect macrophage phagocytosis. It is important to assess macrophage function upon Filamin A mutation, as one could hypothesized that the recruitment of macrophages in the context of MV remodeling could be linked to an inability of macrophages to resolve the remodeling due to Filamin A mutation. Additionally, as an actin-binding protein, Filamin A plays a key role in the cytoskeleton dynamic and interaction with the extracellular space, which are also key aspects of the phagocytosis process.

However, our results indicate that the FLNA mutation increases the ability of VICs to bind monocytes *in vitro*. Adhesion of monocytes naturally occurs with endothelial cells, to allow the extravasation of circulating monocytes into the tissue where they differentiate into mature macrophages. Our experiment could not have been performed with endothelial cells because dissociation of rat's MV provides too few endothelial cells to generate primary culture of VECs.

Nonetheless, it shows that *FLNA*-KI VICs increases the attachment of monocytes, which is consistent with our findings of chemotactic signaling in the MV of *FLNA*-KI rats. A more detailed *in vitro* study of those mechanisms is ongoing, by evaluating the role of adhesion molecules to this process.

V. Discussion

Myxomatous mitral valve dystrophy (MVD) is the main etiology of mitral valve prolapse, and its prevalence is increasing with the aging of the population in western countries.[4] MVD is associated with cardiovascular morbidity and mortality as it can lead to mitral insufficiency, arrythmias, heart failure, and cardiac death. Despite years of research, no pharmacological treatment is yet available and the only therapies are surgical repair or replacement of the diseased valve for the most severe cases. Within those years of research, many pathways have been highlighted as key player a part in the development or progression of MVD. But the pathophysiology of MVD is more complex and is largely due to a dysregulation of several, if not all the pathways. Indeed, TGF-β, serotonin, primary cilia, endothelial-mesenchymal transition, and mechanotransduction signaling pathways are strongly interconnected and may be regulated each other's.

Inflammation and immune cells were for a long time left aside as MVD was thought to be non-inflammatory and mostly related to aging and to the mechanical constraints applied to the valve leaflets. But our comprehension of the disease mechanisms evolved when $CD45^+$ hematopoietic cells were identified in the valves of Human, sheep, and mice.[40,156,204,285–287] The interest in the immune processes leading or contributing to MVD has since been growing. The more recent findings reveals that the immune cells present in the MV are predominantly macrophages, and that their number increases over the disease progression.[41] They were successfully targeted in a model of Marfan syndrome-related MVD, and blocking the recruitment of macrophages in the tissue prevented the myxomatous remodeling of the MV.[204,205] A limit of those studies is that they were conducted on the Marfan syndrome mice model, which develop a myxomatous remodeling of MV but the mechanisms behind cannot resume the non-syndromic forms. Marfan

syndrome is a connective tissue disorders caused by mutations in the Fibrillin-1 gene that induces a strong increase of TGF-β levels and signaling in the MV, but also large disruption of elastin fibers that could act as potent chemoattractant. The combination of increase TGF-β signaling, and elastin fragmentation could thus induce the activation of resident macrophages and/or recruitment of circulating monocytes. Indeed, numerous studies have investigated the immune functions of TGF-β.[288,289] Notably, endothelial cell-derived TGF-β1 participates to lungs interstitial macrophages (IM) development by promoting the core IM transcriptional program in monocytes.[290]

Our group recently generated and phenotyped the first rat model of MVD that recapitulates the Human pathology, and better represents the non-syndromic form of MVD.[207,208] Our enrichment analysis of bulk transcriptomic data highlighted a major role of immune cells in MVD as 30% of GO-terms were related to chemotaxis and immune cells. These results and the previous work from other groups on different forms of MVD lead to the genesis of this project with the aim of understanding how macrophages contribute to the development or the maintenance of non-syndromic MVD.

1. Dynamic of MVD progression and macrophage recruitment in the *FLNA*-KI rat model

The first step of our analysis was to determine if the 'Immune cells' signature found in the transcriptomic data at three weeks[208] was induced by an increased number of macrophages in the MV or a local activation of the tissue-resident macrophages of the MV. Flow cytometry experiments revealed that the proportion of macrophages was increased in *FLNA*-KI MV at the age of three weeks, clearly indicating either recruitment of circulating monocytes or local

proliferation of resident macrophages. However, we weren't able to discriminate more precisely the different macrophages population or phenotype due to a limited antibody panel for flow cytometry of rat samples. To determine the timeframe of macrophages expansion in the tissue and if they could actively contribute to the remodeling of the tissue, we performed a time-course phenotyping of the *FLNA*-KI rats MV. It is well described that the MV leaflets undergo a post-natal maturation process that includes remodeling of the ECM to switch from a proteoglycan-rich cardiac jelly to a collagen and elastin layered structure.[32,66,291] Therefore, differentiating a pathological or a physiological remodeling of the leaflets was not possible in newborn and 2-days old rats MV. Nonetheless, we did find the molecular signature of ECM remodeling at birth with overexpression of *Has1*, and overexpression of the endothelial dysfunction marker *Esm1* at 2 days post-natal but not at birth. This suggest that filamin A mutation induces ECM defect as early as birth, marked by increased hyaluronan production, rapidly followed by endothelial dysfunction, probably related to the drastic circulatory modification after birth with closure of the oval foramen and increased pressure in the heart chambers.[292] It remains uncertain if those two mechanisms are interdependent or act as a "double-hit" to initiate the vicious cercle of MV remodeling.

At 7-days post-natal, the leaflets of WT animals are thinner and more structured, whereas those of KI rats appeared enlarged with high proteoglycan content, consistent with the remodeling observed in more advanced stages. The transcriptomic signature of ECM remodeling and cellular activation was also present at this stage, with dysregulation of the typical markers of MVD that we had previously identified in our RNA-seq analysis at three weeks (overexpression of *Has1* and *Esm1*, downregulation of *Hyal1*).[208] More interestingly, we also found an enrichment for immune cells process and chemotaxis in the MV of *FLNA*-KI rats, but macrophages proportion were similar in both genotypes as assessed by flow cytometry. The single nuclei RNA-seq experiment allowed us to refine these finding, as the immune signature

was only found in VECs at seven days. Interestingly, the immune signature later extended to the VICs population in three weeks old rats.

Overall, our results indicate that ECM remodeling is the first process of *FLNA*-MVD development, followed by endothelial dysfunction. By 7-days old, VECs secrete chemoattractant factors leading to the increase of macrophage proportion that we can observe in three weeks-old animals. How Filamin A mutation causes early ECM defects is still unclear, but we also found an upregulation of *Has1* in E19.5 embryos MV (data not shown) that indicate a developmental origin of *FLNA*-MVD, consistent with the previous studies conducted with Filamin A knock-out mice model.[193,206] It is likely that the chemotactic signaling observed at 7 days is a normal response to the accumulation of ECM. However, the fact that this immune microenvironment persists over time and even extend to the VICs population at Three weeks suggest an inability of macrophages to resolve the remodeling. Whether the macrophages then participate to the remodeling is still unknown, and a better characterization of the macrophage's subpopulations is needed.

2. Contribution of macrophages to Human sporadic forms of MVD

In the general population, *FLNA* mutation are extremely rare and represents a very minor number of MVD cases, the vast majority being sporadic forms of MVD. It is thus legitimate to question if the findings from the *FLNA*-KI rats are translatable to Human sporadic form of MVD. To this aim, we collected a unique cohort of 78 samples of MV obtained from patients with severe myxomatous MVD undergoing surgery, and performed bulk RNA sequencing. As we could have expected, the 2000 most expressed genes of the tissue were enriched in pathways related to extracellular matrix and cytoskeleton, adhesion, and TGF-β signaling. But

interestingly, there were also two immune pathways over-represented: 'Humoral immune response', and 'Leukocyte transendothelial migration'. This first indication of leukocytes recruitment was supported by a deconvolution analysis using xCell algorithm[293], which inferred macrophage molecular signature as the most predominant in the expression data. Furthermore, we validated by immunohistochemistry against CD68, that there were more macrophages invading MVD samples compared to the control sample. Additionally, macrophages exhibited the same localization as we observed in the *FLNA*-KI rat model. In control MV, macrophages were located beneath the endothelium at the atrial side, but were also found in the spongiosa of MVD patients, specifically in areas of intense remodeling and proteoglycan content. Numerous studies have highlighted that macrophage have different functions depending on their surrounding niches.[228,253,294,295] We can hypothesize that sub-endothelial macrophages are resident macrophages and serve as sentinel to maintain tissue homeostasis. Their physical proximity with endothelial cells would allow them to quickly respond to a stress or physical insult. The additional macrophages observed in *FLNA*-KI or in Human MVD samples are found in highly remodeled area of the spongiosa, and in some area of the fibrosa. It is likely that those macrophages are monocyte-derived, and recruited in the tissue with the purpose of tissue repair, but additional experiments are required to consolidate those hypotheses.

Eventually, we compared the similarities between human MVD and the *FLNA*-KI rats. Among the 2000 most expressed genes of Human sporadic MVD and *FLNA*-KI rats MVD, we found 47% common genes. More interestingly, the over-representation analysis of these common genes highlighted 'Leukocyte migration' as the most enriched pathways, followed by actin cytoskeleton, collagen, adhesion, integrin and TGF-β. This important result strongly consolidates our previous findings. We had already demonstrated that the *FLNA*-KI rat model recapitulates the Human phenotype at the morphological level, we now have a clear common

transcriptional signature, and the confirmation that macrophages are not specific to FLNA- or Marfan syndrome-related MVD.

Overall, our analysis provides the first evidence for a contribution of macrophages in the pathophysiology of MVD in a large cohort. We also described the similarities between *FLNA*-KI and Human sporadic MVD with a common phenotypic and molecular signature. Those results highlight the pertinence of the *FLNA*-KI rat as a model for sporadic MVD, and its relevance to decipher the role of macrophages in the disease.

3. Macrophages in the mitral valve niche

The role of macrophages in the disease progression is still unclear. Our first hypothesis was that macrophages acquire a pro-inflammatory phenotype, consistent with the increased expression of pro-inflammatory cytokines *Ccl7* and *S100a8* that we previously described in the *FLNA*-KI rat.[208] Our current analysis also revealed upregulation of several pro-inflammatory cytokines, as we found increased expression of *Ccl7*, *Tnfsf18*, or *Il1b* in the bulk RNA-seq of 7 days old rats. This hypothesis was also supported by the fact that ECM components can act as damage-associated molecular patterns (DAMP), and induce the pro-inflammatory nuclear factor-kappa B (NF-κB) pathway through their recognition by toll-like receptors (TLR2 and TLR4) from immune cells, including macrophages.[296–300] For example, hyaluronan, a major component of the MV ECM and increased in *FLNA*-KI MVD, serve as a platform for leukocytes and modulates inflammation.[301–303] Notably, it was shown that *HAS3*-null mice had decreased inflammation and tissue damage in a model of colitis, disease in which hyaluronan deposition is altered.[304,305] However, the single nuclei RNAseq analysis performed on *FLNA*-KI rats failed to identify an abundant population of pro-inflammatory macrophages. Instead, macrophages seem to adopt a pro-healing phenotype without significant differences between KI and WT

genotype. Consistently, the xCell deconvolution algorithm revealed that the "M2 macrophage" molecular signature was the most enriched in the Human cohort of MVD. Although the M1/M2 macrophage paradigm has been refuted *in vivo* and should not be used, the M2 signature refers to a pro-resolving/pro-healing phenotype, as opposed to the pro-inflammatory M1 phenotype. Despite being contradictory to our hypothesis, those results were consistent with another report from 2024 in which authors used MVD microarray data and performed a digital cell quantification with the already validated LM22 dataset (22 human immune cell type signature) as reference.[276,306] They found the same 'M2 macrophage' as the predominant immune signature in their dataset. The choice of LM22 reference dataset to compute for a digital cell quantification is questionable, as the reference used for the M1 and M2 macrophages signature is an in vitro polarization of bone-marrow derived macrophages using a cocktail of LPS, IFN-γ or IL-4. Such experiment cannot resume the diversity and complexity of endogenous macrophages.[307] Therefore, we selected the xCell algorithm that rely on 6 dataset compiling a total of 1725 samples and 64 cell types, to compute immune cell type enrichment in our samples, and found the same results.[293]

The *FLNA* P637Q mutation is located in the actin-binding domain of Filamin A. Therefore, it is possible that the mutation affects macrophage core functions, phagocytosis. In an attempt to answer this question, we assessed phagocytosis using primary culture of peritoneal macrophages and revealed no differences between non-mutated and *FLNA*-mutated macrophages. It will be important in the near future to also assess efferocytosis of the valvular macrophages instead of phagocytosis.[220,308] Indeed, efferocytosis refers to the specific process of apoptotic cell clearance, an essential mechanism of development and tissue homeostasis, and is therefore more relevant in the context of myxomatous remodeling of the MV.

A few limitations arise from these experiments. Peritoneal macrophages are thioglycolate-activated monocyte-derived macrophages, and therefore doesn't represent the ontogenic and phenotypic diversity of endogenous valvular macrophages.[309] One of the objectives of this project was to develop inducible Pluripotent Stem Cells (iPSC)-derived macrophages. The protocol is well-established, and implies the formation of embryoid bodies (EBs) for mesodermal differentiation. The EBs are then differentiated into hemogenic endothelium that will produce non-adherent macrophage precursors (preMac) that can be easily harvested from the media. The advantages offered by this approach are numerous: first, iPSC-derived macrophages are a better model for yolk-sac derived macrophages. Second, the macrophages precursor obtained are "naïve" and can further be differentiated into specific macrophage population. Finally, as we already have *FLNA* patients-derived iPSC, we could have assessed the effect of the mutation on resident macrophages. However, despite numerous attempts, we were not able to achieve the EBs formation from *FLNA*-iPSC. One of the hypotheses is that *FLNA*-iPSC are unable to form EBs due to adhesion defect in the absence of extracellular matrix Indeed, although the *FLNA*-iPSC grew normally on Matrigel coating, they didn't survive during the generation of EBs. It is possible that the *FLNA* mutation impairs their ability to form intercellular adhesion in this context.[189]

Overall, it seems that macrophages in the diseased MV does not have a pro-inflammatory phenotype as it was initially thought but rather acquire a pro-healing phenotype. This raises new questions regarding their role in the disease. Consistently with the specific distribution of macrophages (i.e. in areas of intense remodeling) that we described, it is probable that the monocyte-derived macrophages are recruited to resolve the accumulation of ECM. However, the interactions between valvular macrophages and VICs remains largely unknown. The field of macrophage-fibroblast interactions is raising interest, notably in tumor research, and it is now established that they are capable of regulating each other's functions.[310–312] The influence

of ECM on macrophages phenotype should also be studied more closely as it is more and more clear that the ECM can directly influence macrophage response and phenotype.[313–315] Deciphering more precisely those interactions would benefit to the comprehension of MVD pathogenesis, and potentially provide new therapeutic targets.

4. The *FLNA*-KI rat model

Our study was conducted using the Filamin A P637Q Knock-in rat model. The phenotype has been previously published by our group and shows that it recapitulates the Human phenotype. The results obtained in the current study support and extend those findings, as we have provided the first evidences of macrophage expansion in a Human cohort of MV samples, as well as a shared molecular signature between Human sporadic MVD and *FLNA*-KI pointing out leukocyte migration as the most enriched pathway. Rat model are much larger than mice, making it convenient for the characterization of the heart and for the MV morphology and function with imaging techniques such as echocardiography and micro-computed tomography. In addition, rats MV can be used to generate primary culture of VICs, which can subsequently be used for *in vitro* assays. Nonetheless the rat model has limitations that leaves some of our questions unanswered. Firstly, designing a flow cytometry panel is very limited for rat markers. Despite many trials, we haven't been able to design one that would have allowed the identification of the different macrophage populations. It would have been interesting to investigate if the valvular macrophage populations are similar to the resident cardiac macrophages already described, with $CCR2^-$ and $CCR2^+$ populations, and to decipher which population is expanded upon MVD development. The single nuclei RNA-seq seems to indicate that the monocyte-derived $CCR2^+$ macrophage population is expanded in KI rats but this result should be taken cautiously because of the non-quantitative nature of snRNA-seq data.

The use of a rat model was also a limit for the depletion of macrophages. Indeed, despite two different methods: clodronate (data not shown) and CCR2 inhibitor, the depletion of macrophages in the *FLNA*-KI rats was incomplete, and it remains uncertain why it couldn't be achieved. The possibility of genetic depletion of macrophages was explored, but the only rat strain available is the *Csf1r* $^{-/-}$ Dark Agouti rat. The *FLNA*-KI rat was created from the Sprague-Dawley strain, meaning it would have required a long genetic backcross to generate *Csf1r* $^{-/-}$; *FLNA*-KI rats.

Instead, our group chose to generate a mice model carrying the *FLNA* P637Q mutation. Having a mice model instead of rat will allow us to overcome several of the limitations described above. Indeed, mice models offer much more tools that will be of particular interest to investigate the role of macrophages in MVD.[316–320] First of all, once MVD phenotype will be confirmed in the new mice model, new flow cytometry experiment will allow us identify the relevant markers for valvular macrophages to discriminate the different sub-population, and identify how these populations behave upon MVD. Fate mapping experiment would allow to precisely identify the origin of each sub-population, and follow their fate during the development and progression of the disease. Finally, several genetic depletion models are available in order to selectively deplete a specific population of macrophages. For example, it would be possible to deplete monocyte-derived macrophages by using a CCR2$^{-/-}$ mice, or deplete resident yolk-sac derived macrophages with a Cx3cr1$^{-/-}$ mice. Those genetic models also exist as Tamoxifen-inducible model by combining the Cre recombinase to the estrogen receptor ER. Therefore, it is possible to selectively and temporally deplete a population of macrophages to decipher their contribution to MVD development, but also to valvulogenesis.

5. Conclusions and perspectives

This thesis has attached to decipher the dynamic of MVD and more precisely to understand the role of macrophages in the development or the maintenance of the disease. It has successfully showed the dynamic of MVD development in the Filamin A P637Q rat model, highlighting the early extracellular matrix disturbance. This was rapidly followed by endothelial activation and resulted in a myxomatous remodeling of the MV as detected in 7-days old rats. We also demonstrated that it is from this timepoint that the valvular endothelial cells upregulate chemotactic signaling. This led to a recruitment of monocyte-derived macrophages in the tissue in advanced stage of MVD. The precise mechanisms behind macrophage activation and recruitment are still unclear, but experiments are ongoing to understand the mechanisms of macrophage recruitment and the role of adhesion molecules. Although we made significant progress in the definition of the macrophage population with the single nuclei experiment, it does not allow us to precisely conclude on their ontogeny. Future experiments are needed to answers those important questions. Notably, the development of a mice model of MVD carrying the *FLNA* mutation will allow fate mapping and selective depletion of macrophages, to bring valuable insight in our understanding of MVD.

We successfully demonstrated that macrophages did not participate or played an active role in the early process of MVD but rather contribute to its progression. We have established that the early mechanisms leading to MVD are related to the ECM homeostasis, and endothelial activation most likely induce by mechanical stress. However, how those mechanisms are initiated and how they temporally and spatially regulate MV remodeling remains unknown. Our group is committed to elucidate those questions, and an ongoing project aims to decipher the role of mechanical stress using *in vitro* models of stress and 3D cultures of VICs.

Eventually, this thesis paves the way to change the current views of the MV physiology and pathophysiology. By recognizing the role of macrophages in MV development as well as their unique contribution to MVD, we have a unique opportunity to discover new therapeutic targets in order to better detect and potentially treat patients suffering from MVD.

VI. References

1. Iung, B. *et al.* Contemporary Presentation and Management of Valvular Heart Disease: The EURObservational Research Programme Valvular Heart Disease II Survey. *Circulation* **140**, 1156–1169 (2019).

2. Iung, B. & Vahanian, A. Epidemiology of Acquired Valvular Heart Disease. *Canadian Journal of Cardiology* **30**, 962–970 (2014).

3. Praz, F. *et al.* 2025 ESC/EACTS Guidelines for the management of valvular heart disease. *European Heart Journal* ehaf194 (2025) doi:10.1093/eurheartj/ehaf194.

4. Nkomo, V. T. *et al.* Burden of valvular heart diseases: a population-based study. *The Lancet* **368**, 1005–1011 (2006).

5. Enriquez-Sarano, M., Messika-Zeitoun, D., Nkomo, V. & Tajik, A. J. Quantitative Determinants of the Outcome of Asymptomatic Mitral Regurgitation. *The new england journal of medicine* (2005).

6. Tumenas, A., Tamkeviciute, L., Arzanauskiene, R. & Arzanauskaite, M. Multimodality Imaging of the Mitral Valve: Morphology, Function, and Disease. *Curr Probl Diagn Radiol* **50**, 905–924 (2021).

7. Dal-Bianco, J. P., Beaudoin, J., Handschumacher, M. D. & Levine, R. A. Basic mechanisms of mitral regurgitation. *Can J Cardiol* **30**, 971–981 (2014).

8. Chen, S. *et al.* Mechanical and morphometric study of mitral valve chordae tendineae and related papillary muscle. *J Mech Behav Biomed Mater* **111**, 104011 (2020).

9. Debonnaire, P., Palmen, M., Marsan, N. A. & Delgado, V. Contemporary imaging of normal mitral valve anatomy and function. *Curr Opin Cardiol* **27**, 455–464 (2012).

10. Du Plessis, L. A. & Marchand, P. The Anatomy of the Mitral Valve and its Associated Structures. *Thorax* **19**, 221–227 (1964).

11. Gross, L. Topographic anatomy and histology of the valves in the human heart.

12. Hjortnaes, J. *et al.* Comparative Histopathological Analysis of Mitral Valves in Barlow Disease and Fibroelastic Deficiency. *Semin Thorac Cardiovasc Surg* **28**, 757–767 (2016).

13. Gupta, V. *et al.* Abundance and location of proteoglycans and hyaluronan within normal and myxomatous mitral valves. *Cardiovasc Pathol* **18**, 191–197 (2009).

14. Cole, W. G., Chan, D., Hickey, A. J. & Wilcken, D. E. L. Collagen composition of normal and myxomatous human mitral heart valves. *Biochemical Journal* **219**, 451–460 (1984).

15. Canty, E. G. & Kadler, K. E. Procollagen trafficking, processing and fibrillogenesis. *J Cell Sci* **118**, 1341–1353 (2005).

16. Merryman, W. D. *et al.* Correlation between heart valve interstitial cell stiffness and transvalvular pressure: implications for collagen biosynthesis. *American Journal of Physiology-Heart and Circulatory Physiology* **290**, H224–H231 (2006).

17. Ponta, H., Sherman, L. & Herrlich, P. A. CD44: from adhesion molecules to signalling regulators. *Nat Rev Mol Cell Biol* **4**, 33–45 (2003).

18. Lockhart, M., Wirrig, E., Phelps, A. & Wessels, A. Extracellular matrix and heart development. *Birth Defects Research* **91**, 535–550 (2011).

19. Grande-Allen, K. J. *et al.* Glycosaminoglycans and proteoglycans in normal mitral valve leaflets and chordae: association with regions of tensile and compressive loading. *Glycobiology* **14**, 621–633 (2004).

20. Wight, T. N. Versican: a versatile extracellular matrix proteoglycan in cell biology. *Curr Opin Cell Biol* **14**, 617–623 (2002).

21. Combs, M. D. & Yutzey, K. E. Heart Valve Development: Regulatory Networks in Development and Disease. *Circulation Research* **105**, 408–421 (2009).

22. De Vlaming, A. *et al.* Atrioventricular valve development: New perspectives on an old theme. *Differentiation* **84**, 103–116 (2012).

23. Butcher, J. T., Penrod, A. M., García, A. J. & Nerem, R. M. Unique Morphology and Focal Adhesion Development of Valvular Endothelial Cells in Static and Fluid Flow Environments. *ATVB* **24**, 1429–1434 (2004).

24. Butcher, J. T. & Nerem, R. M. Valvular endothelial cells and the mechanoregulation of valvular pathology. *Phil. Trans. R. Soc. B* **362**, 1445–1457 (2007).

25. Blomme, B. *et al.* Mechanical strain induces a pro-fibrotic phenotype in human mitral valvular interstitial cells through RhoC/ROCK/MRTF-A and Erk1/2 signaling pathways. *Journal of Molecular and Cellular Cardiology* **135**, 149–159 (2019).

26. Ahuja, N., Ostwald, P., Bark, D. & Garrity, D. Biomechanical Cues Direct Valvulogenesis. *JCDD* **7**, 18 (2020).

27. Vignes, H. *et al.* Extracellular mechanical forces drive endocardial cell volume decrease during zebrafish cardiac valve morphogenesis. *Developmental Cell* **57**, 598-609.e5 (2022).

28. Sluiter, T. J., van Buul, J. D., Huveneers, S., Quax, P. H. A. & de Vries, M. R. Endothelial Barrier Function and Leukocyte Transmigration in Atherosclerosis. *Biomedicines* **9**, 328 (2021).

29. Medrano-Bosch, M., Simón-Codina, B., Jiménez, W., Edelman, E. R. & Melgar-Lesmes, P. Monocyte-endothelial cell interactions in vascular and tissue remodeling. *Front Immunol* **14**, 1196033 (2023).

30. Parra-Izquierdo, I. *et al.* Interferons Are Pro-Inflammatory Cytokines in Sheared-Stressed Human Aortic Valve Endothelial Cells. *Int J Mol Sci* **22**, 10605 (2021).

31. Shu, S. *et al.* Cellular Landscapes of Nondiseased Human Cardiac Valves From End-Stage Heart Failure–Explanted Heart. *ATVB* 10.1161/ATVBAHA.122.318314 (2022) doi:10.1161/ATVBAHA.122.318314.

32. Hulin, A. *et al.* Maturation of heart valve cell populations during postnatal remodeling. *Development* dev.173047 (2019) doi:10.1242/dev.173047.

33. O'Donnell, A. *et al.* Localized Prox1 Regulates Aortic Valve Endothelial Cell Diversity and Extracellular Matrix Stratification in Mice. *ATVB* **43**, 1478–1493 (2023).

34. von Gise, A. & Pu, W. T. Endocardial and Epicardial Epithelial to Mesenchymal Transitions in Heart Development and Disease. *Circ Res* **110**, 1628–1645 (2012).

35. Liu, A. C., Joag, V. R. & Gotlieb, A. I. The Emerging Role of Valve Interstitial Cell Phenotypes in Regulating Heart Valve Pathobiology. *The American Journal of Pathology* **171**, 1407–1418 (2007).

36. Liu, A. C., Joag, V. R. & Gotlieb, A. I. The Emerging Role of Valve Interstitial Cell Phenotypes in Regulating Heart Valve Pathobiology. *The American Journal of Pathology* **171**, 1407–1418 (2007).

37. Fu, X. *et al.* Specialized fibroblast differentiated states underlie scar formation in the infarcted mouse heart. *Journal of Clinical Investigation* **128**, 2127–2143 (2018).

38. Visconti, R. P. *et al.* An In Vivo Analysis of Hematopoietic Stem Cell Potential: Hematopoietic Origin of Cardiac Valve Interstitial Cells. *Circ Res* **98**, 690–696 (2006).

39. Hajdu, Z. *et al.* Recruitment of bone marrow-derived valve interstitial cells is a normal homeostatic process. *Journal of Molecular and Cellular Cardiology* **51**, 955–965 (2011).

40. Sauls, K. *et al.* Increased Infiltration of Extra-Cardiac Cells in Myxomatous Valve Disease. *J Cardiovasc Dev Dis.* **2**, 200–213 (2015).

41. Hulin, A. *et al.* Macrophage Transitions in Heart Valve Development and Myxomatous Valve Disease. *ATVB* **38**, 636–644 (2018).

42. Zubrzycki, M. *et al.* Cardiac Development and Factors Influencing the Development of Congenital Heart Defects (CHDs): Part I. *IJMS* **25**, 7117 (2024).

43. Person, A. D., Klewer, S. E. & Runyan, R. B. Cell Biology of Cardiac Cushion Development. in *International Review of Cytology* vol. 243 287–335 (Elsevier, 2005).

44. Farhat, B. *et al.* Understanding the cell fate and behavior of progenitors at the origin of the mouse cardiac mitral valve. *Developmental Cell* S1534580723006561 (2024) doi:10.1016/j.devcel.2023.12.006.

45. Lin, C.-J., Lin, C.-Y., Chen, C.-H., Zhou, B. & Chang, C.-P. Partitioning the heart: mechanisms of cardiac septation and valve development. *Development* **139**, 3277–3299 (2012).

46. Goddard, L. M. *et al.* Hemodynamic Forces Sculpt Developing Heart Valves through a KLF2-WNT9B Paracrine Signaling Axis. *Developmental Cell* **43**, 274-289.e5 (2017).

47. Pham, D. H., Dai, C. R., Lin, B. Y. & Butcher, J. T. Local fluid shear stress operates a molecular switch to drive fetal semilunar valve extension. *Developmental Dynamics* **251**, 481–497 (2022).

48. Astrof, S., Crowley, D. & Hynes, R. O. Multiple cardiovascular defects caused by the absence of alternatively spliced segments of fibronectin. *Developmental Biology* **311**, 11–24 (2007).

49. Wang, Y. *et al.* Endocardial to myocardial notch-wnt-bmp axis regulates early heart valve development. *PLoS One* **8**, e60244 (2013).

50. Rivera-Feliciano, J. & Tabin, C. J. Bmp2 instructs cardiac progenitors to form the heart-valve-inducing field. *Dev Biol* **295**, 580–588 (2006).

51. Liu, N. *et al.* Notch and retinoic acid signals regulate macrophage formation from endocardium downstream of Nkx2-5. *Nat Commun* **14**, 5398 (2023).

52. Wu, B. *et al.* Nfatc1 Coordinates Valve Endocardial Cell Lineage Development Required for Heart Valve Formation. *Circulation Research* **109**, 183–192 (2011).

53. Johnson, E. N. *et al.* NFATc1 mediates vascular endothelial growth factor-induced proliferation of human pulmonary valve endothelial cells. *J Biol Chem* **278**, 1686–1692 (2003).

54. Armstrong, E. J. & Bischoff, J. Heart valve development: endothelial cell signaling and differentiation. *Circ Res* **95**, 459–470 (2004).

55. De La Pompa, J. L. *et al.* Role of the NF-ATc transcription factor in morphogenesis of cardiac valves and septum. *Nature* **392**, 182–186 (1998).

56. Ranger, A. M. *et al.* The transcription factor NF-ATc is essential for cardiac valve formation. *Nature* **392**, 186–190 (1998).

57. Lange, A. W. & Yutzey, K. E. NFATc1 expression in the developing heart valves is responsive to the RANKL pathway and is required for endocardial expression of cathepsin K. *Developmental Biology* **292**, 407–417 (2006).

58. Gunawan, F., Gentile, A., Gauvrit, S., Stainier, D. Y. R. & Bensimon-Brito, A. Nfatc1 Promotes Interstitial Cell Formation During Cardiac Valve Development in Zebrafish. *Circ Res* **126**, 968–984 (2020).

59. Armesilla, A. L. *et al.* Vascular endothelial growth factor activates nuclear factor of activated T cells in human endothelial cells: a role for tissue factor gene expression. *Mol Cell Biol* **19**, 2032–2043 (1999).

60. Stankunas, K., Ma, G. K., Kuhnert, F. J., Kuo, C. J. & Chang, C.-P. VEGF signaling has distinct spatiotemporal roles during heart valve development. *Dev Biol* **347**, 325–336 (2010).

61. Miquerol, L., Gertsenstein, M., Harpal, K., Rossant, J. & Nagy, A. Multiple developmental roles of VEGF suggested by a LacZ-tagged allele. *Dev Biol* **212**, 307–322 (1999).

62. Combs, M. D. & Yutzey, K. E. Heart Valve Development: Regulatory Networks in Development and Disease. *Circulation Research* **105**, 408–421 (2009).

63. Heckel, E. *et al.* Oscillatory Flow Modulates Mechanosensitive klf2a Expression through trpv4 and trpp2 during Heart Valve Development. *Current Biology* **25**, 1354–1361 (2015).

64. da Silva, A. R. *et al.* egr3 is a mechanosensitive transcription factor gene required for cardiac valve morphogenesis. *Sci Adv* **10**, eadl0633 (2024).

65. Camenisch, T. D. *et al.* Disruption of hyaluronan synthase-2 abrogates normal cardiac morphogenesis and hyaluronan-mediated transformation of epithelium to mesenchyme. *J. Clin. Invest.* **106**, 349–360 (2000).

66. Aikawa, E. *et al.* Human Semilunar Cardiac Valve Remodeling by Activated Cells From Fetus to Adult: Implications for Postnatal Adaptation, Pathology, and Tissue Engineering. *Circulation* **113**, 1344–1352 (2006).

67. Hinton, R. B. *et al.* Extracellular Matrix Remodeling and Organization in Developing and Diseased Aortic Valves. *Circulation Research* **98**, 1431–1438 (2006).

68. Peacock, J. D., Lu, Y., Koch, M., Kadler, K. E. & Lincoln, J. Temporal and spatial expression of collagens during murine atrioventricular heart valve development and maintenance. *Dev Dyn* **237**, 3051–3058 (2008).

69. Chandrashekhar, Y., Westaby, S. & Narula, J. Mitral stenosis. *The Lancet* **374**, 1271–1283 (2009).

70. Carpentier, A. *et al.* Reconstructive surgery of mitral valve incompetence. *The Journal of Thoracic and Cardiovascular Surgery* **79**, 338–348 (1980).

71. Carpentier, A. Cardiac valve surgery—the "French correction". *The Journal of Thoracic and Cardiovascular Surgery* **86**, 323–337 (1983).

72. Stone, G. W. *et al.* Clinical Trial Design Principles and Endpoint Definitions for Transcatheter Mitral Valve Repair and Replacement: Part 1: Clinical Trial Design Principles. *Journal of the American College of Cardiology* **66**, 278–307 (2015).

73. Monteagudo Ruiz, J. M. *et al.* Overview of mitral regurgitation in Europe: results from the European Registry of mitral regurgitation (EuMiClip). *Eur Heart J Cardiovasc Imaging* **19**, 503–507 (2018).

74. Freed, L. A. *et al.* Prevalence and clinical outcome of mitral-valve prolapse. *N Engl J Med* **341**, 1–7 (1999).

75. Messika-Zeitoun, D. *et al.* Clinical Presentation and Outcomes After Surgery for Mitral Regurgitation: Real-World Insights From the MITRACURE International Registry. *Circulation* **152**, 927–938 (2025).

76. Dietz, H. FBN1-Related Marfan Syndrome. 24.

77. Attias, D. *et al.* Comparison of Clinical Presentations and Outcomes Between Patients With *TGFBR2* and *FBN1* Mutations in Marfan Syndrome and Related Disorders. *Circulation* **120**, 2541–2549 (2009).

78. Le Tourneau, T. *et al.* Genetics of syndromic and non-syndromic mitral valve prolapse. *Heart* **104**, 978–984 (2018).

79. Morningstar, J. E. *et al.* Mitral Valve Prolapse and Its Motley Crew-Syndromic Prevalence, Pathophysiology, and Progression of a Common Heart Condition. *JAHA* **10**, e020919 (2021).

80. Loeys, B. L. *et al.* A syndrome of altered cardiovascular, craniofacial, neurocognitive and skeletal development caused by mutations in TGFBR1 or TGFBR2. *Nat Genet* **37**, 275–281 (2005).

81. Gouda, P. *et al.* Clinical features and complications of Loeys-Dietz syndrome: A systematic review. *International Journal of Cardiology* **362**, 158–167 (2022).

82. Atzinger, C. L., Meyer, R. A., Khoury, P. R., Gao, Z. & Tinkle, B. T. Cross-Sectional and Longitudinal Assessment of Aortic Root Dilation and Valvular Anomalies in Hypermobile and Classic Ehlers-Danlos Syndrome. *The Journal of Pediatrics* **158**, 826-830.e1 (2011).

83. van Wijngaarden, A. L., Kruithof, B. P. T., Vinella, T., Barge-Schaapveld, D. Q. C. M. & Ajmone Marsan, N. Characterization of Degenerative Mitral Valve Disease: Differences between Fibroelastic Deficiency and Barlow's Disease. *JCDD* **8**, 23 (2021).

84. Anyanwu, A. C. & Adams, D. H. Etiologic Classification of Degenerative Mitral Valve Disease: Barlow's Disease and Fibroelastic Deficiency. *Seminars in Thoracic and Cardiovascular Surgery* **19**, 90–96 (2007).

85. Levine, R. A. *et al.* Mitral valve disease—morphology and mechanisms. *Nat Rev Cardiol* **12**, 689–710 (2015).

86. Cuffer, M. & Barbillion, M. Nouvelles recherches sur le bruit de galop cardiaque. *Archives générales de médecine* 19:129-149 (1887).

87. Barlow, J. B. & Pocock, W. A. The significance of late systolic murmurs and mid-late systolic clicks. *Md State Med J* **12**, 76–77 (1963).

88. Criley, J. M., Lewis, K. B., Humphries, J. O. & Ross, R. S. Prolapse of the mitral valve: clinical and cine-angiocardiographic findings. *Heart* **28**, 488–496 (1966).

89. Pomerance, A. Ballooning deformity (mucoid degeneration) of atrioventricular valves. *Br Heart J* **31**, 343–351 (1969).

90. Trent, J. K., Adelman, A. G., Wigle, E. D. & Silver, M. D. Morphology of a prolapsed posterior mitral valve leaflet. *Am Heart J* **79**, 539–543 (1970).

91. Hayek, E., Gring, C. N. & Griffin, B. P. Mitral valve prolapse. *Lancet* **365**, 507–518 (2005).

92. Le Tourneau, T. *et al.* New insights into mitral valve dystrophy: a Filamin-A genotype–phenotype and outcome study. *European Heart Journal* **39**, 1269–1277 (2018).

93. Mentias, A. *et al.* Prognostic Utility of Brain Natriuretic Peptide in Asymptomatic Patients With Significant Mitral Regurgitation and Preserved Left Ventricular Ejection Fraction. *Am J Cardiol* **117**, 258–263 (2016).

94. Basso, C. *et al.* Arrhythmic Mitral Valve Prolapse and Sudden Cardiac Death. *Circulation* **132**, 556–566 (2015).

95. Feldman, T. *et al.* Randomized Comparison of Percutaneous Repair and Surgery for Mitral Regurgitation. *Journal of the American College of Cardiology* **66**, 2844–2854 (2015).

96. Mauri, V. *et al.* Early Outcomes of 2 Mitral Valve Transcatheter Leaflet Approximation Devices. *JACC: Cardiovascular Interventions* **15**, 2541–2551 (2022).

97. Makkar, R. *et al.* CLASP IID Trial and Registry: 2-Year Outcomes of Transcatheter Repair for Degenerative Mitral Regurgitation. *JACC Cardiovasc Interv* **18**, 2392–2404 (2025).

98. Heimansohn, D. A. *et al.* Mid-term outcomes of the COMMENCE trial investigating mitral valve replacement using a bioprosthesis with a novel tissue. *JTCVS Open* **15**, 151–163 (2023).

99. Hunt, D. & Sloman, G. Prolapse of the posterior leaflet of the mitral valve occurring in eleven members of a family. *Am Heart J* **78**, 149–153 (1969).

100. Devereux, R. B., Brown, W. T., Kramer-Fox, R. & Sachs, I. Inheritance of mitral valve prolapse: effect of age and sex on gene expression. *Ann Intern Med* **97**, 826–832 (1982).

101. Kyndt, F. *et al.* Mapping of X-Linked Myxomatous Valvular Dystrophy to Chromosome Xq28. *The American Journal of Human Genetics* **62**, 627–632 (1998).

102. Kyndt, F. *et al.* Mutations in the Gene Encoding Filamin A as a Cause for Familial Cardiac Valvular Dystrophy. *Circulation* **115**, 40–49 (2007).

103. Bernstein, J. A., Bernstein, D., Hehr, U. & Hudgins, L. Familial cardiac valvulopathy due to filamin A mutation. *Am J Med Genet A* **155A**, 2236–2241 (2011).

104. Aalberts, J. J. J. *et al.* Screening of TGFBR1, TGFBR2, and FLNA in familial mitral valve prolapse. *Am J Med Genet A* **164A**, 113–119 (2014).

105. Durst, R. *et al.* Mutations in DCHS1 cause mitral valve prolapse. *Nature* **525**, 109–113 (2015).

106. Toomer, K. A. *et al.* Primary cilia defects causing mitral valve prolapse. *Sci. Transl. Med.* **11**, eaax0290 (2019).

107. Clark, H. F. *et al.* Dachsous encodes a member of the cadherin superfamily that controls imaginal disc morphogenesis in Drosophila. *Genes Dev.* **9**, 1530–1542 (1995).

108. PROMESA investigators *et al.* Genetic association analyses highlight biological pathways underlying mitral valve prolapse. *Nat Genet* **47**, 1206–1211 (2015).

109. Roselli, C. *et al.* Genome-wide association study reveals novel genetic loci: a new polygenic risk score for mitral valve prolapse. *European Heart Journal* **43**, 1668–1680 (2022).

110. Shpitzen, S. Characterization of LTBP2 mutation causing mitral valve prolapse.

111. Shpitzen, S. *et al.* Characterization of LTBP2 mutation causing mitral valve prolapse. *European Heart Journal Open* **5**, oeae106 (2024).

112. Le Vely, B., Delwarde, C. & Capoulade, R. Physiopathologie du prolapsus valvulaire mitral. *Archives des Maladies du Coeur et des Vaisseaux - Pratique* **2024**, 26–29 (2024).

113. Delwarde, C. *et al.* Genetics and pathophysiology of mitral valve prolapse. *Front. Cardiovasc. Med.* **10**, 1077788 (2023).

114. Guignabert, C. & Humbert, M. Targeting transforming growth factor-β receptors in pulmonary hypertension. *Eur Respir J* **57**, 2002341 (2021).

115. Ng, C. M. *et al.* TGF-β–dependent pathogenesis of mitral valve prolapse in a mouse model of Marfan syndrome. *J. Clin. Invest.* **114**, 1586–1592 (2004).

116. Hagler, M. A. *et al.* TGF-β signalling and reactive oxygen species drive fibrosis and matrix remodelling in myxomatous mitral valves. *Cardiovascular Research* **99**, 175–184 (2013).

117. Keszthelyi, D., Troost, F. J. & Masclee, A. A. M. Understanding the role of tryptophan and serotonin metabolism in gastrointestinal function. *Neurogastroenterology Motil* **21**, 1239–1249 (2009).

118. Imamdin, A. & Van Der Vorst, E. P. C. Exploring the Role of Serotonin as an Immune Modulatory Component in Cardiovascular Diseases. *IJMS* **24**, 1549 (2023).

119. Strawn, J. R., Geracioti, L., Rajdev, N., Clemenza, K. & Levine, A. Pharmacotherapy for generalized anxiety disorder in adult and pediatric patients: an evidence-based treatment review. *Expert Opinion on Pharmacotherapy* **19**, 1057–1070 (2018).

120. Pytliak, M., Vargová, V., Mechírová, V. & Felšöci, M. Serotonin Receptors – From Molecular Biology to Clinical Applications. *Physiol Res* 15–25 (2011) doi:10.33549/physiolres.931903.

121. Ayme-Dietrich, E., Lawson, R., Da-Silva, S., Mazzucotelli, J. P. & Monassier, L. Serotonin contribution to cardiac valve degeneration: new insights for novel therapies? *Pharmacological Research* **140**, 33–42 (2019).

122. Lundin, L., Norheim, I., Landelius, J., Oberg, K. & Theodorsson-Norheim, E. Carcinoid heart disease: relationship of circulating vasoactive substances to ultrasound-detectable cardiac abnormalities. *Circulation* **77**, 264–269 (1988).

123. Møller, J. E. *et al.* Prognosis of Carcinoid Heart Disease: Analysis of 200 Cases Over Two Decades. *Circulation* **112**, 3320–3327 (2005).

124. Connolly, H. M. & Edwards, B. S. Valvular Heart Disease Associated with Fenfluramine–Phentermine. (1997).

125. Volmar, K. E. & Hutchins, G. M. Aortic and Mitral Fenfluramine-Phentermine Valvulopathy in 64 Patients Treated With Anorectic Agents. *Archives of Pathology & Laboratory Medicine* **125**, 1555–1561 (2001).

126. Lancellotti, P. *et al.* High-dose oral intake of serotonin induces valvular heart disease in rabbits. *International Journal of Cardiology* **197**, 72–75 (2015).

127. Fitzgerald, L. W. *et al.* Possible role of valvular serotonin 5-HT(2B) receptors in the cardiopathy associated with fenfluramine. *Mol Pharmacol* **57**, 75–81 (2000).

128. Rothman, R. B. *et al.* Evidence for Possible Involvement of 5-HT_{2B} Receptors in the Cardiac Valvulopathy Associated With Fenfluramine and Other Serotonergic Medications. *Circulation* **102**, 2836–2841 (2000).

129. Xu, J. *et al.* Serotonin Mechanisms in Heart Valve Disease II. *The American Journal of Pathology* **161**, 2209–2218 (2002).

130. Driesbaugh, K. H. *et al.* Serotonin receptor 2B signaling with interstitial cell activation and leaflet remodeling in degenerative mitral regurgitation. *J Mol Cell Cardiol* **115**, 94–103 (2018).

131. Gustafsson, B. I. *et al.* Long-Term Serotonin Administration Induces Heart Valve Disease in Rats. *Circulation* **111**, 1517–1522 (2005).

132. Mekontso-Dessap, A. *et al.* Deficiency of the 5-hydroxytryptamine transporter gene leads to cardiac fibrosis and valvulopathy in mice. *Circulation* **113**, 81–89 (2006).

133. Castillero, E. *et al.* Decreased serotonin transporter activity in the mitral valve contributes to progression of degenerative mitral regurgitation. *Sci. Transl. Med.* **15**, eadc9606 (2023).

134. Satir, P., Pedersen, L. B. & Christensen, S. T. The primary cilium at a glance. *Journal of Cell Science* **123**, 499–503 (2010).

135. Gopalakrishnan, J. *et al.* Emerging principles of primary cilia dynamics in controlling tissue organization and function. *The EMBO Journal* **42**, e113891 (2023).

136. Sorokin, S. P. Reconstructions of centriole formation and ciliogenesis in mammalian lungs. *Journal of Cell Science* **3**, 207–230 (1968).

137. Reiter, J. F. & Leroux, M. R. Genes and molecular pathways underpinning ciliopathies. *Nat Rev Mol Cell Biol* **18**, 533–547 (2017).

138. Morleo, M., Pezzella, N. & Franco, B. Proteome balance in ciliopathies: the OFD1 protein example. *Trends in Molecular Medicine* **29**, 201–217 (2023).

139. Hale, Z. E. & Sadoshima, J. Primary Cilia and Their Role in Acquired Heart Disease. *Cells* **11**, 960 (2022).

140. Li, Y. *et al.* Global genetic analysis in mice unveils central role for cilia in congenital heart disease. *Nature* **521**, 520–524 (2015).

141. Nesta, F. *et al.* New Locus for Autosomal Dominant Mitral Valve Prolapse on Chromosome 13: Clinical Insights From Genetic Studies. *Circulation* **112**, 2022–2030 (2005).

142. Tay, S. Y. *et al.* The iguana/DZIP1 protein is a novel component of the ciliogenic pathway essential for axonemal biogenesis. *Dev Dyn* **239**, 527–534 (2010).

143. Bischoff, J. Endothelial-to-Mesenchymal Transition.

144. Alvandi, Z. & Bischoff, J. Endothelial-Mesenchymal Transition in Cardiovascular Disease. *ATVB* **41**, 2357–2369 (2021).

145. Piera-Velazquez, S. & Jimenez, S. A. Endothelial to Mesenchymal Transition: Role in Physiology and in the Pathogenesis of Human Diseases. *Physiological Reviews* **99**, 1281–1324 (2019).

146. Dal-Bianco, J. P. *et al.* Active Adaptation of the Tethered Mitral Valve: Insights Into a Compensatory Mechanism for Functional Mitral Regurgitation. *Circulation* **120**, 334–342 (2009).

147. Zhang, H. *et al.* Yap1 Is Required for Endothelial to Mesenchymal Transition of the Atrioventricular Cushion. *Journal of Biological Chemistry* **289**, 18681–18692 (2014).

148. Kovacic, J. C. *et al.* Endothelial to Mesenchymal Transition in Cardiovascular Disease. *Journal of the American College of Cardiology* **73**, 190–209 (2019).

149. Debnath, P., Huirem, R. S., Dutta, P. & Palchaudhuri, S. Epithelial–mesenchymal transition and its transcription factors. *Bioscience Reports* **42**, BSR20211754 (2022).

150. Paranya, G. *et al.* Aortic Valve Endothelial Cells Undergo Transforming Growth Factor-β-Mediated and Non-Transforming Growth Factor-β-Mediated Transdifferentiation in Vitro. *The American Journal of Pathology* **159**, 1335–1343 (2001).

151. Paruchuri, S. *et al.* Human Pulmonary Valve Progenitor Cells Exhibit Endothelial/Mesenchymal Plasticity in Response to Vascular Endothelial Growth Factor-A and Transforming Growth Factor-β_2. *Circulation Research* **99**, 861–869 (2006).

152. Wylie-Sears, J., Aikawa, E., Levine, R. A., Yang, J.-H. & Bischoff, J. Mitral Valve Endothelial Cells With Osteogenic Differentiation Potential. *ATVB* **31**, 598–607 (2011).

153. Geirsson, A. *et al.* Modulation of Transforming Growth Factor-β Signaling and Extracellular Matrix Production in Myxomatous Mitral Valves by Angiotensin II Receptor Blockers. *Circulation* **126**, (2012).

154. Shapero, K., Wylie-Sears, J., Levine, R. A., Mayer, J. E. & Bischoff, J. Reciprocal interactions between mitral valve endothelial and interstitial cells reduce endothelial-to-mesenchymal transition and myofibroblastic activation. *Journal of Molecular and Cellular Cardiology* **80**, 175–185 (2015).

155. Wylie-Sears, J., Levine, R. A. & Bischoff, J. Losartan inhibits endothelial-to-mesenchymal transformation in mitral valve endothelial cells by blocking transforming growth factor-β-induced phosphorylation of ERK. *Biochemical and Biophysical Research Communications* **446**, 870–875 (2014).

156. Kim, A. J., Alfieri, C. M. & Yutzey, K. E. Endothelial Cell Lineage Analysis Does Not Provide Evidence for EMT in Adult Valve Homeostasis and Disease. *The Anatomical Record* **302**, 125–135 (2019).

157. Kaiser, A. D., McQueen, D. M. & Peskin, C. S. Modeling the mitral valve. *Numer Methods Biomed Eng* **35**, e3240 (2019).

158. Vermot, J. *et al.* Reversing Blood Flows Act through klf2a to Ensure Normal Valvulogenesis in the Developing Heart. *PLoS Biol* **7**, e1000246 (2009).

159. Zhou, Z. *et al.* The Cerebral Cavernous Malformation Pathway Controls Cardiac Development via Regulation of Endocardial MEKK3 Signaling and KLF Expression. *Developmental Cell* **32**, 168–180 (2015).

160. Steed, E. *et al.* klf2a couples mechanotransduction and zebrafish valve morphogenesis through fibronectin synthesis. *Nat Commun* **7**, 11646 (2016).

161. Shou, Y. *et al.* Dynamic Stimulations with Bioengineered Extracellular Matrix-Mimicking Hydrogels for Mechano Cell Reprogramming and Therapy. *Advanced Science* **10**, 2300670 (2023).

162. Ławkowska, K., Bonowicz, K., Jerka, D., Bai, Y. & Gagat, M. Integrins in Cardiovascular Health and Disease: Molecular Mechanisms and Therapeutic Opportunities. *Biomolecules* **15**, 233 (2025).

163. Aman, J. & Margadant, C. Integrin-Dependent Cell–Matrix Adhesion in Endothelial Health and Disease. *Circulation Research* **132**, 355–378 (2023).

164. Kechagia, J. Z., Ivaska, J. & Roca-Cusachs, P. Integrins as biomechanical sensors of the microenvironment. *Nat Rev Mol Cell Biol* **20**, 457–473 (2019).

165. Hynes, R. O. Integrins: bidirectional, allosteric signaling machines. *Cell* **110**, 673–687 (2002).

166. Seetharaman, S. & Etienne-Manneville, S. Integrin diversity brings specificity in mechanotransduction. *Biology of the Cell* **110**, 49–64 (2018).

167. Balcioglu, H. E., van Hoorn, H., Donato, D. M., Schmidt, T. & Danen, E. H. J. The integrin expression profile modulates orientation and dynamics of force transmission at cell-matrix adhesions. *J Cell Sci* **128**, 1316–1326 (2015).

168. Humphries, J. D., Byron, A. & Humphries, M. J. Integrin ligands at a glance. *Journal of Cell Science* **119**, 3901–3903 (2006).

169. Calderwood, D. A., Shattil, S. J. & Ginsberg, M. H. Integrins and Actin Filaments: Reciprocal Regulation of Cell Adhesion and Signaling. *Journal of Biological Chemistry* **275**, 22607–22610 (2000).

170. Jian, B. *et al.* Serotonin mechanisms in heart valve disease I: serotonin-induced up-regulation of transforming growth factor-beta1 via G-protein signal transduction in aortic valve interstitial cells. *Am J Pathol* **161**, 2111–2121 (2002).

171. Hutcheson, J. D., Ryzhova, L. M., Setola, V. & Merryman, W. D. 5-HT(2B) antagonism arrests non-canonical TGF-β1-induced valvular myofibroblast differentiation. *J Mol Cell Cardiol* **53**, 707–714 (2012).

172. Transcriptional cofactor dyxin mediates hypertrophic response in the heart during angiotensin II-induced hypertension. *Journal of Physiology and Pharmacology* https://doi.org/10.26402/jpp.2023.6.03 (2023) doi:10.26402/jpp.2023.6.03.

173. Wang, K., Ash, J. F. & Singer, S. J. Filamin, a new high-molecular-weight protein found in smooth muscle and non-muscle cells. *Proc Natl Acad Sci U S A* **72**, 4483–4486 (1975).

174. Hartwig, J. H. & Stossel, T. P. Isolation and properties of actin, myosin, and a new actinbinding protein in rabbit alveolar macrophages. *J Biol Chem* **250**, 5696–5705 (1975).

175. Stossel, T. P. & Hartwig, J. H. Interactions between actin, myosin, and an actin-binding protein from rabbit alveolar macrophages. Alveolar macrophage myosin Mg-2+-adenosine triphosphatase requires a cofactor for activation by actin. *J Biol Chem* **250**, 5706–5712 (1975).

176. Guiet, R. *et al.* Macrophage mesenchymal migration requires podosome stabilization by filamin A. *J Biol Chem* **287**, 13051–13062 (2012).

177. Zhou, A.-X., Hartwig, J. H. & Akyürek, L. M. Filamins in cell signaling, transcription and organ development. *Trends in Cell Biology* **20**, 113–123 (2010).

178. Stossel, T. P. *et al.* Filamins as integrators of cell mechanics and signalling. *Nat Rev Mol Cell Biol* **2**, 138–145 (2001).

179. Hartwig, J. H., Tyler, J. & Stossel, T. P. Actin-binding protein promotes the bipolar and perpendicular branching of actin filaments. *J Cell Biol* **87**, 841–848 (1980).

180. Pudas, R., Kiema, T.-R., Butler, P. J. G., Stewart, M. & Ylänne, J. Structural basis for vertebrate filamin dimerization. *Structure* **13**, 111–119 (2005).

181. Nakamura, F., Osborn, T. M., Hartemink, C. A., Hartwig, J. H. & Stossel, T. P. Structural basis of filamin A functions. *J Cell Biol* **179**, 1011–1025 (2007).

182. Iwamoto, D. V. *et al.* Structural basis of the filamin A actin-binding domain interaction with F-actin. *Nat Struct Mol Biol* **25**, 918–927 (2018).

183. Gorlin, J. B. *et al.* Human endothelial actin-binding protein (ABP-280, nonmuscle filamin): a molecular leaf spring. *J Cell Biol* **111**, 1089–1105 (1990).

184. Duval, D. *et al.* Valvular dystrophy associated filamin A mutations reveal a new role of its first repeats in small-GTPase regulation. *Biochim Biophys Acta* **1843**, 234–244 (2014).

185. Ohta, Y., Suzuki, N., Nakamura, S., Hartwig, J. H. & Stossel, T. P. The small GTPase RalA targets filamin to induce filopodia. *Proc Natl Acad Sci U S A* **96**, 2122–2128 (1999).

186. Zhou, J., Kang, X., An, H., Lv, Y. & Liu, X. The function and pathogenic mechanism of filamin A. *Gene* **784**, 145575 (2021).

187. Feng, Y. *et al.* Filamin A (FLNA) is required for cell–cell contact in vascular development and cardiac morphogenesis. *Proc. Natl. Acad. Sci. U.S.A.* **103**, 19836–19841 (2006).

188. Duval, D. *et al.* MVP-Associated Filamin A Mutations Affect FlnA-PTPN12 (PTP-PEST) Interactions. *JCDD* **2**, 233–247 (2015).

189. Kim, H., Sengupta, A., Glogauer, M. & McCulloch, C. A. Filamin A regulates cell spreading and survival via beta1 integrins. *Exp Cell Res* **314**, 834–846 (2008).

190. Nakamura, F. FilGAP and its close relatives: a mediator of Rho-Rac antagonism that regulates cell morphology and migration. *Biochem J* **453**, 17–25 (2013).

191. Ohta, Y., Hartwig, J. H. & Stossel, T. P. FilGAP, a Rho- and ROCK-regulated GAP for Rac binds filamin A to control actin remodelling. *Nat Cell Biol* **8**, 803–814 (2006).

192. Ehrlicher, A. J., Nakamura, F., Hartwig, J. H., Weitz, D. A. & Stossel, T. P. Mechanical strain in actin networks regulates FilGAP and integrin binding to filamin A. *Nature* **478**, 260–263 (2011).

193. Hart, A. W. *et al.* Cardiac malformations and midline skeletal defects in mice lacking filamin A. *Human Molecular Genetics* **15**, 2457–2467 (2006).

194. Stourm, L. *et al.* Pulmonary hypertension in patients carrying FLNA loss-of-function variants. *Eur Respir J* **65**, 2401132 (2025).

195. Parrini, E. *et al.* Periventricular heterotopia: phenotypic heterogeneity and correlation with Filamin A mutations. *Brain* **129**, 1892–1906 (2006).

196. Cannaerts, E. *et al.* FLNA mutations in surviving males presenting with connective tissue findings: two new case reports and review of the literature. *BMC Med Genet* **19**, 140 (2018).

197. Billon, C. *et al.* Cardiovascular and connective tissue disorder features in FLNA-related PVNH patients: progress towards a refined delineation of this syndrome. *Orphanet J Rare Dis* **16**, 504 (2021).

198. Haataja, T. J. K. *et al.* Critical Structural Defects Explain Filamin A Mutations Causing Mitral Valve Dysplasia. *Biophys J* **117**, 1467–1475 (2019).

199. Haataja, T. J. K. *et al.* Non-syndromic Mitral Valve Dysplasia Mutation Changes the Force Resilience and Interaction of Human Filamin A. *Structure* **27**, 102-112.e4 (2019).

200. O'Brien, M. J., Beijerink, N. J. & Wade, C. M. Genetics of canine myxomatous mitral valve disease. *Animal Genetics* **52**, 409–421 (2021).

201. Oyama, M. A. *et al.* Comparative pathology of human and canine myxomatous mitral valve degeneration: 5HT and TGF-β mechanisms. *Cardiovascular Pathology* **46**, 107196 (2020).

202. Kim, Y.-M., Kim, S.-W. & Kim, J.-H. Galectin-3 is able to differentiate dogs with myxomatous mitral valve disease from healthy control dogs. *ajvr* 1–8 (2023) doi:10.2460/ajvr.23.03.0063.

203. Zhou, Q. *et al.* Differentially expressed platelet activation-related genes in dogs with stage B2 myxomatous mitral valve disease. *BMC Vet Res* **19**, 271 (2023).

204. Kim, A. J. *et al.* Deficiency of Circulating Monocytes Ameliorates the Progression of Myxomatous Valve Degeneration in Marfan Syndrome. *Circulation* **141**, 132–146 (2020).

205. Xu, N. & Yutzey, K. E. Therapeutic CCR2 Blockade Prevents Inflammation and Alleviates Myxomatous Valve Disease in Marfan Syndrome. *JACC: Basic Trans Sci.* **7**, 1143–1157 (2022).

206. Sauls, K. *et al.* Developmental basis for filamin-A-associated myxomatous mitral valve disease. *Cardiovascular Research* **96**, 109–119 (2012).

207. Remy, S. *et al.* Generation of gene-edited rats by delivery of CRISPR/Cas9 protein and donor DNA into intact zygotes using electroporation. *Sci Rep* **7**, 16554 (2017).

208. Delwarde, C. *et al.* Multimodality imaging and transcriptomics to phenotype mitral valve dystrophy in a unique knock-in Filamin-A rat model. *Cardiovascular Research* **119**, 759–771 (2023).

209. Aristizábal, B. & González, Á. Chapter 2 Innate immune system. in *Autoimmunity: from bench to bedside* (eds Anaya, J.-M., Shoenfeld, Y., Rojas-Villarraga, A., Levy, R. A. & Cervera, R.) (Center for Autoimmune Diseases Research, School of Medicine and Health Sciences, El Rosario University, Bogota, Colombia, 2013).

210. Yatim, K. M. & Lakkis, F. G. A Brief Journey through the Immune System. *Clinical Journal of the American Society of Nephrology* **10**, 1274–1281 (2015).

211. Delves, P. J. & Roitt, I. M. The Immune System. *N Engl J Med* **343**, 37–49 (2000).

212. Muntjewerff, E. M., Meesters, L. D. & Van Den Bogaart, G. Antigen Cross-Presentation by Macrophages. *Front. Immunol.* **11**, 1276 (2020).

213. Pegram, H. J., Andrews, D. M., Smyth, M. J., Darcy, P. K. & Kershaw, M. H. Activating and inhibitory receptors of natural killer cells. *Immunology & Cell Biology* **89**, 216–224 (2011).

214. Dunkelberger, J. R. & Song, W.-C. Complement and its role in innate and adaptive immune responses. *Cell Res* **20**, 34–50 (2010).

215. Kemper, C. *et al.* Complement: The Road Less Traveled. *J Immunol* **210**, 119–125 (2023).

216. Rosales, C. & Uribe-Querol, E. Phagocytosis: A Fundamental Process in Immunity. *BioMed Research International* **2017**, 1–18 (2017).

217. Cockram, T. O. J., Dundee, J. M., Popescu, A. S. & Brown, G. C. The Phagocytic Code Regulating Phagocytosis of Mammalian Cells. *Front Immunol* **12**, 629979 (2021).

218. Brown, G. C. Cell death by phagocytosis. *Nat Rev Immunol* **24**, 91–102 (2024).

219. Rabinovitch, M. Professional and non-professional phagocytes: an introduction. *Trends Cell Biol* **5**, 85–87 (1995).

220. Boada-Romero, E., Martinez, J., Heckmann, B. L. & Green, D. R. The clearance of dead cells by efferocytosis. *Nat Rev Mol Cell Biol* **21**, 398–414 (2020).

221. Doran, A. C., Yurdagul, A. & Tabas, I. Efferocytosis in health and disease. *Nat Rev Immunol* **20**, 254–267 (2020).

222. Michiels, R., Gensch, N., Erhard, B. & Rohrbach, A. Pulling, failing, and adaptive mechanotransduction of macrophage filopodia. *Biophysical Journal* **121**, 3224–3241 (2022).

223. Kundu, S., Pal, K., Pyne, A. & Wang, X. Force-bearing phagocytic adhesion rings mediate the phagocytosis of surface-bound particles. *Nat Commun* **16**, 984 (2025).

224. Richards, D. M. & Endres, R. G. The Mechanism of Phagocytosis: Two Stages of Engulfment. *Biophysical Journal* **107**, 1542–1553 (2014).

225. Ma, Z. *et al.* Regulation of Rac1 activation by the low density lipoprotein receptor–related protein. *The Journal of Cell Biology* **159**, 1061–1070 (2002).

226. Gordon, S. Elie Metchnikoff: father of natural immunity. *Eur J Immunol* **38**, 3257–3264 (2008).

227. Guilliams, M., Thierry, G. R., Bonnardel, J. & Bajenoff, M. Establishment and Maintenance of the Macrophage Niche. *Immunity* **52**, 434–451 (2020).

228. T'Jonck, W., Guilliams, M. & Bonnardel, J. Niche signals and transcription factors involved in tissue-resident macrophage development. *Cellular Immunology* **330**, 43–53 (2018).

229. Mass, E. *et al.* Specification of tissue-resident macrophages during organogenesis. *Science* **353**, aaf4238 (2016).

230. Mass, E. Delineating the origins, developmental programs and homeostatic functions of tissue-resident macrophages. *International Immunology* **30**, 493–501 (2018).

231. Ginhoux, F. *et al.* Fate mapping analysis reveals that adult microglia derive from primitive macrophages. *Science* **330**, 841–845 (2010).

232. Yona, S. *et al.* Fate mapping reveals origins and dynamics of monocytes and tissue macrophages under homeostasis. *Immunity* **38**, 79–91 (2013).

233. Kierdorf, K. *et al.* Microglia emerge from erythromyeloid precursors via Pu.1- and Irf8-dependent pathways. *Nat Neurosci* **16**, 273–280 (2013).

234. Gomez Perdiguero, E. *et al.* Tissue-resident macrophages originate from yolk-sac-derived erythro-myeloid progenitors. *Nature* **518**, 547–551 (2015).

235. Calvanese, V. & Mikkola, H. K. A. The genesis of human hematopoietic stem cells. *Blood* **142**, 519–532 (2023).

236. Lux, C. T. *et al.* All primitive and definitive hematopoietic progenitor cells emerging before E10 in the mouse embryo are products of the yolk sac. *Blood* **111**, 3435–3438 (2008).

237. Ginhoux, F. & Guilliams, M. Tissue-Resident Macrophage Ontogeny and Homeostasis. *Immunity* **44**, 439–449 (2016).

238. Mo, S. & Yen, K. Developmental Origins of the Heterogeneous Hematopoiesis. *Am J Hematol* **100**, 2074–2090 (2025).

239. Lacaud, G. & Kouskoff, V. Hemangioblast, hemogenic endothelium, and primitive versus definitive hematopoiesis. *Experimental Hematology* **49**, 19–24 (2017).

240. Mass, E. Delineating the origins, developmental programs and homeostatic functions of tissue-resident macrophages. *International Immunology* https://doi.org/10.1093/intimm/dxy044 (2018) doi:10.1093/intimm/dxy044.

241. Nakano, H. *et al.* Haemogenic endocardium contributes to transient definitive haematopoiesis. *Nat Commun* **4**, 1564 (2013).

242. Shigeta, A. *et al.* Endocardially Derived Macrophages Are Essential for Valvular Remodeling. *Developmental Cell* **48**, 617-630.e3 (2019).

243. Zamir, L. *et al.* Nkx2.5 marks angioblasts that contribute to hemogenic endothelium of the endocardium and dorsal aorta. *eLife* **6**, e20994 (2017).

244. Liu, K. *et al.* Lineage tracing clarifies the cellular origin of tissue-resident macrophages in the developing heart. *Journal of Cell Biology* **221**, e202108093 (2022).

245. Epelman, S. *et al.* Embryonic and Adult-Derived Resident Cardiac Macrophages Are Maintained through Distinct Mechanisms at Steady State and during Inflammation. *Immunity* **40**, 91–104 (2014).

246. Epelman, S., Lavine, K. J. & Randolph, G. J. Origin and functions of tissue macrophages. *Immunity* **41**, 21–35 (2014).

247. Lavine, K. J. *et al.* The Macrophage in Cardiac Homeostasis and Disease. *J Am Coll Cardiol* **72**, 2213–2230 (2018).

248. Dick, S. A. *et al.* Three tissue resident macrophage subsets coexist across organs with conserved origins and life cycles. *Sci Immunol* **7**, eabf7777 (2022).

249. Zaman, R. & Epelman, S. Resident cardiac macrophages: Heterogeneity and function in health and disease. *Immunity* **55**, 1549–1563 (2022).

250. Bajpai, G. *et al.* Tissue Resident CCR2- and CCR2+ Cardiac Macrophages Differentially Orchestrate Monocyte Recruitment and Fate Specification Following Myocardial Injury. *Circ Res* **124**, 263–278 (2019).

251. Heidt, T. *et al.* Differential Contribution of Monocytes to Heart Macrophages in Steady-State and After Myocardial Infarction. *Circulation Research* **115**, 284–295 (2014).

252. Isidoro, C. A. & Deniset, J. F. The role of macrophage subsets in and around the heart in modulating cardiac homeostasis and pathophysiology. *Front. Immunol.* **14**, 1111819 (2023).

253. Chakarov, S. *et al.* Two distinct interstitial macrophage populations coexist across tissues in specific subtissular niches. *Science* **363**, eaau0964 (2019).

254. Suku, M., Forrester, L., Biggs, M. & Monaghan, M. G. Resident Macrophages and Their Potential in Cardiac Tissue Engineering. *Tissue Engineering Part B: Reviews* **28**, 579–591 (2022).

255. Bajpai, G. *et al.* The human heart contains distinct macrophage subsets with divergent origins and functions. *Nat Med* **24**, 1234–1245 (2018).

256. Nicolás-Ávila, J. A. *et al.* A Network of Macrophages Supports Mitochondrial Homeostasis in the Heart. *Cell* **183**, 94-109.e23 (2020).

257. Sugita, J. *et al.* Cardiac macrophages prevent sudden death during heart stress. *Nat Commun* **12**, 1910 (2021).

258. Hulsmans, M. *et al.* Macrophages Facilitate Electrical Conduction in the Heart. *Cell* **169**, 510-522.e20 (2017).

259. Zaman, R. *et al.* Selective loss of resident macrophage-derived insulin-like growth factor-1 abolishes adaptive cardiac growth to stress. *Immunity* **54**, 2057-2071.e6 (2021).

260. Revelo, X. S. *et al.* Cardiac Resident Macrophages Prevent Fibrosis and Stimulate Angiogenesis. *Circulation Research* **129**, 1086–1101 (2021).

261. Pinto, A. R. *et al.* Revisiting Cardiac Cellular Composition. *Circ Res* **118**, 400–409 (2016).

262. Anstine, L. J., Horne, T. E., Horwitz, E. M. & Lincoln, J. Contribution of Extra-Cardiac Cells in Murine Heart Valves is Age-Dependent. *J Am Heart Assoc* **6**, e007097 (2017).

263. Bischoff, J. *et al.* CD45 Expression in Mitral Valve Endothelial Cells After Myocardial Infarction. *Circ Res* **119**, 1215–1225 (2016).

264. Dick, S. A. *et al.* Self-renewing resident cardiac macrophages limit adverse remodeling following myocardial infarction. *Nat Immunol* **20**, 29–39 (2019).

265. Rizzo, G. *et al.* Dynamics of monocyte-derived macrophage diversity in experimental myocardial infarction. *Cardiovascular Research* **119**, 772–785 (2023).

266. Haider, N. *et al.* Transition of Macrophages to Fibroblast-Like Cells in Healing Myocardial Infarction. *Journal of the American College of Cardiology* **74**, 3124–3135 (2019).

267. Kong, Y. *et al.* Mitochondrial metabolism regulated macrophage phenotype in myocardial infarction. *Biomedicine & Pharmacotherapy* **180**, 117494 (2024).

268. Goody, P. R. *et al.* Aortic Valve Stenosis: From Basic Mechanisms to Novel Therapeutic Targets. *Arterioscler Thromb Vasc Biol* **40**, 885–900 (2020).

269. Mueller, K. A. L. *et al.* Macrophage Migration Inhibitory Factor Promotes Thromboinflammation and Predicts Fast Progression of Aortic Stenosis. *ATVB* ATVBAHA.124.321000 (2024) doi:10.1161/ATVBAHA.124.321000.

270. Lee, S. H. *et al.* Single-cell transcriptomics reveal cellular diversity of aortic valve and the immunomodulation by PPARγ during hyperlipidemia. *Nat Commun* **13**, 5461 (2022).

271. Grim, J. C. *et al.* Secreted Factors From Proinflammatory Macrophages Promote an Osteoblast-Like Phenotype in Valvular Interstitial Cells. *ATVB* **40**, (2020).

272. Issa, N. *et al.* Macrophages as key modulators of calcific aortic valve disease. *Front. Cardiovasc. Med.* **12**, 1664067 (2025).

273. Zhang, X. *et al.* Integrating bioinformatics and machine learning analyses to identify immune-related secretory proteins and therapeutic small-molecule drugs in calcific aortic valve disease with type 2 diabetes. *Front. Immunol.* **16**, 1634655 (2025).

274. Guo, G. *et al.* Induction of Macrophage Chemotaxis by Aortic Extracts from Patients with Marfan Syndrome Is Related to Elastin Binding Protein. *PLoS ONE* **6**, e20138 (2011).

275. Guo, G. *et al.* Induction of Macrophage Chemotaxis by Aortic Extracts of the mgR Marfan Mouse Model and a GxxPG-Containing Fibrillin-1 Fragment. *Circulation* **114**, 1855–1862 (2006).

276. Minvielle Moncla, L.-H. *et al.* Mendelian randomization reveals interactions of the blood proteome and immunome in mitral valve prolapse. *Commun Med* **4**, 108 (2024).

277. Bandaru, S. *et al.* Targeting Filamin A Reduces Macrophage Activity and Atherosclerosis. *Circulation* **140**, 67–79 (2019).

278. Bandaru, S., Ala, C., Zhou, A.-X. & Akyürek, L. M. Filamin A Regulates Cardiovascular Remodeling. *IJMS* **22**, 6555 (2021).

279. Wolf, F. A., Angerer, P. & Theis, F. J. SCANPY: large-scale single-cell gene expression data analysis. *Genome Biol* **19**, 15 (2018).

280. Wolock, S. L., Lopez, R. & Klein, A. M. Scrublet: Computational Identification of Cell Doublets in Single-Cell Transcriptomic Data. *Cell Systems* **8**, 281-291.e9 (2019).

281. Kolberg, L. *et al.* g:Profiler—interoperable web service for functional enrichment analysis and gene identifier mapping (2023 update). *Nucleic Acids Research* **51**, W207–W212 (2023).

282. Jin, S. *et al.* Inference and analysis of cell-cell communication using CellChat. *Nat Commun* **12**, 1088 (2021).

283. Jin, S., Plikus, M. V. & Nie, Q. CellChat for systematic analysis of cell-cell communication from single-cell transcriptomics. *Nat Protoc* **20**, 180–219 (2025).

284. Leung, R. *et al.* Filamin A Regulates Monocyte Migration Through Rho Small GTPases During Osteoclastogenesis. *Journal of Bone and Mineral Research* 091123192444063–36 (2009) doi:10.1359/jbmr.091114.

285. Bartko, P. E. *et al.* Effect of Losartan on Mitral Valve Changes After Myocardial Infarction. *Journal of the American College of Cardiology* **70**, 1232–1244 (2017).

286. Dal-Bianco, J. P. *et al.* Myocardial Infarction Alters Adaptation of the Tethered Mitral Valve. *J Am Coll Cardiol* **67**, 275–287 (2016).

287. Hulin, A., Moore, V., James, J. M. & Yutzey, K. E. Loss of Axin2 results in impaired heart valve maturation and subsequent myxomatous valve disease. *Cardiovasc Res* **113**, 40–51 (2017).

288. Larson, C. *et al.* TGF-beta: a master immune regulator. *Expert Opin Ther Targets* **24**, 427–438 (2020).

289. Batlle, E. & Massagué, J. Transforming Growth Factor-β Signaling in Immunity and Cancer. *Immunity* **50**, 924–940 (2019).

290. Peng, W. *et al.* Endothelial-driven TGFβ signaling supports lung interstitial macrophage development from monocytes. *Sci Immunol* **10**, eadr4977 (2025).

291. Liu, Z. *et al.* APOE–NOTCH axis governs elastogenesis during human cardiac valve remodeling. *Nat Cardiovasc Res* **3**, 933–950 (2024).

292. Morton, S. U. & Brodsky, D. Fetal Physiology and the Transition to Extrauterine Life. *Clin Perinatol* **43**, 395–407 (2016).

293. Aran, D., Hu, Z. & Butte, A. J. xCell: digitally portraying the tissue cellular heterogeneity landscape. *Genome Biol* **18**, 220 (2017).

294. Huang, H.-Y. *et al.* Alternations in inflammatory macrophage niche drive phenotypic and functional plasticity of Kupffer cells. *Nat Commun* **15**, 9337 (2024).

295. Vannan, A. *et al.* Spatial transcriptomics identifies molecular niche dysregulation associated with distal lung remodeling in pulmonary fibrosis. *Nat Genet* https://doi.org/10.1038/s41588-025-02080-x (2025) doi:10.1038/s41588-025-02080-x.

296. Adair-Kirk, T. L. & Senior, R. M. Fragments of extracellular matrix as mediators of inflammation. *Int J Biochem Cell Biol* **40**, 1101–1110 (2008).

297. Sorokin, L. The impact of the extracellular matrix on inflammation. *Nat Rev Immunol* **10**, 712–723 (2010).

298. Riley, H. J. & Bradshaw, A. D. The Influence of the Extracellular Matrix in Inflammation: Findings from the SPARC-Null Mouse. *Anat Rec (Hoboken)* **303**, 1624–1629 (2020).

299. Moretti, L., Stalfort, J., Barker, T. H. & Abebayehu, D. The interplay of fibroblasts, the extracellular matrix, and inflammation in scar formation. *J Biol Chem* **298**, 101530 (2022).

300. Roh, J. S. & Sohn, D. H. Damage-Associated Molecular Patterns in Inflammatory Diseases. *Immune Netw* **18**, e27 (2018).

301. Petrey, A. C. & De La Motte, C. A. Hyaluronan, a Crucial Regulator of Inflammation. *Front. Immunol.* **5**, (2014).

302. Heldin, P., Lin, C.-Y., Kolliopoulos, C., Chen, Y.-H. & Skandalis, S. S. Regulation of hyaluronan biosynthesis and clinical impact of excessive hyaluronan production. *Matrix Biology* **78–79**, 100–117 (2019).

303. De La Motte, C. A. & Kessler, S. P. The Role of Hyaluronan in Innate Defense Responses of the Intestine. *International Journal of Cell Biology* **2015**, 1–5 (2015).

304. Kessler, S. P., Obery, D. R. & De La Motte, C. Hyaluronan Synthase 3 Null Mice Exhibit Decreased Intestinal Inflammation and Tissue Damage in the DSS-Induced Colitis Model. *International Journal of Cell Biology* **2015**, 1–13 (2015).

305. Filpa, V. *et al.* Changes in hyaluronan deposition in the rat myenteric plexus after experimentally-induced colitis. *Sci Rep* **7**, 17644 (2017).

306. Newman, A. M. *et al.* Robust enumeration of cell subsets from tissue expression profiles. *Nat Methods* **12**, 453–457 (2015).

307. Cho, H. J. *et al.* Induction of dendritic cell-like phenotype in macrophages during foam cell formation. *Physiol Genomics* **29**, 149–160 (2007).

308. Aranda-Pardos, I., Imam-Chasan, A. & Alonso-Gonzalez, N. Studying Efferocytosis Dynamics in Tissue-Resident Macrophages Ex Vivo. in *Tissue-Resident Macrophages* (ed. Mass, E.) vol. 2713 389–405 (Springer US, New York, NY, 2024).

309. Pridans, C. *et al.* Transcriptomic Analysis of Rat Macrophages. *Front. Immunol.* **11**, 594594 (2021).

310. Grove, L. M. *et al.* Transient Receptor Potential Vanilloid 4 in Macrophages Mediates TGF-β Activation to Drive Myofibroblast Differentiation and Pulmonary Fibrosis. *J Biol Chem* 111135 (2026) doi:10.1016/j.jbc.2026.111135.

311. Keerthivasan, S. *et al.* Homeostatic functions of monocytes and interstitial lung macrophages are regulated via collagen domain-binding receptor LAIR1. *Immunity* **54**, 1511-1526.e8 (2021).

312. Makdissi, N. & Mass, E. Of myeloid cells and fibroblasts—A love story. *Immunity* **54**, 1371–1373 (2021).

313. Duann, P. & Lin, P.-H. Wound Matrix Stiffness Imposes on Macrophage Activation. *Methods Mol Biol* **2193**, 111–120 (2021).

314. Taufalele, P. V. *et al.* Matrix stiffness enhances cancer-macrophage interactions and M2-like macrophage accumulation in the breast tumor microenvironment. *Acta Biomater* **163**, 365–377 (2023).

315. Wang, Y. *et al.* Matrix stiffness regulates macrophage polarization in atherosclerosis. *Pharmacol Res* **179**, 106236 (2022).

316. Hua, L., Shi, J., Shultz, L. D. & Ren, G. Genetic Models of Macrophage Depletion. in *Macrophages* (ed. Rousselet, G.) vol. 1784 243–258 (Springer New York, New York, NY, 2018).

317. Mauel, K. & Mass, E. Fate-Mapping of Hematopoietic Stem Cell-Derived Macrophages. in *Tissue-Resident Macrophages* (ed. Mass, E.) vol. 2713 139–148 (Springer US, New York, NY, 2024).

318. Splichalova, I. & Mass, E. Fate-Mapping of Yolk Sac-Derived Macrophages. in *Tissue-Resident Macrophages* (ed. Mass, E.) vol. 2713 129–137 (Springer US, New York, NY, 2024).

319. Huang, S. *et al.* Genetic and Immunohistochemistry Tools to Visualize Rat Macrophages In Situ. in *Tissue-Resident Macrophages* (ed. Mass, E.) vol. 2713 99–115 (Springer US, New York, NY, 2024).

320. Ahlback, A. & Gentek, R. Fate-Mapping Macrophages: From Ontogeny to Functions. in *Tissue-Resident Macrophages* (ed. Mass, E.) vol. 2713 11–43 (Springer US, New York, NY, 2024).